DOI: 10.1070/RCR4800

Tri- and tetranuclear molybdenum and tungsten chalcogenide clusters: on the way to new materials and catalysts †

Artem L. Gushchin,[a, b] Yuliya A. Laricheva,[a] Maxim N. Sokolov,[a, b, c] Rosa Llusar [d]

[a] *Nikolaev Institute of Inorganic Chemistry, Siberian Branch of the Russian Academy of Sciences ul. Akad. Lavrentieva 3, 630090 Novosibirsk, Russian Federation*
[b] *Novosibirsk National Research State University ul. Pirogova 1, 630090 Novosibirsk, Russian Federation*
[c] *Kazan (Volga Region) Federal University ul. Kremlevskaya 18, 420008 Kazan, Russian Federation*
[d] *Department of Physical and Analytical Chemistry, Jaume I University Str. Sos Baynat s/n, 12071 Castellón de la Plana, Spain*

Data on the electronic structure and redox, magnetic, luminescent, nonlinear optical and catalytic properties of tri- and tetranuclear molybdenum and tungsten chalcogenide clusters are analyzed and integrated. The prospects for the applications of this family of clusters for the design of new materials for molecular electronics, nonlinear optics and catalysis are considered.
The bibliography includes 202 references.

Contents

1. Introduction 670
2. Electronic structure and redox and magnetic properties 672
3. Luminescent properties 683
4. Optical limiting properties 683
5. Catalytic properties 684
6. Conclusion 701

A.L.Gushchin. Doctor of Chemical Sciences, Leading Researcher at the Laboratory of Synthesis of Complex Compounds of the NIIC SB RAS, Assistant Professor at the Department of Inorganic Chemistry of the NSU.
Telephone: +7(383)316 – 5845, e-mail: gushchin@niic.nsc.ru
Current research interests: chemistry of coordination and cluster compounds of transition metals, chalcogenide clusters of early transition metals, transition metal complexes with redox active ligands.
Yu.A.Laricheva. PhD, Researcher at the same Laboratory of the NIIC SB RAS
Telephone: +7(383)316 – 5845, e-mail: laricheva@niic.nsc.ru
Current research interests: molybdenum and tungsten chalcogenide clusters, electronic structure of coordination compounds.
M.N.Sokolov. Doctor of Chemical Sciences, Professor of the RAS, Head of the same Laboratory, Professor at the Department of Inorganic Chemistry of the NSU, Leading Researcher at the KFU.
Telephone: +7(383)316 – 5845, e-mail: caesar@niic.nsc.ru
Current research interests: coordination chemistry of 4d and 5d metals.
R.Llusar. PhD, Professor, Head of the group of Molecular Materials, University Jaume I. E-mail: rosa.llusar@qfa.uji.es
Current research interests: cluster compounds of transition metals, molecular materials, catalysis.

Received 24 November 2017
Translation: Z.P.Svitanko

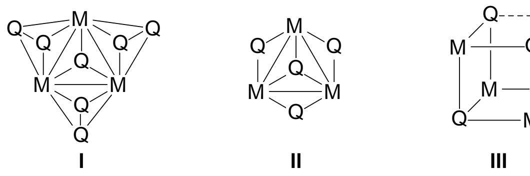
1. Introduction

Trinuclear molybdenum and tungsten (M) chalcogenide clusters and their heterometallic tetranuclear (cubane type) derivatives form the basis of an extensive and comprehensively studied family of cluster compounds of early transition metals. These compounds contain a stable group of three or four metal atoms linked by bridging chalcogen atoms (Q = S, Se, Te). The other coordination sites of the metal atoms are occupied by terminal ligands. The following structural types are most abundant: chalcogen-saturated clusters $\{M_3Q_7\}$ with three bridging dichalcogenide ligands (structure **I**) and chalcogen-unsaturated clusters $\{M_3Q_4\}$ with monochalcogenide ligands (structure **II**). In both cases, direct metal – metal contacts are present and metal atoms form a triangle. The heterometallic cubane type clusters $\{M_3Q_4M'\}$ (structure **III**) can be considered as resulting from coordination of a chalcophilic transition or post-transition metal heteroatom M′ (in a low oxidation

† The review is dedicated to Professor V.E.Fedorov on the occasion of his 80th birthday.

© 2018 Uspekhi Khimii, Russian Academy of Sciences and Turpion Ltd.

Structures I–III



state) to the triangular $\{M_3Q_4\}$ core. This coordination gives rise to a cluster in which the metal heteroatom is coordinated by three bridging chalcogenide ligands and does not form, most often, metal–metal bonds with other metal atoms; the number of vacant sites for ligand coordination to the metal heteroatom depends on its nature. In the case of $\{M_3Q_7\}$ clusters, the molybdenum or tungsten atom has (without considering the metal–metal bonds) a distorted pentagonal bipyramidal environment composed of five bridging chalcogen atoms and two donor atoms of terminal ligands. In the $\{M_3Q_4\}$ and $\{M_3Q_4M'\}$ clusters, the metal has a distorted octahedral environment of three chalcogen atoms and three donor atoms of terminal ligands.

The chemistry of these tri- and tetranuclear clusters with various mono- and polydentate ligands has been intensively developed since the beginning of 1980s in various research centres of the world. The first trinuclear molybdenum clusters $Mo_3Q_7X_4$ (Q = S, Se; X = Cl, Br) were described [1] in 1968. A lot of published reviews and book chapters are devoted to various aspects of the chemistry of these compounds (methods of synthesis, molecular and electronic structure, reactivity, physicochemical properties);[2–7] however, the issues related to their functional properties and the search for potential applications are touched on only fragmentarily. To some extent, this is caused by the fact that intensive research along this line started only in the 2000s. For example, studies of the catalytic activity of trinuclear molybdenum and tungsten clusters were initiated only approximately 10 years ago.

Currently, a large body of information has been accumulated on the potential use of these clusters for the design of new functional materials. This information has not yet been systematized in any survey publication. We made an attempt to fill this gap. The review presents data on the electronic structures and redox, magnetic, luminescent and nonlinear-optical properties of complexes formed by $\{M_3Q_7\}$, $\{M_3Q_4\}$ and $\{M_3Q_4M'\}$ clusters and catalytic systems based on them. The prospects for application of these compounds in such areas as molecular electronics, nonlinear optics and catalysis are outlined.

The review is timed to the 60th year anniversary of the A.V.Nikolaev Institute of Inorganic Chemistry, Siberian Branch of the Russian Academy of Sciences. The research carried out at this Institute makes a considerable contribution to the development of chemistry of the chalcogenide clusters of Group 5 to 7 metals.

The abbreviations used in the text are expanded below.

Organic ligands and groups

Ac — acetyl,
ADP — adenosine diphosphate,
ATP — adenosine triphosphate,
acac — acetylacetonate,
All — allyl,
bdt — benzene-1,2-dithiolate,
bpy — 2,2′-bipyridine,
COD — cycloocta-1,5-diene,
COE — cyclooctene,
Cp′ — methylcyclopentadienyl,
Cp* — pentamethylcyclopentadienyl,
Cy — cyclohexyl,
Cys — cysteine,
dba — dibenzylideneacetone,
dbbpy — 4,4′-di-*tert*-butyl-2,2′-bipyridine,
dcmbpy — 4,4′-dimethoxycarbonyl-2,2′-bipyridine,
dmbpy — 4,4′-dimethyl-2,2′-bipyridine,
dmen — *N*,*N*′-dimethylethylenediamine,
dmid —2-oxo-1,3-dithiole-4,5-dithiolate,
dmit — 2-thioxo-1,3-dithiole-4,5-dithiolate,
Dmp — 2,6-dimesitylbenzene,
dmpe — 1,2-bis(dimethylphosphino)ethane,
dpe — diphosphinoethane,
dppe — 1,2-bis(diphenylphosphino)ethane,
dnbpy — 4,4′-dinonyl-2,2′-bipyridine,
dppp — 1,3-bis(diphenylphosphino)propane,
dsit — 2-thioxo-1,3-dithiole-4,5-diselenolate,
dtp — diethyl dithiophoshate,
IPDOP — 1*H*-imidazo[4,5-*f*]-1,10-phenanthroline-2-[3,4-bis(dodecyloxy)phenyl],
mnt — 1,2-dicyanoethene-1,2-dithiolate,
MPTES — (3-mercaptopropyl)triethoxysilane,
nor — norbornene,
o-P2 — 3,4-dimethyl-3′,4′-bis(diphenylphosphino)tetrathiafulvalene,
p-cymene — 1-methyl-4-(1-methylethyl)benzene,
PCy_3 — tricyclohexylphosphine,
phen — 1,10-phenanthroline,
Pi — phosphate,
PNP — 2,6-bis(di-*tert*-butylphosphinomethyl)pyridine,
PPh_3 — triphenylphosphine,
pts — *p*-toluenesulfonate,
py — pyridine,
py_5Me_2 — 2,6-bis[1,1-bis(2-pyridyl)ethyl]pyridine,
Pyr — pyrrolidino,
tacn — 1,4,7-triazacyclononane,
tdas — 1,2,5-thiadiazole-3,4-dithiolate,
tdci — *cis*-1,3,5-tris(dimethylamino)-*cis*-inositol,
tfd — 1,2-bis(trifluoromethyl)ethene-1,2-dithiolate,
Tol — tolyl,
Tp — hydrotris(pyrazol-1-yl)borate,
TTF — tetrathiafulvalene,
TCNQ — 7,7′,8,8′-tetracyanoquinodimethane,
TRISPHAT — tris(tetrachlorocatecholate)phosphate.

Other abbreviations

CID — collision induced dissociation,
DFT — density functional theory,
ELF — electron localization function,
ESI MS — electrospray ionization mass spectrometry,
HDF — hydrodefluorination,
HDM — hydrodemetallation,
HDN — hydrodenitrogenation,
HDO — hydrodeoxygenation (oxygen removal from oxygenated compounds),
HDS — hydrodesulfurization,
HER — hydrogen evolution reaction (water reduction to give hydrogen),
His — histidine,
HOMO — highest occupied molecular orbital,
ILCT — intraligand charge transfer,

LUMO — lowest unoccupied molecular orbital,
TOF — catalyst turnover frequency,
TON — reaction turnover number,
ZFS — zero field splitting,
MO — molecular orbital,
NHE — normal hydrogen electrode,
NLO — nonlinear optics,
CSE — cluster skeletal electrons,
XPES — X-ray photoelectron spectroscopy.

2. Electronic structure and redox and magnetic properties

2.1. Complexes of trinuclear $\{M_3Q_7\}$ clusters

2.1.1. Electronic structure

The major difference between the $\{M_3(\mu_3\text{-}Q)(\mu_2\text{-}Q_2)_3\}$ and $\{M_3(\mu_3\text{-}Q)(\mu_2\text{-}Q)_3\}$ clusters (M = Mo, W; Q = S, Se) is the nature of the μ_2-bridging ligands. In the former case, the triangular M_3 moiety is surrounded by dichalcogenide ligands μ_2-Q_2 (see structure **I**), while in the latter case, it is surrounded by monochalcogenide ligands μ_2-Q (see structure **II**). Furthermore, the chalcogen atoms in the axial positions of complexes based on $\{M_3Q_7\}$ are electrophilic, unlike those in the $\{M_3Q_4\}$-based complexes.

The molecular orbital diagram for metal–metal interaction in the $\{M_3Q_7\}$ clusters with idealized C_{3v} symmetry has three bonding (one $1a_1$ and two 1e) and three antibonding (two 2e and one a_2) MOs (Fig. 1 *a*).[8] The $\{M_3Q_7\}$ clusters are stable if six d electrons of the metal (two electrons from each Mo^{IV} atom with the d^2 configuration) are available for filling the low-lying metal-centred $1a_1$ and 1e orbitals, which formally corresponds to three localized M–M single bonds. Thus, the number of cluster skeletal electrons in $\{M_3Q_7\}$ is 6. In this simplified scheme, a change in the electronic nature of the external ligands may lead to a change in the relative energy positions of the orbitals.

2.1.2. Redox properties

A distinctive feature of complexes of the $\{M_3Q_7\}$ clusters is that, irrespective of the charge state and the nature of terminal ligands, they undergo irreversible reaction involving reduction of three bridging dichalcogenide ligands to give $\{M_3Q_4\}$ cluster complexes [9–15]

$$\{M_3Q_7\}^{4+} + 6\,e \longrightarrow \{M_3Q_4\}^{4+} + 3\,Q^{2-} \qquad (1)$$

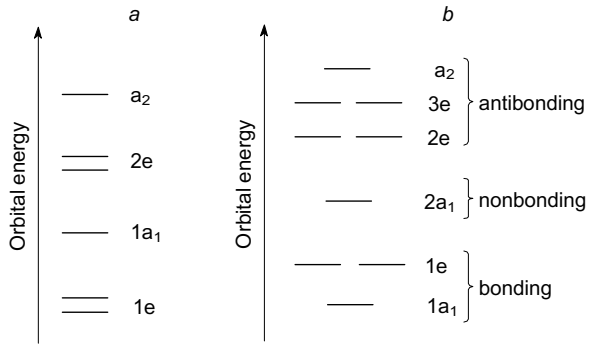


Figure 1. Simplified molecular orbital diagrams for the $\{M_3Q_7\}$ (*a*) and $\{M_3Q_4\}$ (*b*) clusters (M = Mo, W; Q = S, Se) for idealized C_{3v} symmetry.[8,22]

The electrochemical potentials of some $\{M_3Q_7\}$ complexes are summarized in Table 1. Generally, the coordination environment of the $\{Mo_3S_7\}$ cluster affects little the course of the reduction.[9] This is consistent with the fact that lower vacant molecular orbitals of $\{Mo_3S_7\}$ are mainly localized on the bridging S_2^{2-} ligands and make an antibonding contribution ($p-\pi^*/\sigma^*$) to the S–S bond.[16]

An interesting situation arises when electroactive ligands capable of being reduced, in particular, 1,10-phenanthroline, is introduced into the coordination sphere of $\{M_3Q_7\}$. Thus, the results of CV investigation of the complex $[Mo_3Se_7(phen)_3]Br_4$ immobilized on a graphite electrode attest to a completely reversible electron exchange reaction occurring at cathodic and anodic half-wave potentials of −0.086 V *versus* Ag/AgCl, which can be interpreted as three-electron reduction of $[Mo_3Se_7(phen)_3]^{4+}$ (structure **IV**) to give $[Mo_3Se_7(phen)_3]^{+}$ (Ref. 17). In the case of the tungsten complex $[W_3Se_7(phen)_3]Br_4$, the electrode potential shifts by −0.51 V, which may imply either metal-centred reduction ($M_3^{IV} \rightleftarrows M_3^{III}$) or mixed metal-(ligand)-centred reduction in which the electron density is delocalized between the ligand π* orbitals and metal d orbitals. This situation is intermediate between two limiting cases, $\{[M_3^{IV}Se_7(phen^-)_3]Br\}$ and $\{[M_3^{III}Se_7(phen)_3]Br\}$, and is confirmed by quantum chemical calculations, which showed the possibility for three electrons to be located in the 15A2 (LUMO) and 60E1 (LUMO + 1) orbitals that have

Table 1. Electrochemical potentials (E) for some trinuclear molybdenum $\{Mo_3Q_7\}$ cluster complexes.

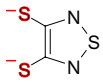
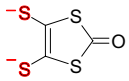
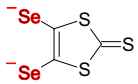
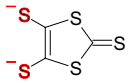
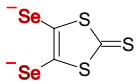
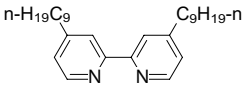
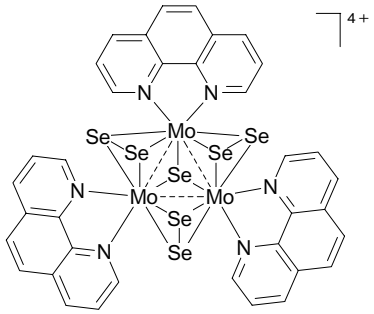
Complex	Organic ligand	E/V *versus* Ag/AgCl			Ref.
		I	*II*	*III*	
$[Mo_3S_7(S_2)_6]^{2-}$		−1.22	–	–	10
$[Mo_3S_7(tdas)_3]^{2-}$		−1.31	+0.72	–	11
$[Mo_3S_4Se_3Br_6]^{2-}$		from −1.2 to −1.4	–	–	11
$[Mo_3S_7Cl_6]^{2-}$		from −1.2 to −1.4	–	–	11
$[Mo_3S_7(tfd)_3]^{2-}$		−1.22	+0.51	+0.89	12
$[Mo_3S_7(bdt)_3]^{2-}$		−1.26	+0.23	+0.41	12

Table 1 (continued).

Complex	Organic ligand	*E*/V *versus* Ag/AgCl			Ref.
		I	*II*	*III*	
$[Mo_3S_7(dmid)_3]^{2-}$		−1.27	+0.36	–	12
$[Mo_3S_7(dsit)_3]^{2-}$		−1.69	+0.34	–	12
$[Mo_3S_7(dmit)_3]^{2-}$		−1.20	+0.38	–	12
$[Mo_3Se_7(dmit)_3]^{2-}$		−0.92	+0.15	–	13
$[Mo_3Se_7(dsit)_3]^{2-}$		−0.87	+0.16	–	13
$[Mo_3S_7Br_4(dnbpy)]$		−1.06	–	–	14
$[Mo_3S_7Br_6]^{2-}$		−1.15 to −1.68	–	–	15
$[Mo_3S_7(mnt)_3]^{2-}$		−1.04	+0.77	+1.16	15

Note. Here and in other Tables, the Roman numbers designate the electrochemical potentials of the successive redox processes.

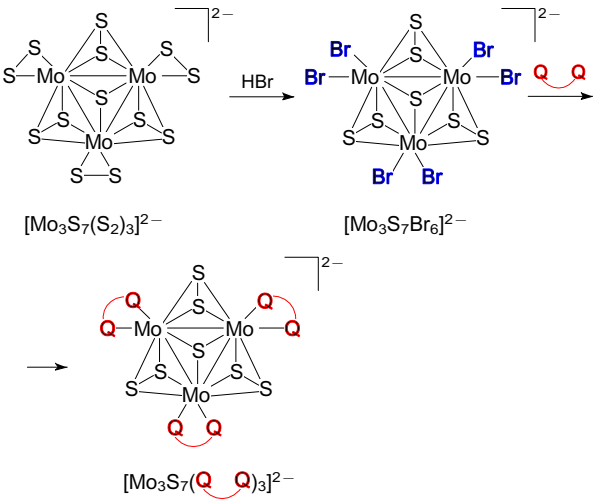
Structure IV



comparable contributions from the molybdenum (4d) and carbon (2p) atomic orbitals. This is the first and the only example of reversible reduction of $\{M_3Q_7\}^{4+}$clusters.

The $\{M_3Q_7\}$ clusters are less prone to oxidation, because this requires removal of electrons from the bonding metal-centred orbitals (HOMOs) and is expected to decrease the cluster core stability. In some complexes, the contribution of metal orbitals to the HOMO is no longer dominant. For example, the highest occupied MO in the $[Mo_3S_7(S_2)_3]^{2-}$ complex (Scheme 1) is mainly formed by weakly interacting π* orbitals of the terminal S_2^{2-} ligands, which rules out the possibility of any oxidation. Nevertheless, the $\{Mo_3S_7\}$ clusters become electroactive towards oxidation as a result of coordination of redox-active ligands such as dithiolates (Q Q = $S_2C_2R_2$) or diselenolates (Q Q = $Se_2C_2R_2$). In this case, the electrochemical response comes mainly from

Scheme 1



the ligand, *i.e.*, the oxidation is mainly a ligand-centred process. The oxidation reactions are reversible and proceed at moderate potentials (ranging from +0.2 to +0.8 V) (see Table 1). The corresponding dithiolate (diselenolate) complexes $[Mo_3S_7(Q\ Q)_3]^{2-}$ (Q Q = $S_2C_2R_2$, $Se_2C_2R_2$) are formed in moderate yields in the reactions of the bromide

complex $[Mo_3S_7Br_6]^{2-}$ with $(Bu_4N)_2[M(\overset{\frown}{Q\,Q})_2]$ (M = Zn, Sn; $\overset{\frown}{Q\,Q} = S_2C_2R_2$, Se_2 C_2R_2) or $Na_2(mnt)$.[11,12,18]

Similar complexes were also prepared for the $\{Mo_3Se_7\}$ cluster (see Table 1). The selenide complexes $[Mo_3Se_7(dmit)_3]^{2-}$ and $[Mo_3Se_7(dsit)_3]^{2-}$ are more easily oxidized than their sulfide analogues.[13] This trend is also followed for the $\{Mo_3Q_4\}$ and $\{Mo_4Q_4\}$ clusters (Q = S, Se).[19]

The calculations showed that the HOMOs in $[Mo_3S_7(\overset{\frown}{Q\,Q})_3]^{2-}$ ($\overset{\frown}{Q\,Q} = S_2C_2R_2$) are fully occupied mainly ligand-centred orbitals of 'e' symmetry. The contribution of ligands to the HOMO varies from 62% for $[Mo_3S_7(bdt)_3]^{2-}$ (Fig. 2) to 82% for $[Mo_3S_7(dsit)_3]^{2-}$. The major contribution to the HOMO-1 of 'a' symmetry is made by three external ligands and equatorial sulfur atoms of the cluster core (without involvement of the molybdenum atoms).[18]

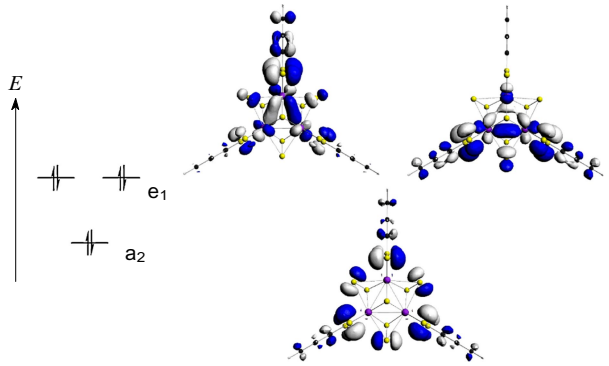


Figure 2. Form of the HOMO (above) and HOMO-1 (below) for the $[Mo_3S_7(bdt)_3]^{2-}$ dianion.[13]
Different colours (blue and grey) designate the areas of different parity.

The number of observed oxidation reactions of the $[Mo_3S_7(\overset{\frown}{Q\,Q})_3]^{2-}$ dianions ($\overset{\frown}{Q\,Q} = S_2C_2R_2$) and/or the diselenolate analogues depends on the nature of the external ligand. In the case of tfd, bdt, tdas or mnt derivatives, two successive reversible one-electron oxidation reactions take place; for the dmid, dmit and dsit ligands, there is only one two-electron oxidation process, which is asymmetric because of deposition of the neutral conductive product, $[Mo_3S_7(\overset{\frown}{Q\,Q})_3]$ ($\overset{\frown}{Q\,Q} = S_2C_2R_2$), on the electrode (see below).[20]

The ease of oxidation increases with decreasing electron-withdrawing (increasing electron-donating) ability of substituents in $S_2C_2R_2$ and varies in the series

bdt > dmid = dsit = dmit > tfd > tdas > mnt

Only in the case of $(Bu_4N)_2[Mo_3S_7L_3]$ (L = dmid, dmit and dsit), does the chemical or electrochemical oxidation give neutral products $[Mo_3S_7L_3]$ exhibiting electronic conductivity (see below).

2.1.3. Magnetic properties

The above-mentioned oxidation of $[Mo_3S_7(\overset{\frown}{Q\,Q})_3]^{2-}$ to $[Mo_3S_7(\overset{\frown}{Q\,Q})_3]$ ($\overset{\frown}{Q\,Q} = S_2C_2R_2$) changes the $1a_1^21e^4$ ground state to the $1a_1^21e^2$ state with partially occupied degenerate orbitals of 'e' symmetry (see Fig. 2), which corresponds to generation of radical anions from two ligands. The stable radicals thus formed can participate in numerous intermolecular interactions of sulfur atoms. For instance, the compound $[Mo_3S_7(dmit)_3]$ crystallizes in a trigonal space group in such a way that the cluster units are directed along the *c* axis and are connected into infinite chains *via* S···S contacts, giving rise to a C_{3v}-symmetric hexagonal network (Fig. 3).

Compounds of this type are of interest regarding both magnetic and electrophysical properties. Measurements of the molar magnetic susceptibility (χ_m) of polycrystalline $[Mo_3S_7L_3]$ samples (L = dmid, dmit and dsit) show continuous decline of the product χ_mT during cooling (Fig. 4*a*). At room temperature, the χ_mT values (~0.8–0.9 e.m.u. K mol^{-1}) are obviously lower than expected for the triplet state with the spin (*S*) equal to unity (1.0 e.m.u. K mol^{-1}). This is indicative of antiferromagnetic exchange interactions between the unpaired electrons of the $[Mo_3S_7L_3]$ molecules. The magnetic behaviour of these compounds can be described in terms of a one-dimensional exchange network formed from randomly distributed spins $S = 0$ and $S = 1$.[20]

For the phase based on $[Mo_3S_7L_3]$ (L = dmid, dmit and dsit), the specific resistance was shown to increase with decreasing temperature, *i.e.*, these phases behave as semiconductors. For example, the electronic conductivity of the single crystals of $[Mo_3S_7(dmit)_3]$ along the *c* axis is 25 Sm cm^{-1} at room temperature; this is a relatively high value for a neutral molecular crystal; the value doubles at high pressures (10 kbar).[18,20]

A distinctive feature of conductors based on $[Mo_3S_7(dmit)_3]$, $[Mo_3S_7(dmid)_3]$ and $[Mo_3S_7(dsit)_3]$ is that the electrons responsible for the conductivity are also responsible for the magnetic properties.[18,20,21] The interactions of sulfur atoms giving rise to conductivity (Fig. 4*b*) were used to simulate the magnetic behaviour considering two competing antiferromagnetic interactions *J* and *J*′ as an

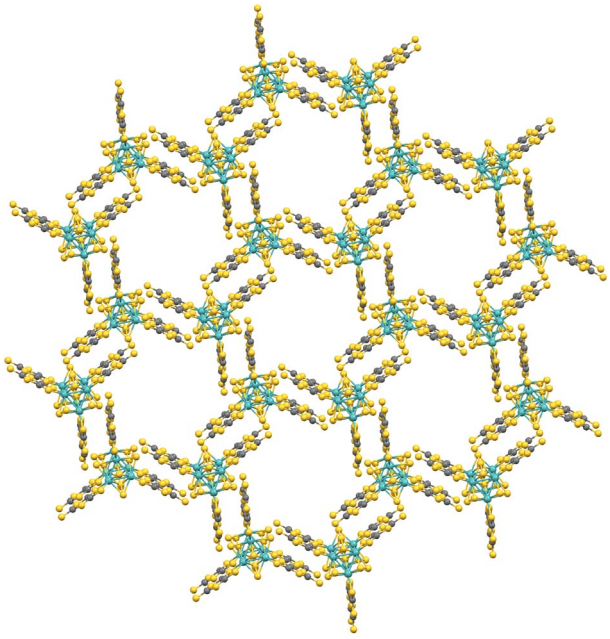


Figure 3. Honeycomb hexagonal packing along the *c* axis for $[Mo_3S_7(dmit)_3]$.[20]

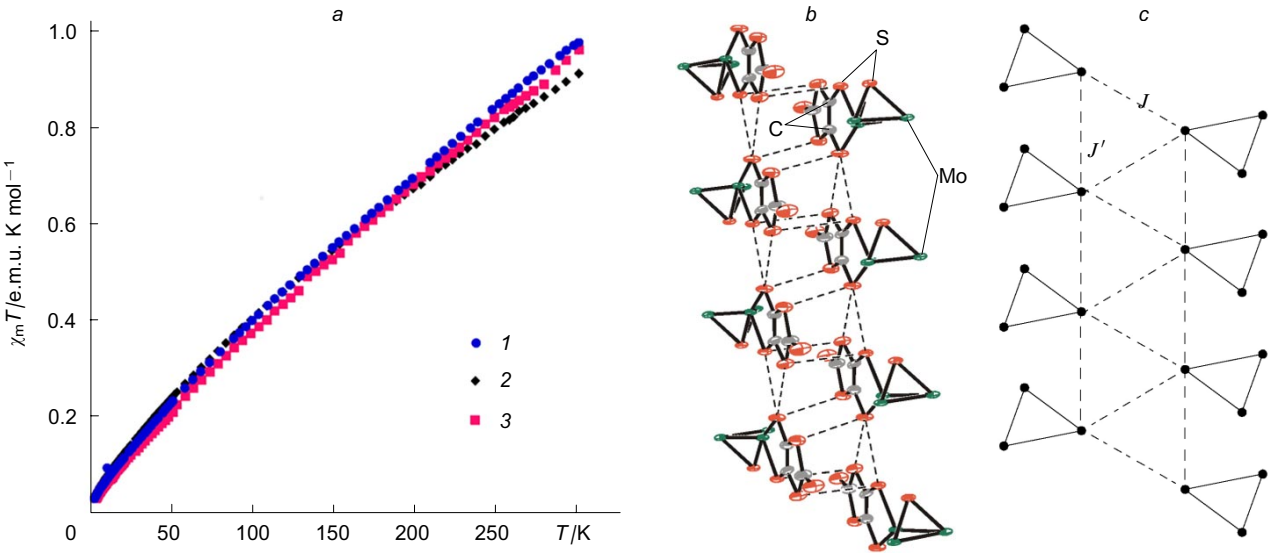


Figure 4. Temperature dependence of the product $\chi_m T$ (see ‡) for $[Mo_3S_7(dmid)_3]$ (*1*), $[Mo_3S_7(dsit)_3]$ (*2*) and $[Mo_3S_7(dmit)_3]$ (*3*) (*a*), fragments of the $[Mo_3S_7(dmit)_3]$ structure (*b*) and an exchange network based on two types of competing antiferromagnetic J and J' interactions (*c*).[20]
(*b*) The view along the *c* axis reflects the S···S contacts responsible for conducting properties; only two neighbouring clusters in the chain and one dmit ligand per cluster are shown; the bridging disulfide groups are omitted.

example (Fig. 4 *c*). The interaction J corresponds to the exchange between dithiolate ligands of different cluster chains and the interaction J' corresponds to the exchange between dithiolate ligands of the same chain. In this model, each magnetic cluster is actually a mixed-valence system which contains two unpaired electrons delocalized among three moieties and in which two types of antiferromagnetic interactions compete. The hypothetical metallic state of $[Mo_3S_7(dmit)_3]$ is only 50 meV mol^{-1} higher in energy than the antiferromagnetic state.

2.2. Complexes of trinuclear $\{M_3Q_4\}$ clusters

2.2.1. Electronic structure

The molecular orbital diagram for metal – metal interactions in the $\{M_3Q_4\}$ clusters (M = Mo, W; Q = S, Se) with idealized C_{3v} symmetry has three bonding ($1a_1$, 1e), one largely nonbonding ($2a_1$) and five antibonding (2e, 3e, a_2) molecular orbitals (see Fig. 1 *b*).[8,22] According to this diagram, the $\{M_3Q_4\}$ clusters, like $\{M_3Q_7\}$, are stable if all three metal-centred bonding orbitals $1a_1$ and 1e are occupied, which corresponds to three M – M bonds (six cluster skeletal electrons). The large energy gap between the 1e and $2a_1$ orbitals prevents the formation of clusters with 7 and 8 CSE (with partially or fully occupied nonbonding $2a_1$ orbital);[23] however, these states (and even the more reduced 9-electron state) can be generated in practice by electrochemical reduction. As regards stable reduced forms, only a few complexes of a seven-electron configuration have been detected, in particular, $[Cp^*_3Mo_3S_4]$,[24] $[Mo_3S_4Cl_3(dppe)_2(PEt_3)]$,[25] $[Mo_3S_4X_3(dppe)_3]$ (X = Br or a 2.6 Br + 0.4 Cl mixture).[26]

‡ The units of measurement of molecular magnetic susceptibility given in the text and in the Figures are the same as in the original source.

The results of XPES investigations of some complexes based on six-electron $\{Mo_3S_4\}$ clusters confirm the 4+ oxidation state for molybdenum.[27–30]

Bond analysis of the $\{Mo_3S_4\}$ cluster performed by advanced methods of quantum chemistry distinguished the $\{Mo_3S_4\}$ group as an individual chemical unit in the first bifurcation ELF diagram (Fig. 5), whereas the metal – metal bond within the Mo_3 triangle is characterized by both disynaptic basins V(Mo, Mo) and trisynaptic basin V(Mo, Mo, Mo). The results of calculations of the basin populations and covariances suggest the existence of delocalized Mo – (μ_2-S) – Mo bonding.[31,32] This delocalization was also suggested by earlier semiempirical calculations, which demonstrated spatially delocalized Mo(d) – S(pπ) bonding, giving rise to a continuous closed $Mo_3(\mu_2\text{-}S)_3$ d – pπ system with a strong interaction between the localized three-centre two-electron Mo – (μ_2-S) – Mo bonds. This delocalization can be described using the concept of quasi-aromaticity, as evidenced from the results of *ab initio* Hartree–Fock calculations.[33–37] The concept of quasi-aromaticity of $\{M_3O_nQ_{4-n}\}$ heterocycles (M = Mo, W; Q = S, Se; n = 0–4) was used to interpret the key reactivity features of the $\{M_3Q_4\}$ clusters, for example, the fact that, unlike the halide analogues $\{M_3O_nX_{4-n}\}$ (X = Cl, Br; n = 0–4), they can form cubane type clusters according to the [3 + 1] pattern.

The electronic structures of halide and the corresponding chalcogenide transition metal clusters are substantially different. A key difference is the relatively weak d – pπ bonding in the halide complexes, which rules out the possibility of pronounced delocalization of the lone pairs of bridging halogen atoms over the vacant d orbitals of the metal. One more difference is the competition of d orbitals for the M – M bond and the M – X π bond in the $\{M_3(\mu_2\text{-}X)_3\}$ moiety of halide complexes. This competition weakens the d – pπ bond and strengthens the metal – metal bond. None of the $\{M_3X_4\}$ halide clusters (M = Mo, W;

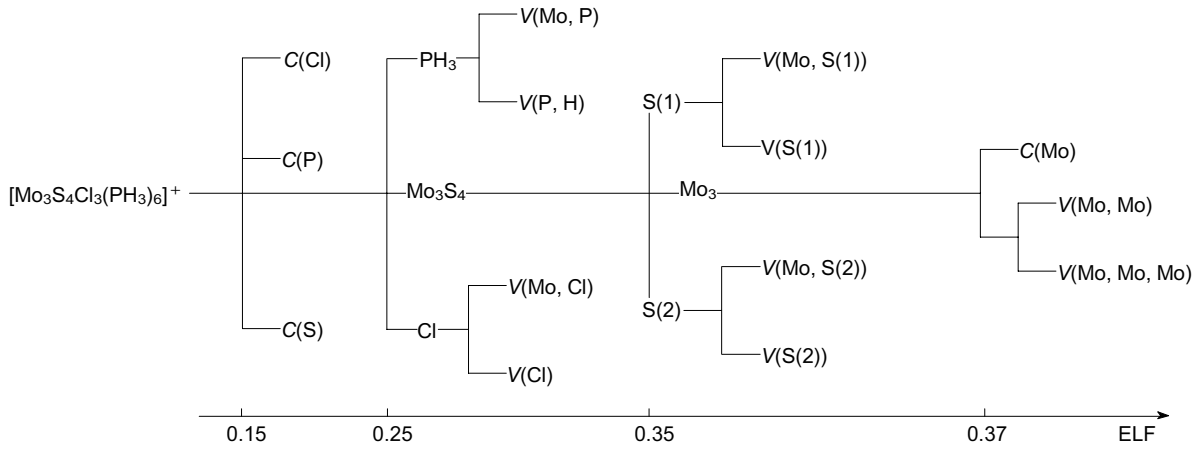


Figure 5. ELF bifurcation tree for the model $[Mo_3S_4Cl_3(PH_3)_6]^+$ complex.[31, 32]
C is the nuclear attractor, *V* is the valence attractor.

X = Cl, Br) shows a quasi-aromatic character inherent in $\{M_3\,Q_4\}$ (Q = S, Se). These two reasons account for the low reactivity of the halide complexes towards [3 + 1]-addition.[38]

2.2.2. Redox properties

The redox properties of trinuclear $\{M_3Q_4\}$ cluster complexes have been studied in detail by the CV technique (Table 2).[21, 39–46] A typical feature is the presence of either three successive one-electron reductions

$$M_3^{IV} \rightleftharpoons M_2^{IV}M^{III} \rightleftharpoons M^{IV}M_2^{III} \rightleftharpoons M_3^{III} \qquad (2)$$

or successive two- and one-electron reductions

$$M_3^{IV} \rightleftharpoons M_2^{III}M^{IV} \rightleftharpoons M_3^{III} \qquad (3)$$

depending on the nature of terminal ligands. This is accompanied by occupation of nonbonding and antibonding metal-centred MOs — $2a_1$ and 2e, respectively. Most often, the first reduction reaction is reversible or quasi-reversible, while the subsequent reactions are irreversible.

Molybdenum complexes are reduced more easily than tungsten counterparts. For instance, the half-wave potential ($E_{1/2}$) of the first one-electron reduction for the diphoshine complexes $[M_3S_4Br_3(dmpe)_3](PF_6)$ is −0.56 (M = Mo) or −0.95 V (M = W).[39] The reduction potential for $[M_3Q_4(dppe)_3X_3](PF_6)$ decreases in the series

Table 2. Electrochemical potentials for some trinuclear $\{M_3Q_4\}$ cluster complexes (M = Mo, W; Q = S, Se).

Complex	*E*/V *versus* Ag/AgCl			Ref.	Complex	*E*/V *versus* Ag/AgCl			Ref.
	I	*II*	*III*			*I*	*II*	*III*	
$[Mo_3S_4(bdt)_3]^{2-}$	−1.42	+0.47	+0.65	21	$[W_3Se_4(dmpe)_3Br_3]^+$	−0.91	−1.12	−1.41	40
$[Mo_3S_4(tdas)_3]^{2-}$	−1.36	+0.86	–	21	$[Mo_3S_4(acac)_3(py)_3]^+$	−0.75	−0.97	–	41
$[Mo_3S_4(dmid)_3]^{2-}$	−1.10	+0.57	–	21	$[Mo_3Se_4(acac)_3(py)_3]^+$	−0.86	−0.99	–	41
$[Mo_3S_4(dmit)_3]^{2-}$	−1.33	+0.57	–	21	$[W_3S_4(acac)_3(py)_3]^+$	−1.36	−1.56	–	41
$[W_3S_4(dppe)_3H_3]^+$	−1.56	−2.03	–	39	$[W_3Se_4(acac)_3(py)_3]^+$	−1.06	−1.19	–	41
$[W_3S_4(dppe)_3Br_3]^+$	−0.94	−1.62	–	39	$[(Cp')_3W_3S_4]^+$	−1.16	+1.60 [a]	–	42
$[W_3S_4(dmpe)_3Br_3]^+$	−0.95	−1.34	–	39	$[(Cp')_3Mo_3S_4]^+$	−0.81	+1.19 [a]	–	42
$[Mo_3S_4(dppe)_3Cl_3]^+$	−0.50	−1.34	–	39	$[Mo_3S_4(o\text{-}P2)_3Cl_3]^+$	−0.46	+0.58	+1.14	43
$[Mo_3S_4(dppe)_3Br_3]^+$	−0.39	−1.15	–	39	$[Mo_3Se_4(o\text{-}P2)_3Cl_3]^+$	−0.48	+0.55	+1.12	43
$[Mo_3Se_4(dmpe)_3Cl_3]^+$	−0.60	−1.21	–	40	$[Mo_3S_4(H_2O)_9]^{4+}$	−0.54	−1.10	−1.83	44
$[Mo_3Se_4(dmpe)_3Br_3]^+$	−0.54	−0.87	−1.20	40	$[Mo_3S_4(dmpe)_3Cl_3]^+$	−0.69	−1.38	–	44
$[Mo_3Se_4(dppe)_3Br_3]^+$	−0.46	−1.09	–	40	$[Mo_3S_4(dmpe)_3Br_3]^+$	−0.56	−1.20	–	44
$[W_3Se_4(dppe)_3Br_3]^+$	−0.92	−1.43	–	40	$[Mo_3S_4Cl_3(dnbpy)_3]^+$	−0.41	−1.21	–	45
$[Mo_3Se_4(dppe)_3Cl_3]^+$	−0.52	−1.25	–	40	$[Mo_3S_4Cl_3(dnbpy)_3]^+$	−0.39	−1.18	–	46

[a] Measured *versus* Hg/Hg_2Cl_2.

$Mo_3S_4 > Mo_3Se_4 > W_3Se_4 > W_3S_4$

whereas the series observed for analogous dmpe derivatives is as follows:[40]

$Mo_3S_4 > Mo_3Se_4 > W_3S_4 > W_3Se_4$

In the case of acetylacetonate complexes $[M_3Q_4(acac)_3(py)_3]^+$ (M = Mo, W; Q = S, Se), the reduction becomes more difficult in the order[41]

$Mo_3S_4 > Mo_3Se_4 > W_3Se_4 > W_3S_4$

It is of interest that the CV measurements for $[Mo_3S_4(dtp)_2(\mu\text{-AcO})Cl(dmbpy)]$ in dichloromethane did not reveal any electrochemical processes associated with the Mo^{IV} reduction in the negative region up to −1.5 V *versus* Ag/AgCl. This is attributable to the fact that the LUMO of this complex responsible for the reducibility is ligand- rather than metal-centred.[47]

The diimine complex $[Mo_3S_4Cl_3(phen)_3]Cl\cdot 4H_2O$ showed reversible two-electron reduction at the half-wave potential of −0.09 V *versus* Ag/AgCl and fully irreversible one-electron reduction at −1.25 V.[48] In this case, considering the possibility for electrons to enter the phenanthroline π-system, as in the case of $[Mo_3Se_7(phen)_3]Br_4$ (see above), this redox process can be regarded as a mixed molybdenum/phenanthroline-centred reduction, resulting in an intermediate between $[Mo_3^{IV}S_4Cl_3(phen^-)_2(phen)]^-$ (one-electron reduction of two phen ligands) and $[Mo^{IV}Mo_2^{III}S_4Cl_3(phen)_3]^-$ (one-electron reduction of two Mo^{IV}).

In the absence of electroactive ligands, $\{M_3Q_4\}$-based complexes are usually not prone to oxidation. As an exception, note methylcyclopentadienyl derivatives $[(Cp')_3M_3S_4]^+$ (M = Mo, W), which undergo, apart from the one-electron reduction, also two-electron oxidation at +1.19 and +1.60 V *versus* Hg/Hg_2Cl_2.[44] This process involves removal of electrons from the bonding metal-centred 1e orbital and can be attributed to the Mo^{IV}/Mo^{V} pair.

Apart from the metal-centred reduction, the cyclic voltammograms of the complexes $[Mo_3Q_4(o\text{-P2})_3Cl_3](PF_6)$ (Q = S, Se) containing electroactive 3,4-dimethyl-3,4-bis(diphenylphosphino)tetrathiafulvalene exhibit oxidation processes resulting in the formation of tetrathiafulvalene radical cation and dication at $E_{1/2} = 0.55$, 1.12 V (for S) and $E_{1/2} = 0.55$, 1.12 V (for Se) and attributable to the $[Mo_3Q_4(o\text{-P2})_3Cl_3]^{+/4+}$ and $[Mo_3Q_4(o\text{-P2})_3Cl_3]^{4+/7+}$ pairs. The products of oxidation of $[Mo_3Q_4(o\text{-P2})_3Cl_3](PF_6)_4$ were isolated upon the reactions of this compound with an excess of $NOPF_6$ in CH_2Cl_2 and were characterized by analytical and spectroscopic methods.[45]

A similar electrochemical behaviour was found for the dithiolate complexes, $[Mo_3S_4(\overset{\frown}{Q\ Q})_3]^{2-}$ and $[Mo_3S_7(\overset{\frown}{Q\ Q})_3]^{2-}$ ($\overset{\frown}{Q\ Q} = S_2C_2R_2$); the former are oxidized at potentials shifted to the anodic region by ~0.2 V compared with the potentials of the $\{Mo_3S_7\}$ derivatives.[21]

2.2.3. Magnetic properties

There are relatively few examples of magnetically active complexes of the trinuclear $\{M_3Q_4\}$ cluster and the number of CSE > 6. The addition of the seventh electron to $\{Mo_3S_4\}$ may reduce the symmetry because of the Jahn–Teller effect, for example, as in $[(Cp^*)_3Mo_3S_4]$.[24]

The paramagnetic complex $[Mo_3S_4Cl_3(dppe)_2(PEt_3)]$ with seven CSE was obtained in the reaction of $Mo_3S_7Cl_4$ with PEt_3 followed by reduction with magnesium at −20 °C with the addition of dppe. The introduction of the seventh electron into the antibonding orbital of the reduced $\{Mo_3S_4\}^{3+}$ cluster leads to elongation of the Mo–Mo bonds (2.806 Å) by 0.05–0.07 Å with respect to analogous bonds in diphosphine complexes of the $\{Mo_3S_4\}^{4+}$ cluster.[25]

The reaction of six-electron $[Mo_3S_4X_3(dppe)_3]^+$ with gallium gives the neutral $[Mo_3S_4X_3(dppe)_3]$ complex (X = Br or a 2.6 Br + 0.4 Cl mixture) with seven CSE.[26] The paramagnetic nature of the reduced complexes was unambiguously confirmed by EPR and by measurement of the molar magnetic susceptibility (Fig. 6). The products of the molar magnetic susceptibility by the temperature ($\chi_m T$) are 0.40 (X = Br) and 0.35 cm^3 K mol^{-1} (X = 2.6 Br + 0.4 Cl) at 300 K, which attests to the presence of one unpaired electron ($S = 1/2$); these values remain almost invariable down to low temperatures, as expected for a nearly ideal paramagnetic system.

The EPR spectra of polycrystalline samples of both complexes (Fig. 7) are very similar and contain a weak single signal at 125 K; the signal intensity increases with decreasing temperature. Below ~80 K both EPR signals are split into six lines as a result of hyperfine coupling of the unpaired electron with the molybdenum nuclei with the 5/2 spin (^{95}Mo and ^{97}Mo with natural abundances of 15.9% and 9.6%, respectively). This fact indicates that below the

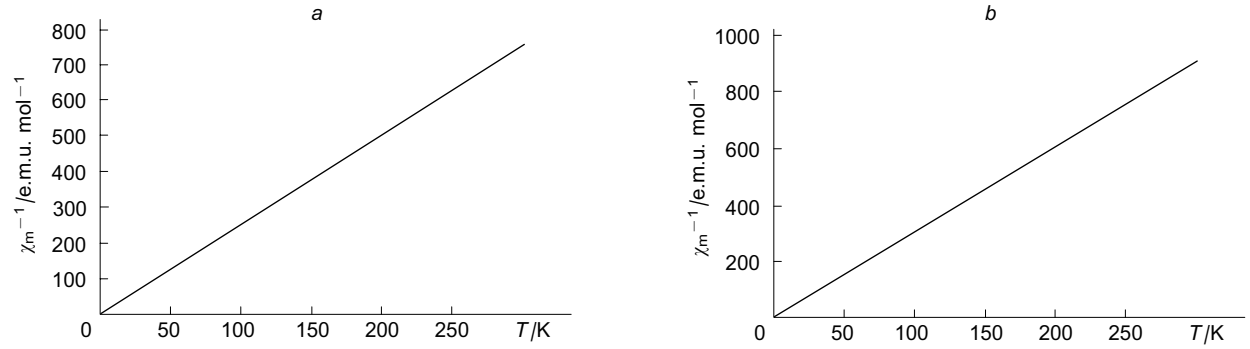


Figure 6. Temperature dependences of the molar magnetic susceptibility of $[Mo_3S_4X_3(dppe)_3]$, X = Br (*a*) and X = 2.6 Br + 0.4 Cl (*b*).[26]

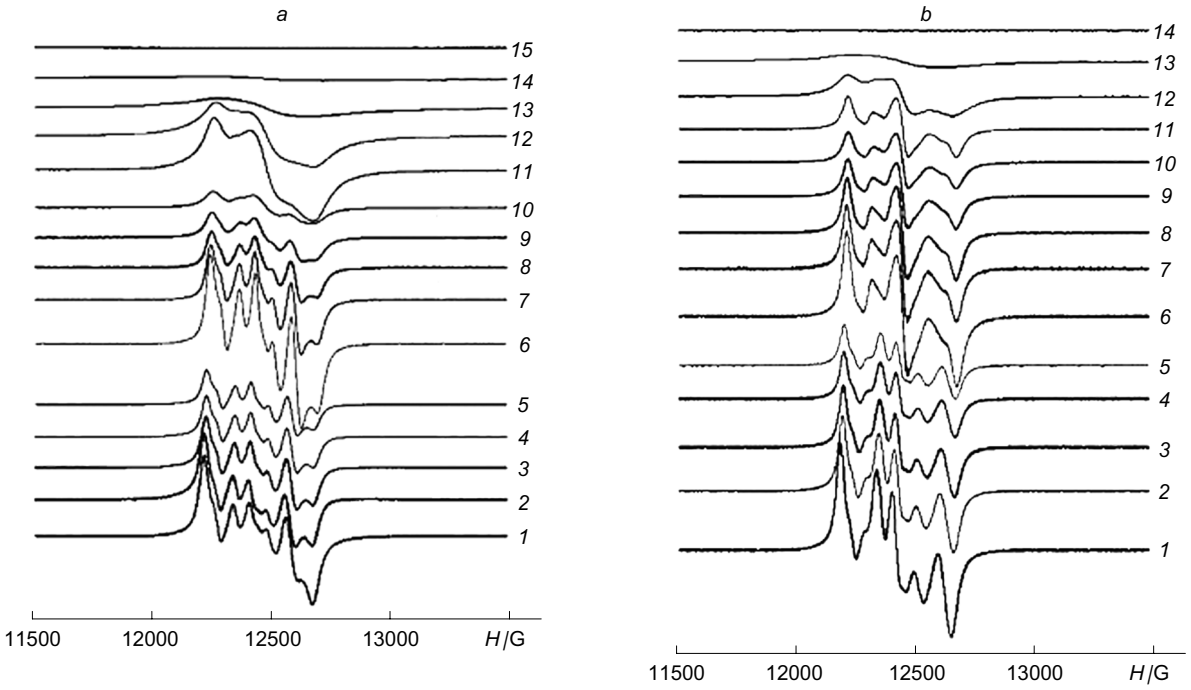


Figure 7. Q-band EPR spectra for $[Mo_3S_4X_3(dppe)_3]$, X = Br (*a*) and X = 2.6 Br + 0.4 Cl (*b*) at various temperatures.
(*a*) T = 5 (*1*), 10 (*2*), 15 (*3*), 20 (*4*), 25 (*5*), 40 (*6*), 50 (*7*), 60 (*8*), 70 (*9*), 80 (*10*), 90 (*11*), 100 (*12*), 125 (*13*), 150 (*14*), 290 K (*15*); amplitude scaling factor: 10 (*1*–*5*), 5 (*6*–*10*);
(*b*) T = 5 (*1*), 8 (*2*), 10 (*3*), 15 (*4*), 20 (*5*), 30 (*6*), 40 (*7*), 50 (*8*), 60 (*9*), 70 (*10*), 80 (*11*), 90 (*12*), 100 (*13*), 300 K (*14*); amplitude scaling factor: 10 (*1*–*6*), 2 (*7*–*12*).[26]

mentioned temperature, the unpaired electron is localized on one of the three atoms of the Mo_3 moiety, which attests to an asymmetrical structure of the moiety.

Quantum chemical calculations for the model $[Mo_3S_4(dpe)_3Br_3]^q$ complex (q = 0, 1+) confirmed the geometric distortion due to the Jahn–Teller effect (caused by the appearance of the seventh electron in the system). For the $[Mo_3S_4(dpe)_3\ Br_3]^+$ cluster with six CSE and a C_3 axis, the lowest unoccupied molecular orbital is doubly degenerate and has 'e' symmetry. The addition of one electron should give rise to the degenerate electronic state ^2E, which can be stabilized by lowering the symmetry and removal of the degeneration. The calculations for neutral $[Mo_3S_4(dpe)_3Br_3]$ (C_1 symmetry) confirmed the geometric distortion of the Mo_3 moiety to an acute-angled triangle and energy splitting of e-orbitals. The unpaired electron occupies the orbital mainly localized on one molybdenum atom, which leads to spin polarization.[26]

In this context, mention should be made of a rare example, the $[Re_3S_4(dppe)_3Br_3]^+$ rhenium(IV) cluster.[49] It was obtained by treatment of $Re_3S_7Br_7$ with phosphine (dppe) in MeCN, and its structure resembles that of $\{Mo_3S_4\}$, but contains nine CSE instead of six. The rhenium cluster has an unusual quadruplet ground state with three unpaired electrons, while the virtually invariable effective magnetic moment (3.87 μ_B) in the temperature range of 30–300 K attests to a nearly ideal paramagnetic system.

It is known that diphosphine complexes $[M_3Q_4(dmpe)_3X_3]^+$ (M = Mo, W; Q = S, Se; X = Cl, Br) react with nucleophiles with replacement of terminal halide ions by H^-, HO^-, SCN^- or CN^-.[39,50] Conversely, when the six-electron $[Mo_3S_4Br_3(dppe)_3](PF_6)$ cluster reacts with Bu^{t}SNa, complete elimination of the bromide anions from the cluster takes place, instead of formation of the expected thiolate-substituted complex; this is accompanied by one-electron reduction and insertion of an additional μ_3-capping sulfur atom into the cluster. This gives rise to a seven-electron paramagnetic complex $[Mo_3(\mu_3\text{-}S)_2(\mu\text{-}S)_3(dppe)_3](PF_6)$ (Fig. 8 *a*)[51] containing a rare trigonal-bipyramidal $\{Mo_3S_5\}$ cluster.[52,53] The reduction of $[Mo_3Se_4Br_3(dppe)_3]Br$ with gallium affords a similar paramagnetic complex $[Mo_3(\mu_3\text{-}Se)_2(\mu\text{-}Se)_3(dppe)_3](GaBr_4)$.[54] This is the only example of a complex with the $\{Mo_3Se_5\}$ cluster. In such complexes, one molybdenum atom occurs in the reduced state (Mo^{III}).

The magnetic nature of the complexes was confirmed by EPR and magnetochemical data. In the diagram of the temperature dependence of $\chi_m T$ for $[Mo_3(\mu_3\text{-}S)_2(\mu\text{-}S)_3(dppe)_3](PF_6)$ (Fig. 8 *b*), the product $\chi_m T$ remains constant down to ~20 K (0.381 cm^3 K mol^{-1} at 300 K), which is indicative of isolated paramagnetic centres. A minor decrease in the product $\chi_m T$ observed at low temperature is, most likely, due to zero field splitting and/or very weak intermolecular interactions.

For $[Mo_3(\mu_3\text{-}Se)_2(\mu\text{-}Se)_3(dppe)_3](GaBr_4)$, the $\chi_m T$ value is 0.372 cm^3 K mol^{-1} at 300 K and remains almost invariable down to 10 K. The Weiss constant is very low (−0.01 K), which was to be expected for a virtually ideal paramagnetic system with very weak antiferromagnetic interactions.[54]

The EPR spectra of solid samples confirm the paramagnetic character of the complexes $[Mo_3S_5(dppe)_3]^+$ and $[Mo_3Se_5(dppe)_3]^+$ in the ground state $S = 1/2$. The unpaired electron of half-occupied HOMO is delocalized

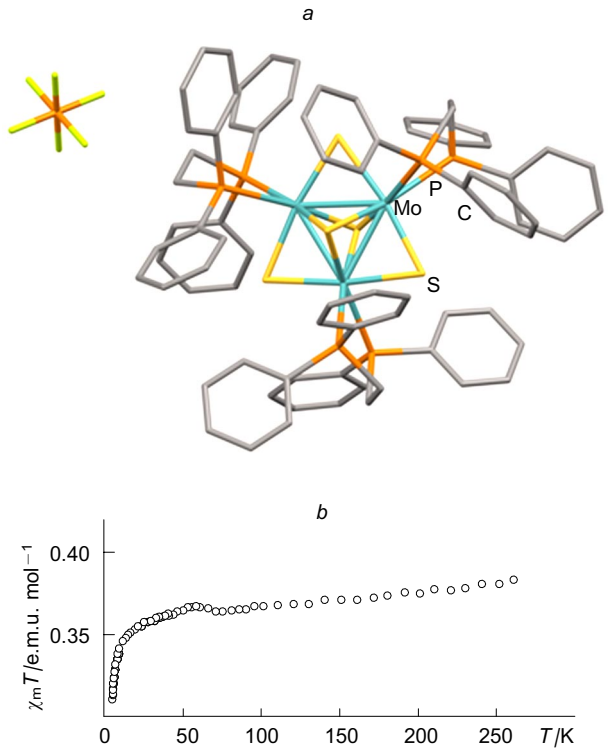


Figure 8. Structure of $[Mo_3(\mu_3\text{-}S)_2(\mu\text{-}S)_3(dppe)_3](PF_6)$ (*a*) and temperature dependence of $\chi_m T$ (*b*).[51]

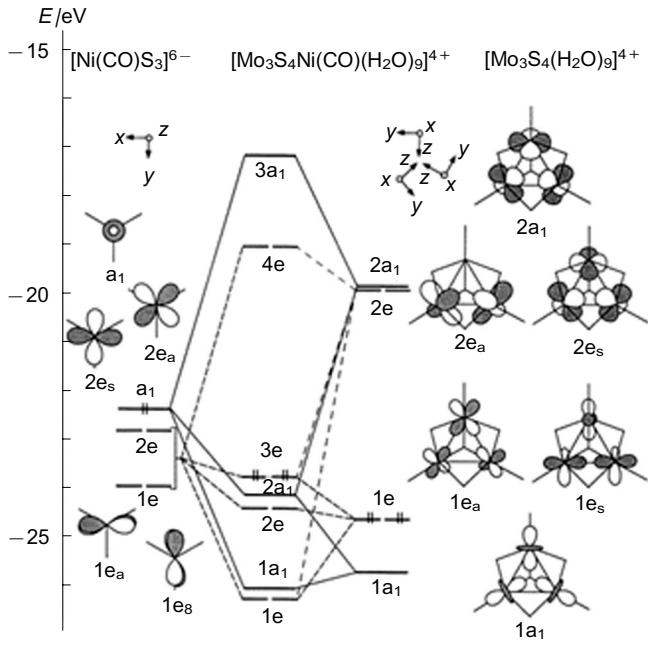


Figure 9. Energy level diagrams for $[Mo_3S_4Ni(CO)(H_2O)_9]^{4+}$ (16 CSE), $[Ni(CO)S_3]^{6-}$ and $[Mo_3S_4(H_2O)_9]^{4+}$ (Ref. 55).

between three molybdenum atoms, which is consistent with the symmetry 'a' obtained in the calculation of the electronic structure. This type of delocalization causes EPR line broadening, which hides the hyperfine coupling of the electron with the ^{95}Mo and ^{97}Mo nuclei.[51] The first order Jahn – Teller effect in these complexes is forbidden because of the non-degenerate nature of the HOMO (a_1). The second-order Jahn – Teller effect is unlikely due to the large difference between the HOMO and LUMO energies as well as the HOMO and HOMO-1 energies.[54]

2.3. Complexes of tetranuclear $\{M_3Q_4M'\}$ clusters

2.3.1. Electronic structure

The MO diagram for metal – metal interactions in $\{M_3Q_4M'\}$ cluster complexes (Fig. 9) shows the presence of a group of three strongly bonding MOs (1e and 1a$_1$), the doubly degenerate bonding orbital (2e) from M′ and a group of weakly antibonding (2a$_1$ and 3e) and strongly antibonding (4e and 3a$_1$) orbitals.[55] In the clusters with the 14 and 16 CSE, twelve electrons occupy the bonding orbitals (1e, 1a$_1$ and 2e) and weakly antibonding orbitals (2a$_1$), while two or four electrons partly or completely fill the 3e orbital (HOMO). In the clusters with >16 CSE, the electrons also occupy the 4e and 3a$_1$ antibonding MOs.

Comparison of the bond lengths for 14- and 16-electron cubane type metal clusters such as M_3M' did not identify a clear relationship between the metal – metal distances and the number of electrons. This may be due to the rather high degree of delocalization of these bonds. Considerable differences between bond lengths are also observed in the $\{Mo_3S_4M'\}$ cluster complexes with equal CSE numbers. This indicates that changes in the donor capacity of external ligands substantially affect the electronic structure of the cluster.

According to the Fenske – Hall calculations, bonding or antibonding nature of the middle group of cluster orbitals (2a$_1$ and 3e) depends on the relative energies of the orbitals of the M′ and M_3 groups.[55] Since the M′ orbitals are higher in energy than the M_3 orbitals, they are mixed to a higher extent with the unoccupied orbitals of the M_3S_4 moiety and, hence, the middle group of cluster orbitals becomes more bonding (or less antibonding). The M′ energy increases in the series

$$Cu < Ni < Co < Fe$$

The antibonding character of the 2a$_1$ and 3e orbitals in this series of elements decreases and, hence, the M – M′ interaction strength increases. The calculated M – M′ bond orders in $[Mo_3S_4Co(Cp')_3(CO)]$ and $[Mo_3S_4Ni(H_2O)_9(CO)]^{4+}$ are 0.561 and 0.432, respectively.

Variational calculations of the discrete X_α levels for $[Mo_3S_4M'(H_2O)_{10}]^{4+}$ (M′ = Fe, Ni) are in line with the overall picture of bonds determined by the Fenske – Hall method, except for the fact that in the case of nickel, the highest occupied MO has 'a' rather than 'e' symmetry.[56] This symmetry coincides with the symmetry of LUMOs for small molecules such as carbon oxide or ethylene; this accounts for the high reactivity of the $\{Mo_3S_4Ni\}$ cluster complexes towards these molecules. The lack of reactivity of $[Mo_3FeS_4(H_2O)_{10}]^{4+}$ can be attributed to the fact that the HOMOs of the $\{Mo_3Fe\}$ core and the LUMOs of small molecules do not coincide in symmetry.

The complexes of $\{Mo_3S_4Cu\}$ have CSE numbers of 16 and 17. In 17-electron complexes $[Mo_3S_4Cu(tdci)_3Br]^{3+}$ and $[Mo_3S_4Cu(H_2O)_{10}]^{4+}$ with isolated cube structure and in the bis-cubane complex $[(H_2O)_9Mo_3S_4CuCuS_4Mo_3(H_2O)_9]^{8+}$, the Mo – Cu distances are longer than those in analogous

16-electron clusters.[57, 58] The extended Hückel calculations for the isolated $\{Mo_3S_4Cu\}$ clusters indicate that the additional electron in the 17-electron cluster occurs in a highly antibonding orbital (4e); this accounts for longer Mo–Mo and Mo–Cu distances.

2.3.2. Redox properties

The electrochemical potentials for some $\{M_3Q_4M'\}$ cluster complexes are summarized in Table 3. Comparison of the electrochemical behaviours of tetranuclear $[Mo_3S_4M'(H_2O)_{10}]^{4+}$ (M′ = Fe, Ni) and their trinuclear precursors based on the $\{Mo_3S_4\}$ cluster revealed that the reduction potential is 0.45 V higher for the former than for the latter.[56] This attests to a change in the metal atom charge state upon the introduction of M′ (which is formally in the zero oxidation state). Indeed, the formal oxidation states of the metal in the cluster are $Mo^{IV}Mo_2^{III}(M')^{II}$, which was confirmed by XPES and Mössbauer spectroscopy data (see below). The three reduction processes observed in CV experiments can be attributed to three successive one-electron steps, namely

$$Mo^{IV}Mo_2^{III}(M')^{II} \rightleftharpoons Mo^{IV}Mo_2^{III}(M')^{I} \rightleftharpoons \rightleftharpoons Mo^{IV}Mo_2^{III}(M')^{0} \rightleftharpoons Mo_3^{III}(M')^{0} \quad (4)$$

It was noted that the potential for the third step is very close to the third reduction potential of the aqua complex of the $\{Mo_3S_4\}^{4+}$ cluster at which $Mo^{IV}Mo_2^{III}$ is reduced to Mo_3^{III}.

A CV study of $[Mo_3(FeCl)S_4Tp_3]$ showed a reversible one-electron reduction and oxidation ($E_{1/2}$ = −1.40 and 0.52 V *versus* Hg/Hg_2Cl_2, respectively) and two irreversible oxidation processes (at 1.54 and 1.66 V *versus* Hg/Hg_2Cl_2).[59] The detected reduction and oxidation steps (except that at 1.66 V) can be assigned to one-electron redox transformations:

reduction

$$Mo^{IV}Mo_2^{III}Fe^{II} \rightleftharpoons Mo^{IV}Mo_2^{III}Fe^{I} \quad (5)$$

oxidation

$$Mo^{IV}Mo_2^{III}Fe^{II} \rightleftharpoons Mo_2^{IV}Mo^{III}Fe^{II} \rightleftharpoons Mo_3^{IV}Fe^{II} \quad (6)$$

Table 3. Electrochemical potentials (E) for tetranuclear molybdenum and tungsten $\{M_3Q_4M'\}$ cluster complexes.

Complex	E/V *versus* Ag/AgCl				Ref.
	I	*II*	*III*	*IV*	
$[(Cp')_3Mo_3S_4Ni(PPh_3)]^+$	−1.20	+0.80	+1.40	–	44
$[(Cp')_3Mo_3S_4Pd(PPh_3)]^+$	−1.07	+0.72	+0.72	–	44
$[(Cp')_3Mo_3S_4Pt(PPh_3)]^+$	−1.16	+0.79	+0.79	–	44
$[(Cp')_3W_3S_4Ni(PPh_3)]^+$	−1.55	+0.57	+1.16	–	44
$[(Cp')_3W_3S_4Pd(PPh_3)]^+$	−1.39	+0.56	+0.56	–	44
$[(Cp')_3W_3S_4Pt(PPh_3)]^+$	−1.40	+0.57	+0.98	–	44
$[Mo_3S_4Fe(H_2O)_{10}]^{4+}$	−0.91	−1.47	−1.81	–	56
$[Mo_3S_4Ni(H_2O)_{10}]^{4+}$	−0.91	−1.48	−1.72	–	56
$[Mo_3S_4FeClTp_3]$	−1.40 [a]	+0.52 [a]	+1.54 [a]	+1.66 [a]	59
$[Mo_3S_4CuCl(dmpe)_3Cl_3]^+$	−0.81	−1.19	–	–	60
$[Mo_3S_4CuBr(dmpe)_3Br_3]^+$	−0.73	−1.08	–	–	60
$[Mo_3Se_4CuBr(dmpe)_3Br_3]^+$	−0.73	−1.31	−1.56	–	61
$[Mo_3S_4CuCN(dmpe)_3Cl_3]^+$	−0.78	–	–	–	62
$[Mo_3S_4Cu\{CN^-\cdots Mo(CO)_5\}(dmpe)_3Cl_3]^+$	−0.76	−0.35	–	–	62
$[Mo_3S_4(CuCl)Cl_3(dbbpy)_3][CuCl_2]$	−0.047	+0.55	–	–	63
$[Mo_3S_4CoCl(dmpe)_3Cl_3]^+$	−0.10	−0.91	–	–	64
$[Mo_3S_4FeCl(dmpe)_3Cl_3]^+$	+0.26	+1.06	–	–	65
$[Mo_3S_4FeCN(dmpe)_3Cl_3]^+$	+0.38	+1.16	–	–	65
$[Mo_3S_4FeN_3(dmpe)_3Cl_3]^+$	+0.25	+1.01	–	–	65
$[Mo_3S_4FeSPh(dmpe)_3Cl_3]^+$	+0.16	+1.03	–	–	65
$[Mo_3S_4CuCl(H_2O)_3(C_2O_4)_3]^{2-}$	−0.35	+0.03	–	–	66
$[Mo_3S_4CuI(H_2O)_3(C_2O_4)_3]^{2-}$	−0.33	+0.21	–	–	66
$[Mo_3S_4CuSCN(H_2O)_3(C_2O_4)_3]^{2-}$	−0.35	–	–	–	66
$[Mo_3Se_4CoCl(dmpe)_3Cl_3]^+$	−0.15	–	–	–	67

[a] Measured *versus* Hg/Hg_2Cl_2.

The introduction of a copper atom (unlike that of iron and nickel) into $[M_3Q_4(dmpe)_3\ X_3]^+$ (X = Cl, Br) leads to an anodic shift of the electrode reduction potentials,[60, 61] *i.e.*, copper-containing complexes with tetranuclear clusters are reduced more easily than their precursors with trinuclear clusters. This fact as well as the distribution of the molybdenum oxidation states, $Mo_2^{IV}Mo^{III}Cu^{I}$, in the 17-electron aqua complex of $\{Mo_3S_4Cu\}^{4+}$, derived from EPR data, make it possible to describe the successive reduction processes as

$$Mo_3^{IV}Cu^{I} \rightleftharpoons Mo_2^{IV}Mo^{III}Cu^{I} \rightleftharpoons Mo^{IV}Mo_2^{III}Cu^{I} \qquad (7)$$

with the copper atoms being unaffected. A similar interpretation can be extended to $\{W_3S_4Cu\}$ complexes. In the general case, selenide derivatives $[Mo_3Q_4CuL(dmpe)_3X_3]^+$ are reduced more easily than the sulfide ones.[46] Different natures of ligands in the $[Mo_3S_4CuL(dmpe)_3X_3]^+$ complexes [L = Cl^-, CN^-, $CN^- \cdots Mo(CO)_5$] do not cause any considerable changes in the redox behaviour. Conversely, the substitution of CN for X (Cl, Br) at molybdenum in both the heterometallic complexes $[Mo_3S_4CuL(dmpe)_3X_3]^+$ and trinuclear precursors $[Mo_3S_4(dmpe)_3X_3]^+$ leads to a considerable anodic shift of potentials. For example, the anodic shift for cyanide complexes $[(CN)_3Mo_3S_4CuL(dmpe)_3]^+$ is 200 – 500 mV with respect to $[Cl_3Mo_3S_4CuL(dmpe)_3]^+$ (Ref. 62).

A CV study of $[Mo_3S_4(CuCl)Cl_3(dbbpy)_3][CuCl_2]$ showed that, apart from the reversible reduction at $E_{1/2} = -0.047$ V (potential difference of 0.077 V *versus* Ag/AgCl), one-electron Cu^+ oxidation to Cu^{2+} takes place in the $[CuCl_2]^-$ anion at $E_{1/2} = 0.55$ V (potential difference of 0.55 V *versus* Ag/AgCl) (Ref. 63).

The introduction of cobalt into $[Mo_3S_4(dmpe)_3Cl_3]^+$ results initially in the neutral complex $[Mo_3S_4CoCl(dmpe)_3Cl_3]$ (15 CSE), which is then readily oxidized to $[Mo_3S_4CoCl(dmpe)_3Cl_3]^+$ (14 CSE).[64] Formally, this can be attributed to Co^0 oxidation to Co^{I} within the cluster. Like the copper coordination to the trinuclear cluster, the introduction of a cobalt atom induces a 0.59 V anodic shift of the first reduction potential. The first reduction process for $[Mo_3S_4CoCl(dmpe)_3Cl_3]^+$ is centred at $E_{1/2} = -0.10$ V and is reversible. The second process (−0.91 V) is completely irreversible and is accompanied by Cl^- elimination from the reduction product.

$$[Mo_3S_4CoCl(dmpe)_3Cl_3]^+ \rightleftharpoons \qquad (8)$$

$$\rightleftharpoons [Mo_3S_4CoCl(dmpe)_3Cl_3] \longrightarrow [Mo_3S_4Co(dmpe)_3Cl_3]^+Cl^-$$

The differences in the electrochemical behaviour are associated with changes in the charge state of molybdenum atoms upon insertion of the metal heteroatom.

Studies of the redox properties of isostructural complexes of a heterometallic tetranuclear cluster, $[(Cp')_3M_3S_4M'L]^{0/+/2+/3+}$ (M = Mo, W; M′ = Ni, Pd, Pt; L = PPh_3, $AsPh_3$) demonstrated[44] that $[(Cp')_3W_3S_4NiPPh_3]^+$ and $[(Cp')_3W_3S_4PtPPh_3]^+$ have similar properties and undergo one reduction (1+/0) and two oxidation reactions (1+/2+ and 2+/3+). A cyclic voltammetry study of $[(Cp')_3W_3S_4PdPPh_3]^+$ revealed one two-electron oxidation process. The addition of the M′(PPh_3) moiety (where M′ = Pd) to $[(Cp')_3W_3S_4]^+$, which tends to undergo reversible one-electron reduction and two-electron oxidation, exerts a simple electron-donating effect on $[(Cp')_3W_3S_4]^+$. In the case of nickel and platinum complexes, the electronic effects induce splitting of the two-electron anodic wave, which attests to two separate one-electron processes. Presumably, in these cases, the addition of the M′(PPh_3) group acts as a molecular electronic switch. Similar molybdenum complexes are more difficult to oxidize (but easier to reduce), probably because of the fact that $[(Cp')_3Mo_3S_4]^+$ damps the electronic effects of M′(PPh_3) more efficiently than $[(Cp')_3W_3S_4]^+$ does.[44]

Study of the electrochemical properties of iron-containing complexes $[Mo_3S_4FeX(dmpe)_3Cl_3]$ with various substituents at the iron atom (X = Cl, CN, N_3, SPh) identified[65] a quasi-reversible oxidation process in the 0.16 – 0.38 V range corresponding to the $\{Mo_3S_4Fe\}^{4+/5+}$ pair. The ligands at the iron atom in these complexes considerably affect the oxidation process. The oxidation potential decreases in the following series of substituents:

$$SPh^- > Cl^- = N_3^- > CN^-$$

The difference between the $E_{1/2}$ values in this series reaches 0.22 V (see Table 3). Thus, the heterometallic derivatives formed upon the insertion of an iron atom into $[Mo_3S_4(dmpe)_3Cl_3]$ are easier to oxidize, but more difficult to reduce than the complex with the trinuclear cluster. It is noteworthy that in the case of $[Mo_3S_4FeX(dmpe)_3Cl_3]$, no reduction processes were found in the potential range suitable for the use of dichloromethane as the solvent.

2.3.3. Magnetic properties

From magnetic susceptibility measurements, the effective magnetic moments of $[Mo_3S_4M'(H_2O)_{10}][pts]_4 \cdot 7H_2O$ (M′ = Fe, Ni) were determined to be 2.78 μ_B at 2.16 K and 3.26 μ_B at 269.95 K for M′ = Fe and 0.11 μ_B at 2.00K and 1.26 μ_B at 260.70 K for M′ = Ni.[56, 68, 69] These results are consistent with the presence of two unpaired electrons (in the 3e orbital) in the 14-electron $\{Mo_3Fe\}$ core and their absence in the 16-electron $\{Mo_3Ni\}$ core. The obtained values of molar magnetic susceptibility (Fig. 10) were analyzed using the vector model formalism of Kambe and the

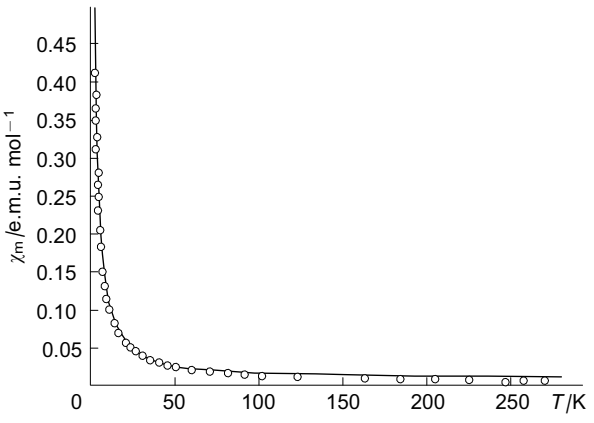


Figure 10. Temperature dependence of the molar magnetic susceptibility of $[Mo_3FeS_4(H_2O)_{10}]^+$ (Refs 67 and 68).
The dots are experimental values and the continuous line is approximation of experimental data with the parameters $J_1/k_B = 25$ K and $J_2/k_B = 75$ K.

formal oxidation states were assigned as $Mo^{IV}Mo_2^{III}(M')^{II}$. This distribution of oxidation states in the ground state is consistent with the iron oxidation state in $\{Mo_3Fe\}$ equal to 2.39+, which was established by ^{57}Fe Mössbauer spectroscopy.

X-Ray photoelectron spectra of the tetranuclear clusters and their trinuclear precursors gave the following $Mo3d_{3/2}$ and $Mo3d_{5/2}$ binding energies: $E(Mo_3) = 233.7$, 230.7 eV; $E(Mo_3Fe) = 233.1$, 230.0 eV and $E(Mo_3Ni) = 233.3$, 230.3 eV. These values are in line with the 4+ formal oxidation state of molybdenum. Also, the decrease in the binding energies upon insertion of the heteroatom (iron or nickel) attests to an increase in the electron density on molybdenum atoms upon electron density transfer from the heteroatom to the Mo_3 core, which is in good agreement with the distribution of oxidation states presented above: $Mo^{IV}Mo_2^{III}(M')^{II}$.

According to EPR studies of the 17-electron heterometallic $[Mo_3S_4Cu(H_2O)_{10}]^{4+}$ cluster cation, which is formed upon dissociation of $[\{Mo_3S_4Cu(H_2O)_9\}_2]^{8+}$, the monomeric cluster is paramagnetic ($S = 1/2$) and the hyperfine splitting of spectral lines is consistent with the distribution of the metal oxidation states in the ground state: $Mo_2^{IV}Mo^{III}Cu^{I}$. The unpaired electron is not located on a particular molybdenum atom, but migrates among all three sites at a rate of about 107 s^{-1} (Ref. 58). Extended Hückel calculations for the $[Mo_3S_4Cu(H_2O)_{10}]^{4+}$ aqua ion also attest to delocalization of the unpaired electron among three molybdenum atoms.

It is of interest that the insertion of Cu^{I} into $[Mo_3S_4Cl_3(dbbpy)_3]^{+}$ to give $[Mo_3S_4(CuCl)Cl_3(dbbpy)_3]^{+}$ with 16 CSE does not induce redistribution of the $Mo_3^{IV}Cu^{I}$ oxidation states determined by XPES. In this case, the $\{Mo_3S_4\}$ cluster can be considered as a Cu^{I}-coordinated metallothiacrown.[70] In view of the ease of oxidation of $[Mo_3S_4(CoCl)(dmpe)_3Cl_3]$ (15 CSE, $S = 1/2$) to $[Mo_3S_4(CoCl)(dmpe)_3Cl_3]^{+}$ (14 CSE, $S = 1$), the complex $[Mo_3S_4(CoCl)(dmpe)_3Cl_3]$ was oxidized by treatment with 7,7,8,8-tetracyanoquinodimethane, which is often used to prepare conducting charge transfer salts. The reaction gave the hybrid salt $[Mo_3S_4(CoCl)(dmpe)_3Cl_3](TCNQ)$, in which both the cation and the anion are paramagnetic.[64] The obtained compound is the first example of a charged transfer complex based on the $\{M_3Q_4M'\}$ cluster that is dielectric.

The plot for the dependence of $\chi_m T$ on T shows a continuous decrease in $\chi_m T$ on cooling from 300 to ~50 K down to the value of 1.1 cm^3 K mol^{-1}, which is indicative of antiferromagnetic interactions in the chains composed of the $TCNQ^{-}$ anions with $S = 1/2$. Only the contribution of the paramagnetic $[Mo_3S_4(CoCl)(dmpe)_3Cl_3]^{+}$ cation with $S = 1$ is present below ~50 K. On cooling below ~10 K, the $\chi_m T$ value sharply decreases, which attests to antiferromagnetic interactions and/or zero field splitting in the cation with $S = 1$. The observed dependence of $\chi_m T$ on T is consistent with the zero field splitting model comprising a regular antiferromagnetic chain with $S = 1/2$ and the monomer ($S = 1$). Conversely, for the selenide complex $[Mo_3Se_4(CoCl)(dmpe)_3Cl_3](TCNQ)$, the $\chi_m T$ value (1.1 cm^3 K mol^{-1}) virtually does not change in the 20–300 K range.[67] This behaviour agrees with the presence of the $[Mo_3Se_4(CoCl)(dmpe)_3Cl_3]^{+}$ cation with $S = 1$, whereas the $TCNQ^{-}$ anion does not contribute to the total magnetic susceptibility. Like for the sulfide complex, $\chi_m T$ sharply decreases below ~15 K. Thus, the magnetic behaviour of the selenide derivative shows only a contribution of the paramagnetic $[Mo_3Se_4(CoCl)(dmpe)_3Cl_3]^{+}$ cation, as opposed to the sulfide analogue in which both the cation and the anion make contributions to the overall magnetic susceptibility, although cooperative magnetic interactions are also not observed.

The oxidation of $[Mo_3S_4(CoCl)(dmpe)_3Cl_3]$ with iodine affords the paramagnetic salt $[Mo_3S_4(CoI)(dmpe)_3Cl_3]I$ (14 CSE, $S = 1$) in a nearly quantitative yield. The replacement of chlorine at the cobalt atom by iodine does not affect considerably the structural or electrochemical properties. The reaction of $[Mo_3S_4(CoI)(dmpe)_3Cl_3]I$ with the paramagnetic nickel dithiolate complex $[Ni(mnt)_2]$ ($S = 1$) affords the hybrid compound $[Mo_3S_4(CoI)(dmpe)_3Cl_3]_2[Ni(mnt)_2]$. In the 10–300 K range, the $\chi_m T$ value of this complex, equal to 0.99 cm^3 K mol^{-1}, virtually does not change, which is consistent with $S = 1$ of the $[Mo_3S_4(CoI)(dmpe)_3Cl_3]^{+}$ cation. The $[Ni(mnt)_2]$ moiety does not contribute to paramagnetism because of formation of the diamagnetic $[Ni(mnt)_2]^{2-}$ anion.[71]

The magnetic properties of 15-electron complexes $[Mo_3S_4FeCl(dmpe)_3Cl_3]$ (Fig. 11), $[Mo_3S_4FeCN(dmpe)_3Cl_3]$, $[Mo_3S_4FeN_3(dmpe)_3Cl_3]$ and $[Mo_3S_4FeSPh(dmpe)_3Cl_3]$ have also been studied.[65] The $[Mo_3S_4FeCl(dmpe)_3Cl_3]$ complex with 15 electrons is oxidized to $[Mo_3S_4FeCl(dmpe)_3Cl_3](PF_6)$ with 14 CSE (for the $\{Mo_3S_4Fe\}^{4+/5+}$ redox pair, see above). Since the 14-electron complex $[Mo_3S_4FeCl(dmpe)_3Cl_3](PF_6)$ was not isolated in a pure state, the magnetic measurements were carried out for its mixture with the 15-electron complex (see Fig. 11). At room temperature, the product $\chi_m T$ for $[Mo_3S_4FeCl(dmpe)_3Cl_3]$ is ~1.15 cm^3 K mol^{-1}, which is consistent with the triplet ground state ($S = 1$). This value linearly decreases with decreasing temperature to reach ~1.02 cm^3 K mol^{-1} at 7 K, and below this temperature $\chi_m T$ decreases more sharply (0.94 cm^3 K mol^{-1} at 2 K). Complexes with other ligands at the iron atom behave in a similar way. The magnetic behaviour of a mixture of

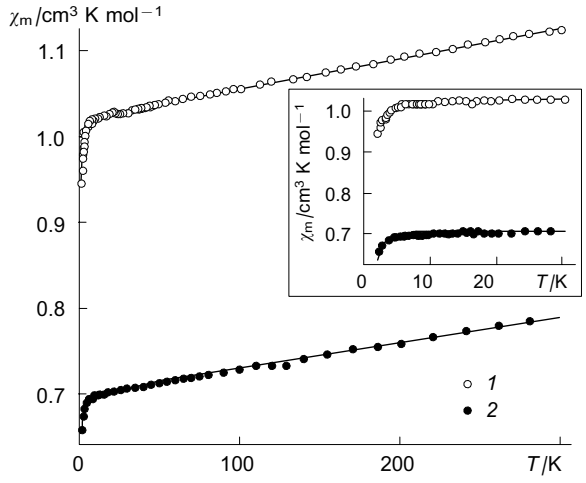


Figure 11. Temperature dependence of $\chi_m T$ for $[Mo_3S_4FeCl(dmpe)_3Cl_3]$ (*1*) and its mixture with $[Mo_3S_4FeCl(dmpe)_3Cl_3](PF_6)$ (*2*).[65]

$[Mo_3S_4FeCl(dmpe)_3Cl_3]$ and $[Mo_3S_4FeCl(dmpe)_3Cl_3](PF_6)$ shows a similar temperature dependence of $\chi_m T$, with the $\chi_m T$ values being lower, as is to be expected for a mixture of compounds with $S = 1$ and $S = 1/2$, respectively.

The reduction of $[Mo_3S_4(dppe)_3Br_3]Br$ and $[Mo_3S_4(dmpe)_3Br_3]Br$ with gallium metal yielded rare gallium-containing tetranuclear $[Mo_3S_4Ga(dppe)_3Br_4]$ and $[Mo_3S_4Ga(dmpe)_3Br_4]$ clusters with nine CSE.[72] Their formation can be described as follows: first, $[Mo_3S_4(dppe/dmpe)_3Br_3]^+$ (six CSE) is reduced to $[Mo_3S_4(dppe/dmpe)_3Br_3]$ (seven CSE) and gallium is oxidized to GaBr, then $[Mo_3S_4(dppe/dmpe)_3Br_3]$ reacts with GaBr to give cubane type derivatives. The obtained compounds are paramagnetic. At 300 K, the $\chi_m T$ value for both complexes is 0.34 cm^3 K mol^{-1} (the expected value for $S = 1/2$ is 0.375 cm^3 K mol^{-1}) and remains almost unchanged as the temperature decreases. The EPR spectra of solid samples exhibit only one signal, the intensity of which increases with decreasing temperature. In both cases, no hyperfine splitting of spectral lines is observed at low temperature, which is indicative of electron density delocalization among the three metal sites. As noted above, in $[Mo_3S_4(dppe)_3\ Br_3]$, the electron density of the unpaired electron is located on one metal atom.[26]

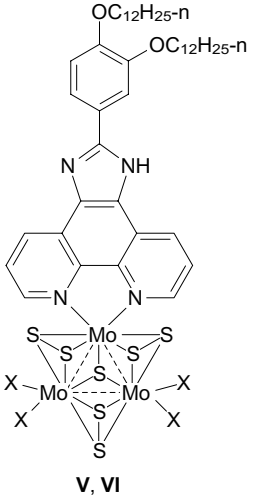
3. Luminescent properties

The photoluminescent properties of heteroleptic $[Mo_3S_7X_4(IPDOP)]$ complexes [X = Cl (**V**), Br (**VI**)] containing imidazophenanthroline moieties were studied by Recatala *et al.*[73]

The emission spectra of both complexes in CH_2Cl_2 (excited at 330 nm) show peaks at 436 nm (Fig. 12). The emission is caused by intraligand transitions. The quantum yield for free IPDOP (0.21) is markedly higher than that for compounds **VI** (0.06) and **V** (0.11). A decrease in the ligand luminescence intensity upon coordination of the ligand to the metal cluster was also detected for binuclear molybdenum complexes with dipyridinodithiolene ligands.[74]

An interesting feature of the fluorescent behaviour of complexes **V** and **VI** is that the emission spectra are sensitive to the presence of some anions. The addition of anions such as F^-, HO^- and AcO^- to a solution of complex **VI** in DMF induced a pronounced ($\sim$90 nm) shift of the emission band towards longer wavelengths (the maximum at

Structures V, VI



X = Cl (**V**), Br (**VI**)

V, **VI**

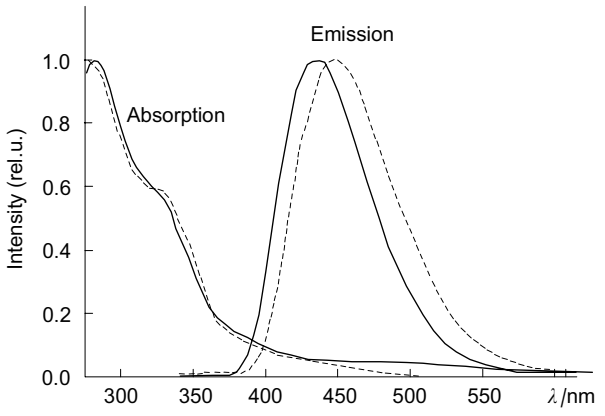


Figure 12. Absorption and emission spectra of a solution of $[Mo_3S_7Br_4(IPDOP)]$ (5 mol $litre^{-1}$) in CH_2Cl_2 (continuous line) and DMF (dashed line). The excitation wavelength is 330 nm.[74]

$\sim$540 nm). Meanwhile, other anions (Cl^-, Br^- and SCN^-) do not affect the fluorescence spectrum of $[Mo_3S_7Br_4(IPDOP)]$. This behaviour is attributable to electron density redistribution induced by interaction between the hydrogen atom of the imidazole N–H group of the ligand and F^-, HO^- and AcO^- anions (capable of hydrogen bonding, unlike Cl^-, Br^- or SCN^-). These are the first examples of luminophores comprising imidazophenanthroline ligands coordinated to molybdenum clusters. The selectivity of these complexes to F^-, Cl^- and Br^- anions could be used in the future to design halide ion sensors.[73]

4. Optical limiting properties

Optical limiting is a physical phenomenon associated with the decrease in the transmission coefficient of a material with increasing intensity of the incident light. In the field of nonlinear optics, a lot of effort has been directed in recent years towards the development of devices based on inorganic semiconductors, organic polymers and fullerene. Inorganic cluster compounds have been less studied. This is due to the fact that cluster complexes are usually deeply coloured, which makes them unsuitable for most NLO applications; they are also unstable on exposure to high-intensity light.[75]

Despite these drawbacks, metal clusters have a number of advantages over other inorganic and organic compounds that are traditionally used in nonlinear optics. First, the heavy atoms that compose the clusters supply higher energy levels; therefore, a larger number of allowed transitions appear compared with organic molecules. Second, the NLO properties can be controlled by changing the cluster core composition (for example, replacement of molybdenum atoms by tungsten, replacement of sulfur by selenium, *etc.*, in trinuclear clusters), its structural type (the number of nuclei, charge, *etc.*) and coordination environment (variation of terminal ligands). For these reasons, metal clusters have attracted considerable attention in recent years.[75–85]

The photochemical stability of metal clusters can be increased by reinforcing the metal–metal bonds with bridging groups. In this respect, the trinuclear $\{M_3(\mu_3\text{-}Q)(\mu_2\text{-}Q_x)_3\}^{4+}$ clusters (M = Mo, W; Q = S, Se, Te; $x = 1, 2$), in which the metal atoms are linked by

bridging chalcogenides, demonstrate high stability against light exposure. The optical limiting properties for the tri- and tetranuclear $\{M_3(\mu_3\text{-}Q)(\mu_2\text{-}Q_x)_3\}^{4+}$ and $\{M_3Cu(\mu_3\text{-}Q)(\mu_2\text{-}Q)_3\}^{5+}$ clusters (M = Mo, W; Q = S, Se) surrounded by diphosphine ligands (dmpe, dppe) were studied by *Z*-scan technique.[15, 40, 60] The high ratio of the excited state effective cross-section (σ_{ef}) to the ground state cross-section (σ_0) serves as a criterion for evaluating the applicability of a compound as an optical limiter. The σ_{ef}/σ_0 values for metal cluster complexes are within one order of magnitude (from 1.1 to 12), which attests to a standard power limiting mechanism, probably, purely thermal one. The threshold density for these optical limiters decreases on going from tetra- to trinuclear complexes and from tungsten to molybdenum derivatives.

Heteroleptic complexes with the $\{Mo_3S_7\}$ cluster containing either π-acceptor diimines (2,2′-bipyridine and 1,10-phenanthroline derivatives) or both π-donor dithiolates (dmit) and π-acceptor diimines (diimino dithiolate complexes) were also studied for the optical limiting properties, because π-conjugated systems are known to increase the NLO properties of materials.[86, 87] For these complexes, too, $\sigma_{ef} > \sigma_0$, which is a criterion for the presence of reverse saturable absorption; the σ_{ef} values increase with increasing π-delocalization of electrons upon the introduction of the π-donor dmit ligands (on going from diimine to diimine dithiolate complexes). In the diimine dithiolate series of complexes, the σ_{ef} value decreases upon the introduction of electron-withdrawing carboxyl or ester groups, which lower the energy of the bipyridine ligand π-system. The highest σ_{ef} value is achieved for the complex $[Mo_3S_7(dnbpy)(dmit)_2]$ containing π-donor dithiolate ligands (dmit) and electron-donating alkyl (n-C_9H_{19}) substituents at the bipyridine moiety.[88]

Similar trends were identified for binuclear niobium complexes $(Et_4N)_2[Nb_2S_4(NCS)_6L]$; the σ_{ef} value decreases in the following series of ligands (L):[89]

dnbpy > bpy > dcmbpy

The introduction of electron-donating nonyl substituents into bipyridine leads to increasing σ_{ef}, whereas electron-withdrawing CO_2Me groups decrease this value. The σ_{ef}/σ_0 ratio varies from 3.4 to 38.3 for both complexes.

5. Catalytic properties

The past decades have seen increasing interest in the catalytic properties of trinuclear molybdenum and tungsten complexes with tetranuclear heterometallic clusters in various chemical transformations, which is caused by the trend towards optimization of composition, lowering the cost and increase in the specificity and selectivity of catalytic reactions. This can be attained by replacing relatively simple metal compounds by more complex metal clusters.

5.1. Catalytic properties of trinuclear cluster complexes

5.1.1. Hydrodefluorination of perfluoroaromatic compounds

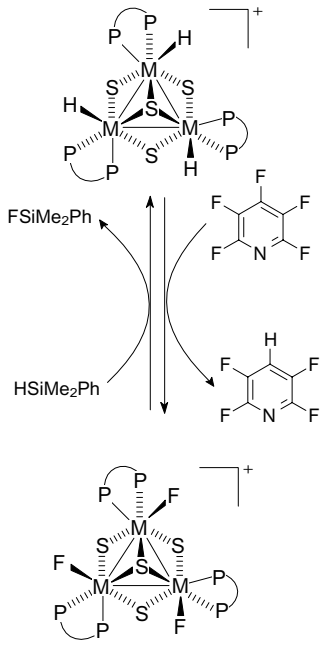
The increasing demand for fluorine-containing pharmaceuticals and agrochemicals has stimulated the development of various synthetic strategies towards easily accessible fluorinated derivatives.[90, 91] The selective elimination of fluorine atoms provides for the diversity of building blocks for the fine organic synthesis of organofluorine products.[92] In this context, the replacement of the C–F bond by the C–H bond *via* hydrodefluorination in the presence of transition metal complexes and a hydrogen source is the most facile and promising approach.[93] A widely used type of reaction described for intermolecular HDF includes hydrogen–fluorine exchange between a transition metal hydride complex and a fluorinated organic substrate to give a hydrogenated organic product and a fluorinated metal complex.

High fluorine affinity of early transition metals makes the HDF of R–F substrates thermodynamically favourable. A variety of compounds, including lanthanide and Group IVa metal hydride complexes are employed as catalysts for hydrogenation of fluorinated aromatic, vinyl and aliphatic substrates.[94, 95] These reactions are deemed to involve the nucleophilic attack by the hydride ligand on the electrophilic centre of the organic substrate, the β-insertion of the alkene and the subsequent β-fluoride elimination (in the case of hydrogenation of vinyl substrates) or σ-bond metathesis to give a four-centre M···H···C···F transition state.[96]

Hydride systems based on trinuclear cluster complexes also proved to be active in these reactions. The hydride complexes $[W_3S_4H_3L_3]A$ (L = dmpe, dppe; A = PF_6, BPh_4) were first obtained in 1989 by the reaction of the chloride precursors $[W_3S_4Cl_3L_3]A$ with lithium borohydride. Later, this synthetic procedure was extended to molybdenum analogues and bromine-containing derivatives.[97] In 2011, fluorine-containing molybdenum and tungsten complexes $[M_3S_4F_3(dmpe)_3]^+$ were prepared for the first time by the reaction of hydride complexes with an excess of HPF_6. The hydride and fluoride complexes are highly efficient and regioselective towards the microwave-assisted HDF of pentafluoropyridine at a temperature of 180 °C in the presence of silanes as a source of hydrogen (Scheme 2).[98] The only product of these reactions is 2,3,5,6-tetrafluoropyridine in which the *para*-fluorine is replaced by hydrogen.

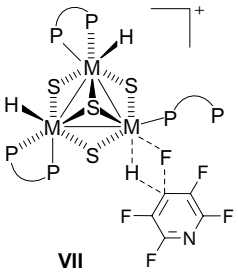
Catalysts based on hydride complexes were more efficient than those based on fluoride complexes, which is attributable to the key role of the hydride intermediate in the reaction. The tungsten hydride complexes are more

Scheme 2



active than the molybdenum complexes; conversely, in the case of fluoride complexes, molybdenum derivatives are more active than tungsten counterparts. For $[W_3S_4H_3(dmpe)_3]^+$, the yield of the product is 90% and TON = 90, whereas in the case of $[Mo_3S_4H_3(dmpe)_3]^+$, a 60% product yield and TON = 60 were attained. The complex $[Mo_3S_4F_3(dmpe)_3]^+$ provides 51% yield of the product (TON = 51) and in the case of $[W_3S_4F_3(dmpe)_3]^+$, the yield is 31% (TON = 31). The reaction is accompanied by partial decoordination of the diphosphine ligand, and the structure of intermediate **VII** accounts for the selective substitution at the *para*-position.[98]

Structure VII



VII

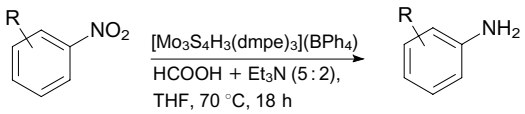
The replacement of the dmpe ligand by the less basic dppe ligand in hydride or fluoride complexes increases the catalytic activity to an extent that the microwave activation of the reaction mixture is no longer necessary and the temperature can be reduced to 115 °C.[99] The tungsten hydride complex $[W_3S_4H_3(dppe)_3]^+$ still remains the most active, with the yield of the product being 55% (87% with additional microwave activation) and the TON increases to 124. The molybdenum complex is inferior in efficiency even to the dmpe analogue; the yield of the product in this case is only 21% and the highest turnover number is 31. Unlike fluoride complexes with dmpe, the tungsten derivatives of $[M_3S_4F_3(dppe)_3]^+$ are more active than molybdenum counterparts and demonstrate 65% yield of the product and TON = 94; in the case of molybdenum, the yield is 19% and the turnover number is 27.

5.1.2. Reduction of nitro and azo compounds

Aromatic amines are important intermediates of the production of pigments and dyes, agrochemicals, pharmaceuticals and polymers. Most often, they are produced by reduction of nitroarenes or (more rarely) azo compounds.[100 – 103] Among various industrial reduction processes that have proved to be efficient, preference is given to catalytic hydrogenation. However, despite the considerable progress made in the last decades, this method still has limitations regarding substrates containing various functional groups capable of being reduced.[103 – 108] For this reason, the use of selective homogeneous catalysts that allow the preparation of structurally complex functionalized amines is still the most reasonable approach. An alternative to the catalytic hydrogenation, which is most often carried out under drastic conditions (high temperature and pressure), is hydrogen transfer hydrogenation with the use of formic acid or hydrosilylation in the presence of silanes under homogeneous conditions. These methods show higher selectivity under relatively mild conditions.

Complexes of the $\{Mo_3S_4\}$ cluster functionalized with diphosphine ligands (dmpe) proved to be efficient and chemoselective homogeneous catalysts for both hydrogen transfer hydrogenation of nitroarenes and hydrosilylation of nitro and azo compounds.[109, 110] In the former case, the reactions are carried out in the presence of an HCOOH and Et_3N mixture as the reducing agent (Scheme 3). In these transformations, the molar content of the catalyst is 5% relative to the substrate.

Scheme 3

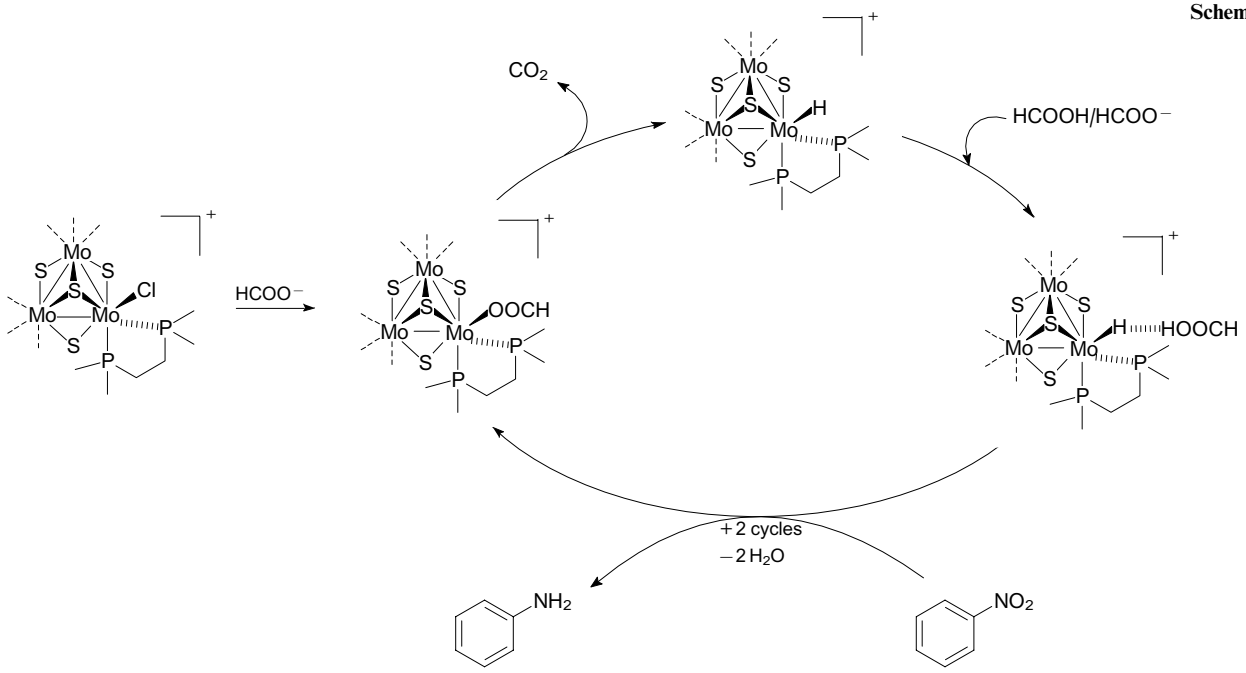


Both the hydride complex $[Mo_3S_4H_3(dmpe)_3]^+$ and the chloride analogue $[Mo_3S_4Cl_3(dmpe)_3]^+$ show high catalytic activity. The chloride complex is the precatalyst (Scheme 4), which reacts with formic acid with subsequent elimination of CO_2 to be converted to catalytically active hydride complex $[Mo_3S_4H_3(dmpe)_3]^+$, which does not undergo fragmentation during the reaction. Initially, HCOOH reacts with the cluster hydride ligand to give a weak hydrogen bond between the hydride and the acid proton. This is followed by elimination of hydrogen to give the formate complex, and hydrogen thus formed reduces nitrobenzene. The hydrogenation of a nitro group is selective with respect to a large number of potentially reducible functional groups R such as alkyl, vinyl, halide, amide, carboxyl, ether, ester, amino, keto, alcohol and thiol groups, also in the presence of several different groups in the ring. The selectivity is higher for the hydride complex than for the chloride one. In the case of hydride complex, the conversion exceeds 99% for all substrates (an exception is 2,5-dimethylnitrobenzene, for which the conversion is 98%). The minimum yield of the product is 89% in the case of the sulfonamide derivative; in most cases, the yield is nearly quantitative. It is noteworthy that these reactions virtually do not proceed if hydrogen is used instead of a mixture of HCOOH with Et_3N. This rules out the possibility of direct hydrogenation with hydrogen formed upon decomposition of formic acid and supports the proposed hydrogen transfer mechanism (see Scheme 4).[109]

The preservation of the cluster structure in the catalytic reactions was proved by mass spectrometry (ESI MS).

The reduction reactions of nitro and azo compounds with silanes were studied for the complex $[Mo_3S_4Cl_3(dmen)_3](BF_4)$, in which the relatively expensive and easily oxidizable phosphine ligand [111] has been replaced by more readily available and stable diamine. The diamine complex was obtained by treatment of $(Bu_4N)_2[Mo_3S_7Cl_6]$ with excess triphenylphosphine followed by the addition of dmen and the freshly prepared $HBF_4 \cdot Et_2O$ adduct. This is the first example of a diamine complex of a trinuclear cluster.[110] The catalytic reactions were carried out under conditions similar to those described above, but with silanes, in particular, Ph_2SiH_2, being used instead of $HCOOH + Et_3N$. In this case, the diamine complex (like the diphosphine one) had high activity and selectivity in the presence of various groups (alkyl, allyl, halide, amide, cyanide, carboxylate, *etc.*). An important distinction of the diamine system is that the conversion and product yield >99% can be attained under milder conditions (at room temperature), whereas the diphosphine complex operates only at 80 °C. The catalyst based on

Scheme 4



$[Mo_3S_4Cl_3(dmen)_3](BF_4)$ is also effective in the case of azo compounds (Scheme 5), although this requires heating.[110]

It is assumed that the reduction of nitroarenes to anilines can follow two different pathways (Scheme 6):

— the first pathway is the direct reduction involving nitrosoarene and hydroxylamine derivatives;

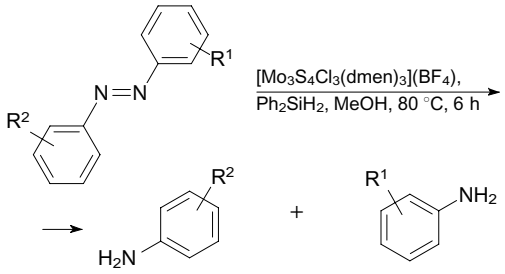
— the second pathway is the condensation of these intermediates to give azoxyarenes followed by reduction *in situ via* the formation of azo and hydrazino derivatives.[112, 113]

If nitrobenzene in these catalytic reactions is replaced by the most probable intermediates formed upon its reduction (*N*-phenylhydroxylamine, nitrosobenzene, azoxybenzene or azobenzene) in the presence of $[Mo_3S_4Cl_3(dmen)_3](BF_4)$, the following situation is observed: azoxybenzene is only partly converted to aniline (39% conversion, 32% yield), whereas *N*-phenylhydroxylamine and nitrosobenzene give aniline in 92% and 86% yields, respectively. This indicates that the reactions predominantly proceed by the direct reduction mechanism (framed in Scheme 6).[110]

Using the ESI MS method, it was shown that during catalytic reactions, the cluster catalyst does not undergo destruction, which suggests the formation of four-centre hydride intermediates Mo···Cl···H···Si, by analogy with diphosphine complexes.[97, 109, 114] However, a more detailed mechanism of hydrogenation is still obscure. Additional experiments with hydrogen being used instead of silane showed the lack of reactivity of nitroarenes, which disproves the possibility of direct hydrogenation with the hydrogen formed upon the reaction of silane with methanol.[110]

It is evident that the catalytic systems considered above for the laboratory synthesis of anilines with various functional groups involving formic acid, triethylamine and silanes compare poorly from the green chemistry standpoint, because they are characterized by low atom efficiency (the ratio of the molar mass of the target product to the sum of molecular masses of all other products in the stoichiometric equation of the chemical reaction). From this stand-

Scheme 5



R^1 = H, Me, NMe_2; R^2 = H, Me, NH_2, NMe_2

Scheme 6

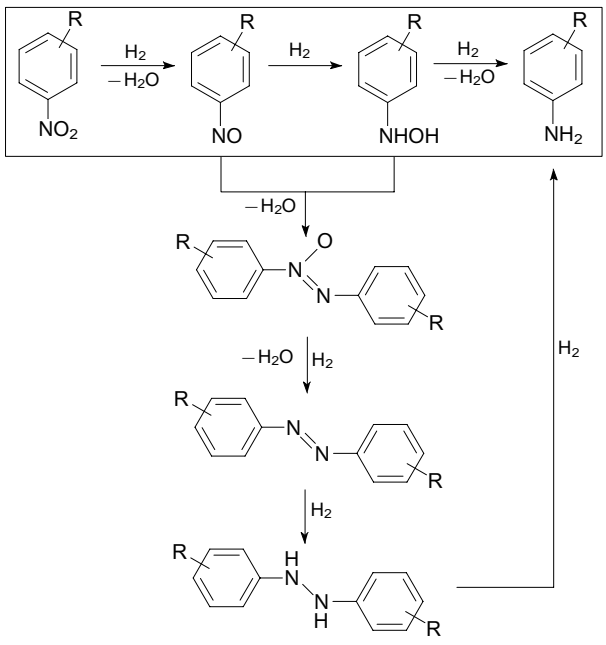


Table 4. Conversion of the substrate and yields of the product in the reduction of nitroarenes catalyzed by the diimine complex $[Mo_3S_4Cl_3(dnbpy)_3](PF_6)$.[45]

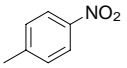
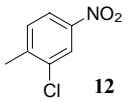
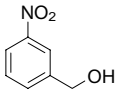
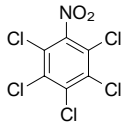
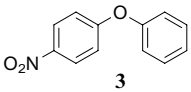
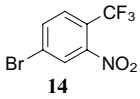
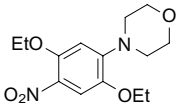
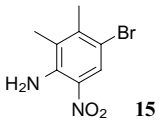
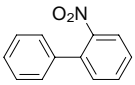
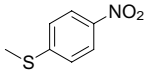
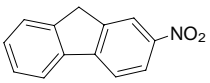
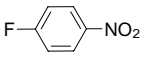
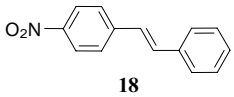
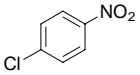
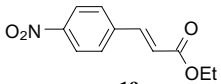
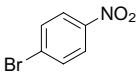
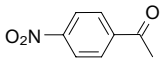
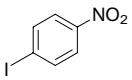
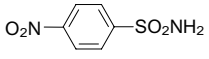
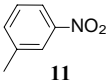
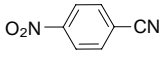
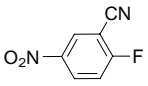
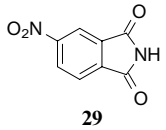
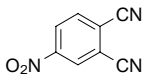
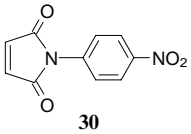
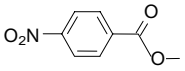
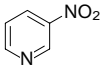
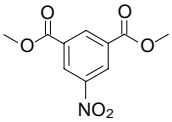
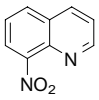
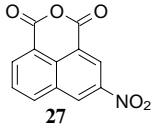
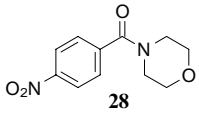
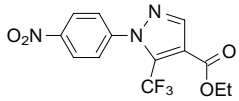
Substrate	Conversion (%)	Yield (%) (see [a])	Substrate	Conversion (%)	Yield (%) (see [a])
 **1**	> 99	> 99	 **12**	> 99	93
 **2**	> 99	> 99	 **13**	> 99	> 99
 **3**	> 99	90 (80)	 **14**	> 99	> 99
 **4**	> 99	> 99	 **15**	> 99	> 99
 **5**	> 99	97 (90) (see [b])	 **16**	> 99	84
 **6**	> 99	98 (91) (see [b])	 **17**	98	85
 **7**	> 99	95	 **18**	> 99	95
 **8**	> 99	92 (80)	 **19**	> 99	87
 **9**	> 99	99 (80)	 **20**	> 99	94
 **10**	> 99	96 (80) (see [c])	 **21**	> 99	80
 **11**	> 99	98	 **22**	> 99	> 99 (96)

Table 4 (continued).

Substrate	Conversion (%)	Yield (%) (see [a])	Substrate	Conversion (%)	Yield (%) (see [a])
 **23**	> 99	94 (87)	 **29**	> 99	95
 **24**	> 99	88	 **30**	> 99	70
 **25**	> 99	80	 **31**	> 99	91
 **26**	> 99	94	 **32**	> 99	> 99
 **27**	> 99	(99)	 **33**	> 99	> 97 (93)
 **28**	> 99	88	 **34**	> 99	> 99

Note. Reaction conditions: substrate amount, 0.1 mmol; H_2 pressure, 20 bar; catalyst content, 5 mol.%; MeOH amount, 2 ml; reaction time, 18 h, $T = 70$ °C.

[a] The yields were determined by gas chromatography (with n-hexadecane as the internal reference), the values in parentheses are the isolated yields of the product. [b] $T = 100$ °C. [c] H_2 pressure 35 bar.

point, catalytic systems using molecular hydrogen, which is a cheap and environmentally clean reducing agent, are more appropriate. An example is provided by catalytic systems based on binuclear $\{Mo_2(\mu\text{-}S)_2(\mu\text{-}SH)_2\}$ cluster, which are closely related to trinuclear $\{Mo_3(\mu_3\text{-}S)(\mu\text{-}S)_3\}$ cluster-based catalysts for hydrogenation of nitroarenes, nitrosobenzene, phenylhydroxylamine and azoxybenzene in the presence of H_2,[115] however the selectivity of these catalysts for substrates containing simultaneously several reactive groups has not been studied. A study of hydrogenation of more than 30 nitroarenes in the presence of H_2 catalyzed by the diimine complex $[Mo_3S_4Cl_3(dnbpy)_3](PF_6)$ has been reported; the results are summarized in Table 4.[45]

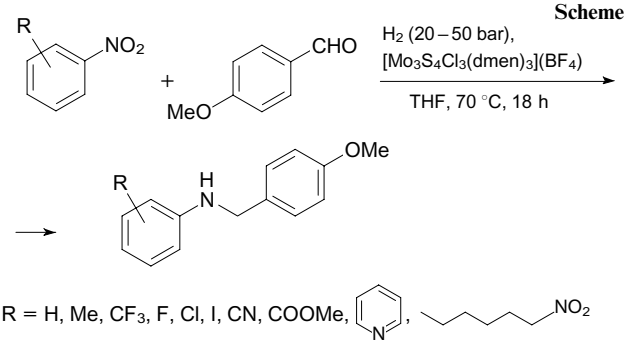
The hydrogenation of nitroarenes containing inert and/or low-reactivity functional groups (alkyl, hydroxyl, alkoxyl, biphenyl) gives the corresponding anilines in up to quantitative yields (compounds **1**–**6** in Table 4). Commercially useful halogen-substituted nitroarenes are hydrogenated without any dehalogenation reactions and the desired halo-substituted anilines are formed in high yields irrespective of the halogen nature or position in the ring (compounds **7**–**13**). In addition, other substituents including trifluoromethyl, amino and thiomethyl groups are also retained in the final aniline derivatives (compounds **14**–**16**).

It is important that the easily reducible alkene groups remain almost intact in these reactions and the expected anilines are formed in high yields (compounds **17**–**19**). Note that ketones and sulfonamides are converted to anilines in good to high yields (substrates **20** and **21**). Cyanide, ester and amide groups are also little affected in these reactions (substrates **22**–**30**). In addition, some heteroaromatic amines that are important building blocks for the preparation of various agrochemicals and pharmaceuticals were obtained in 91%–99% yields (compounds **31**–**34**).[45]

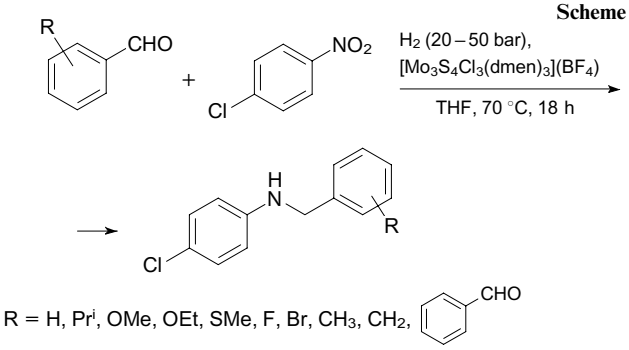
5.1.3. Reductive amination of nitro compounds with aldehydes

The complex $[Mo_3S_4Cl_3(dmen)_3](BF_4)$ mentioned in the previous Section was tested as the catalyst of amine N-alkylation starting from nitro compounds and aldehydes in the presence of H_2 as a reducing agent.[116] The reactions of nitro

Scheme 7



Scheme 8



compounds with *p*-anisaldehyde (Scheme 7) and the reactions of *p*-chloronitrobenzene with various benzaldehydes (Scheme 8), resulting in the formation of secondary amines in high yields, were studied. Electron-donating substituents (alkyl, alkoxy or thiomethyl) in either the nitroarene or the aldehyde promote smoother formation of the reaction products. Meanwhile, in the presence of electron-withdrawing groups, pressure increase is required for these reactions (up to 50 bar), in order to prevent the accumulation of imino derivatives. Halo-substituted nitroarenes and aldehydes give the corresponding haloamines in good yields without any dehalogenation reactions. Other reducible substrates (nitriles, esters, alkenes) are also converted to secondary amines in 82% – 85% yields.

It is noteworthy that these catalytic systems are also efficient for aliphatic nitro compounds (nitrohexane) and aliphatic aldehydes (cyclohexanecarbaldehyde) as substrates. The expected amines are obtained in ~60% yields. The secondary amines can be isolated from the reaction mixture in an individual state. In relation to the model reaction between nitrobenzene and benzaldehyde, it was shown that the reaction can be scaled up and gives *N*-benzylaniline in 90% yield after chromatographic purification. The homogeneous catalytic systems found for these reactions contain no noble metals for the first time.

5.1.4. Photo- and electrocatalytic systems based on the trinuclear $\{Mo_3S_4\}$ and $\{Mo_3S_7\}$ clusters

5.1.4.1. Photo- and electrocatalytic decomposition of water and hydrogen evolution reaction

The photocatalytic decomposition of water using solar energy is a promising way for generation of molecular hydrogen to be used as an environmentally benign renewable energy source.[117,118] In recent years, molybdenum sulfide-based materials for the photo- and electrocatalytic water reduction have been developed;[119] these materials can be considered as an inexpensive alternative to platinum metal complexes.

The evolution of hydrogen upon water photodecomposition includes the following key stages:

— generation of electron–hole pairs in a semiconductor upon light absorption;

— electron and hole migration towards the semiconductor surface;

— efficient transfer of the photogenerated electrons on water molecules by means of a co-catalyst adsorbed on the semiconductor surface; simultaneously, holes must be transferred either on water molecules or on other electron donors in the solution, for example, S^{2-} or SO_3^{2-}.

Photodecomposition of water

$$2\,H_2O \longrightarrow 2\,H_2 + O_2 \qquad (9)$$

Hydrogen evolution reactions
in acidic electrolytes

$$2\,H^+_{aq} + 2\,e \longrightarrow H_2(g) \qquad (10)$$

in alkaline electrolytes

$$2\,H_2O + 2\,e \longrightarrow H_2(g) + 2\,HO^-_{aq} \qquad (11)$$

It should be noted that in alkaline electrolytes, water oxidation with elimination of oxygen can also take place [120]

$$2\,H_2O - 4\,e \longrightarrow 4\,H^+ + O_2 \qquad (12)$$

Nanostructured molybdenum disulfide with developed surface, unlike the amorphous compound, shows high catalytic activity towards H_2 evolution reactions.[121,122] Modifying the surfaces of TiO_2,[122,123] CdS,[124] Si [125,126] and copper(I) and copper(II) oxides [127] with MoS_2 nanoparticles of various morphology leads to increasing photocatalytic activity.

After microscopic determination of the geometry of the catalytically active sites in MoS_2 nanocrystals (Fig. 13), studies of the molecular clusters with a similar topology were initiated.

The molybdenum aqua complex $[Mo_3S_4(H_2O)_9]^{4+}$ has been studied most comprehensively. Like MoS_2, this complex deposited on highly ordered pyrolytic graphite [128] showed high electrocatalytic activity. The number of moles

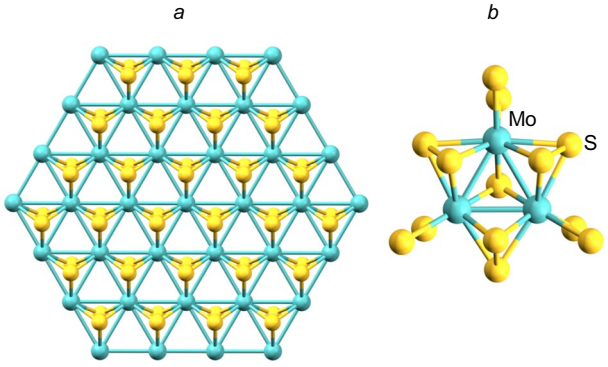


Figure 13. Crystal structures of MoS_2 (*a*) and the $\{Mo_3S_7\}$ cluster core (*b*).

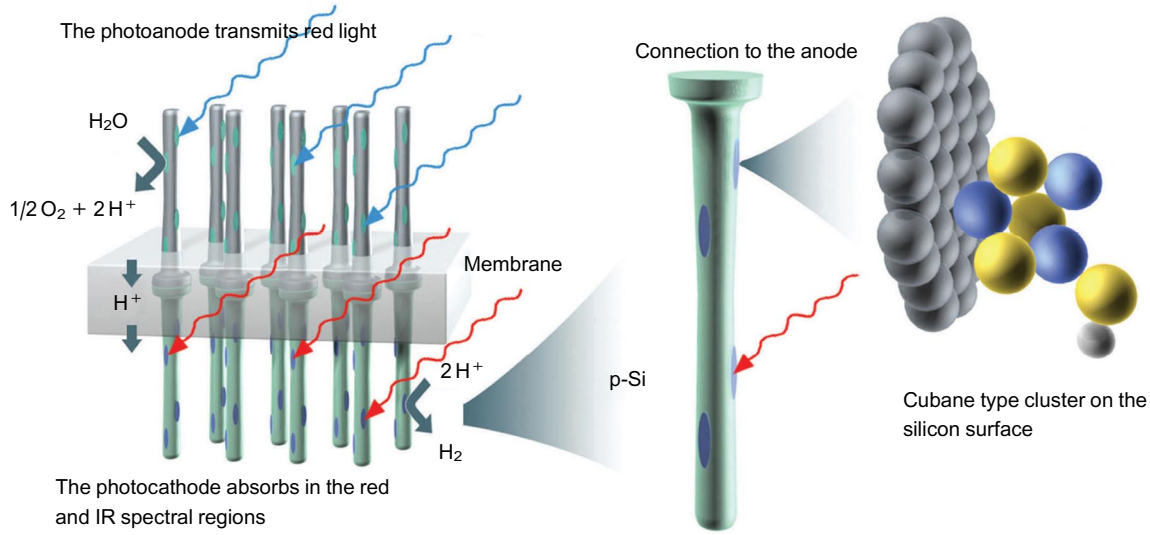


Figure 14. Scheme of the tandem setup for photoelectrocatalytic decomposition of water.[132]

of the substrate converted by one mole of the catalyst per second (TOF) for $[Mo_3S_4(H_2O)_9]^{4+}$ is 0.07 s^{-1}, which is 3.5 times higher than that for nanostructured MoS_2,[129] but an order of magnitude lower than those for Pt or Pd, and is comparable with the values for other catalysts based on non-noble metals (Ni, Cu or W).[130]

The aqua complexes $[M_3S_4(H_2O)_9]^{4+}$ and a number of heterometallic complexes, $[(\eta^5\text{-}Cp')_3M_3S_4M']$(pts) and $[(\eta^5\text{-}Cp')_3M_3S_4M'(X)]$(pts) (M = W, Mo; M′ = Co, Cu; X = CO, Cl), deposited on a p-type semiconductor substrate, for example, silicon (Fig. 14), also catalyze water splitting to oxygen and hydrogen.[131,132]

The use of tungsten-based clusters results in more intense evolution of hydrogen than observed with molybdenum counterparts, and the photoelectrodes decorated with cobalt-containing particles are unstable to radiation because of oxidation and destruction. The photocurrent depends linearly on the light intensity, and the efficiency of conversion of photons to electricity, so-called quantum efficiency of conversion, can reach 80%.

The overvoltage (potential difference between thermodynamically determined half-reaction reduction potential and the experimental redox potential) of hydrogen evolution systems at the current density of 8 mA cm^{-2} is −0.81 (M = W) and −0.55 V *versus* NHE (M = Mo); for the cubane type $\{M_3S_4Cu\}$ derivatives, the values are −0.82 and −0.53 V *versus* NHE, respectively. The undecorated p-Si demonstrates a current density of 8 mA cm^{-2} at the potential of −0.6 V *versus* NHE. The decoration with the clusters (Fig. 15) induces a considerable positive shift of the potential in the range of 0.3 to 0.35 V for tungsten clusters and up to 0.6 V for molybdenum clusters. At this current density, the potential difference between the cluster on silicon in the dark and on exposure to light is ~0.55 V in all cases (except for the $\{Mo_3S_4Co\}$/p-Si systems unstable on irradiation).[131]

The hydrogen evolution rate in these systems is comparable with the rates found with the use of a platinum co-catalyst on the p-Si surface. The resulting two-photon chemical battery (upon absorption of two photons, the electron passes from one bound state to another, the difference between the two states of the electron is equal to the sum of the energies of two photons) evolves hydrogen on exposure to red or IR light.

The adsorption of the $[Mo_3S_4(H_2O)_9]^{4+}$ clusters on the $NaTaO_3$ surface increases the photocatalytic activity of sodium tantalate towards water splitting to oxygen and hydrogen by factors of tens. The catalyst activity depends on the pH value of the solution; the best result was obtained at pH 2. Among the co-catalysts used with $NaTaO_3$, the aqua complex has the smallest size (~1 nm diagonally). If we assume that the characteristic length of $NaTaO_3$ is 1 μm, the $\{Mo_3S_4\}$ and $NaTaO_3$ volume ratio is $\sim 5 \times 10^{-8}$%. The cluster is distributed only over the substrate surface or edge parts, thus providing numerous efficient active sites for H_2 evolution.[133]

Complexes of the $\{Mo_3S_7\}$ clusters also posses catalytic activity towards water reduction. For example, graphite-supported submonolayers of $[Mo_3S_7(S_2)_3]^{2-}$ with terminal disulfide ligands are highly active towards the HER process and are stable in acidic media.[134] The TOF value is 3 s^{-1} for the overvoltage of 0.20 V, which is comparable with performance of a catalyst based on Au^{III} nanoparticles with MoS_2 deposited in a high vacuum, which has TOF of 1 and 10 s^{-1} (per $\{MoS_2\}$ active site) for overvoltages of 0.10 and 0.16 V, respectively.[128] The higher catalytic activity of the $[Mo_3S_7(S_2)_3]^{2-}$ cluster anion compared with the aqua complex of $\{Mo_3S_4\}^{4+}_{aq}$ (TOF = 0.07 s^{-1}) [128] is attributable to the presence of a larger number of sulfur atoms mimicking the electroactive groups of MoS_2. This is also consistent with the high activity of the mononuclear molybdenum complex $[(py_5Me_2)MoS_2]^{2+}$ with the coordinated disulfide group in a similar process with TON reaching $\sim 3.5 \times 10^3$ moles of H_2 per mole of the catalyst.[135]

Recatala *et al.*[88] reported the electro- and photocatalytic properties of *P25* TiO_2 nanoparticles with the adsorbed complex $(Bu_4N)\{[Mo_3S_7Br_4(dcmbpy)]Br\}$ (Fig. 16)[19] for the generation of hydrogen from water in the presence of a $Na_2S + Na_2SO_3$ mixture as an electron donor.

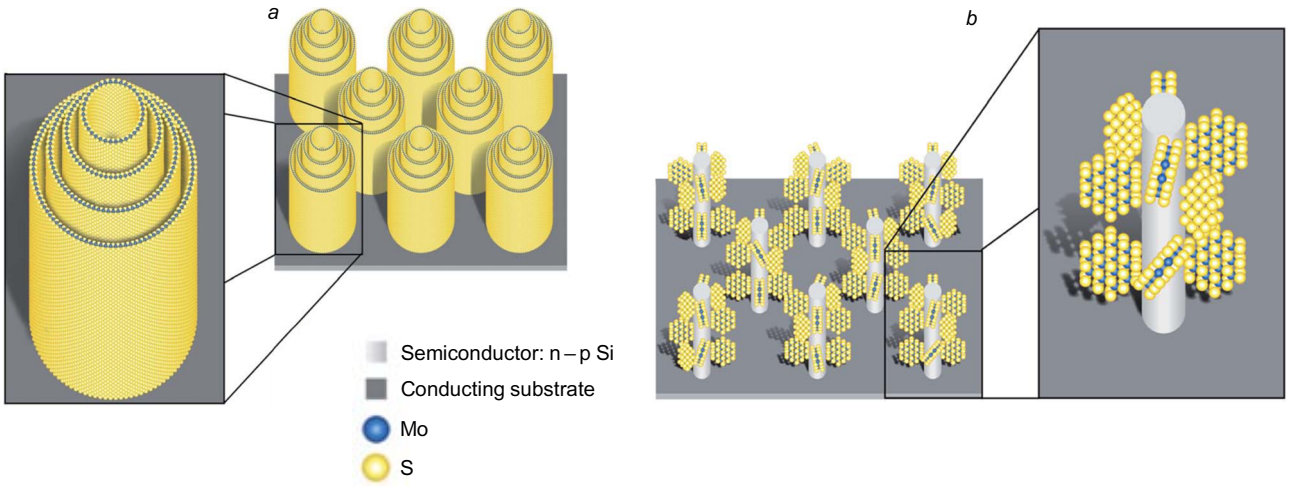


Figure 15. Presumed designs of photocathode decoration with MoS_2 or cubane type clusters.[131]
(*a*) The concentric $\{MoS_x\}$ nanotubes shortened along the radial direction for optimization of the number of active areas with retention of the layered structure are responsible for absorption of photons by the materials. These nanotubes should not be too long. In this design, $\{MoS_x\}$ acts as both a semiconductor and an electrocatalyst.
(*b*) The $\{MoS_x\}$ nanoplates are attached to the semiconductor in the basal plane perpendicular to the semiconductor pillar axis. This design optimizes the energy transport from the light harvesting semiconductor (Si) through the conducting substrate to the active edges of the electrocatalyst.

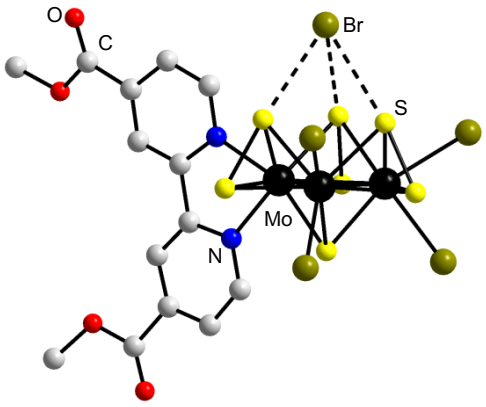


Figure 16. Structure of the $\{[Mo_3S_7X_4(dcmbpy)]Br\}^-$ associate in $(Bu_4N)\{[Mo_3S_7Br_4(dcmbpy)]Br\}$.[14]
Hydrogen atoms are omitted.

Electrochemical experiments with TiO_2 film-coated electrodes with deposited $(Bu_4N)\{[Mo_3S_7Br_4(dcmbpy)]Br\}$ showed that the complex is reduced to give an efficient hydrogen evolution catalyst. The overvoltage (for the polarization current density of 1 mA cm^{-2}) decreases by ~0.30 V (in 0.1 M $Na_2S + 0.02$ M Na_2SO_3) or 0.40 V (in 0.1 M $HClO_4$) in the presence of the complex. The initial overvoltage values are −0.05 V in 0.1 M $HClO_4$ and −0.26 V in 0.1 M $Na_2S + 0.02$ M Na_2SO_3, which is comparable with the published data for MoS_2 on various substrates. The Tafel coefficient (several hundreds in 10^{-1} mV units) and TOF (1.4 s^{-1} in 0.1 M $Na_2S + 0.02$ M Na_2SO_3) are comparable with those for MoS_2.

According to X-ray photoelectron spectroscopy and diffuse reflectance spectroscopy data for modified electrodes, the electrocatalyst has the composition Mo_xS_y and contains molybdenum atoms in the 4+ oxidation state surrounded mainly by S^{2-} groups (instead of S_2^{2-}); in the limiting case, the composition of the electrocatalyst approaches MoS_2.

Molybdenum sulfide-modified TiO_2 nanoparticles dispersed in a 0.1 M $Na_2S + 0.02$ M Na_2SO_3 mixture showed a noticeable hydrogen formation on exposure to light ($\lambda > 410$ nm). The hydrogen evolution rate was 30 nmol min^{-1}, which corresponds to a quantum efficiency of 0.6% and TON = 2.3 after irradiation for 8 h. The calculated TOF, equal to 8×10^{-5} s^{-1} (per Mo atom), is much lower than the value obtained in electrochemical experiments. This is due to the fact that the driving force for charge separation is lower in the photocatalytic experiment than under electrochemical conditions where electrons easily migrate from the electrode to TiO_2. The H_2 evolution rate virtually does not change over a period of 8 h, which is indicative of catalyst stability.

The overall process is described by the following equation:

$$Na_2S + Na_2SO_3 + 2H_2O \longrightarrow H_2 + Na_2S_2O_3 + 2NaOH \quad (13)$$

5.1.4.2. Bleaching of organic dyes

In recent years, bismuth oxohalides BiOX (X = Cl, Br, I) have been used as photocatalysts for photodegradation of organic compounds. Their advantage is operation also in the visible range, unlike the classical TiO_2-based photocatalysts, which operate only in the UV range (spanning only 4% of the whole solar spectrum). The most promising photocatalyst is the stable oxybromide BiOBr with an appropriate band gap, which is active in photodegradation of dyes (rhodamine B, bisphenol A and methylene blue) [136–138] and microcystin-LR (toxin produced by cyanobacteria) and decarboxylation of D-glutamic and methyl-D-aspartic acids.[139] Noble metal complexes can be used as

co-catalysts of these processes. However, they are inappropriate for treatment of liquid wastes of industrial dye production processes, which usually contain considerable amounts of sulfur (in particular, as S^{2-}). Therefore, the search for other co-catalysts containing no noble metals is still a relevant task.

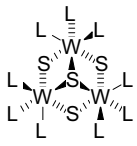
The preparation of $[Mo_3S_{13}]^{2-}$/BiOBr nanocomposite with the sulfide complex $[Mo_3S_{13}]^{2-}$ as the co-catalyst was reported.[140] The composite obtained by impregnation of bismuth oxybromide formed *in situ* from $Bi(NO_3)_3 \cdot 5H_2O$ and cetyltrimethylammonium bromide with a $(NH_4)_2[Mo_3S_{13}]$ solution shows a high photocatalytic activity in the decomposition of rhodamine B. The activity of this photocatalyst is comparable with the activities of the Pt/TiO_2, $[Mo_3S_{13}]^{2-}/TiO_2$ and Pt/BiOBr composites.[140] Spectroscopic studies showed complete bleaching of a rhodamine B solution in the presence of 5 mass % of $[Mo_3S_{13}]^{2-}$/BiOBr and $[Mo_3S_{13}]^{2-}/TiO_2$ and 1 mass % of Pt/BiOBr and Pt/TiO_2. Also, the addition of S^{2-} ions to the reaction mixture does not affect the catalytic activity of the $[Mo_3S_{13}]^{2-}$/BiOBr composite. Conversely, the activity of Pt/BiOBr sharply decreases in the presence of S^{2-}.

5.1.5. Synthesis of aldehydes from alcohols

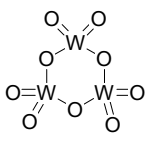
The selective oxidation of alcohols to aldehydes is performed using transition metal oxides, in particular, molybdenum and tungsten oxides, as heterogeneous catalysts.[141, 142] According to the simplest model of interaction of organic substrates with an oxide surface, the surface structure is usually considered as a set of polynuclear M_xO_y groups with various x values and x/y stoichiometry.[14]

Clusters with a clearly defined structure are convenient models for catalytic studies; their reactivity is determined by size effects. For example, the dimeric $[Mo_2O_6(OH)]^-$ anion efficiently catalyzes the gas-phase conversion of methanol to formaldehyde, while its monomeric analogue $[MoO_3(OH)]^-$ does not show a catalytic activity.[143] The gas-phase tungsten(VI) oxide trimer with the presumptive $\{W_3(\mu\text{-}O)_3O_6\}$ structure, either free and/or TiO_2-supported, catalyzes the dehydration of alcohols, for example, propan-2-ol to propene, with high efficiency.[144] The trinuclear $\{W_3(\mu_3\text{-}S)(\mu\text{-}S)_3\}$ clusters (structure **VIII**) resemble the $\{W_3(\mu\text{-}O)_3O_6\}$ group (structure **IX**) and are appropriate models for studying reactions of this type.

Structures VIII, IX



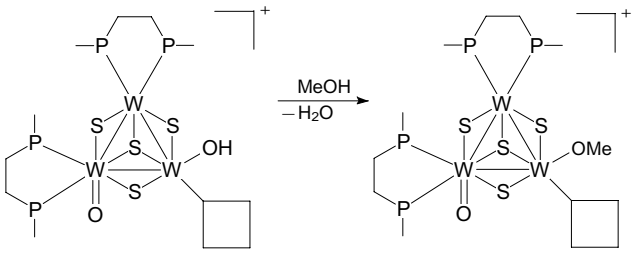
VIII



IX

A variety of tandem mass spectrometric experiments provided a fairly full description of the ionic products formed upon successive fragmentation of diphosphine complex cations $[W_3S_4(dmpe)_3X_3]^+$ (X = Br and OH). The nature of ligands X largely determines the predominant route of gas-phase dissociation. This gives various ionic products containing W–Br, W=O and W–OH groups within the cluster complex. Under electrospray ionization conditions, the cluster cations $[W_3S_4(dmpe)_2(OH)O]^+$ activate methanol to give methoxo complexes (Scheme 9). The methanol O–H bond is activated *via* interaction with the

Scheme 9



hydroxyl group of the cluster followed by elimination of this group and a methanol proton to give water and the $[W_3S_4(dmpe)_2(OMe)O]^+$ cation, which can regenerate $[W_3S_4(dmpe)_2(OH)_3]^+$.[145]

Like the methoxo complex, the ethoxo complex $[W_3S_4(dmpe)_2(OEt)O]^+$ is also formed from $[W_3S_4(dmpe)_2(OH)_3]^+$ upon electrospray ionization in the presence of ethanol. In the CID mass spectrometric experiment, elimination of acetaldehyde takes place to give $[W_3S_4(dmpe)_2(H)O]^+$. Additional experiments with a deuterium label demonstrated that the mechanism involving hydrogen transfer only from the α-position of the ethoxo ligand is most probable.

$$[W_3S_4(dmpe)_2(OCD_2Me)O]^+ \longrightarrow \quad (14)$$

$$\longrightarrow [W_3S_4(dmpe)_2(D)O]^+ + MeC(O)D$$

On the basis of DFT calculations, two competing mechanisms were proposed, one involving hydrogen atom transfer from the α-position of the alkoxo ligand to the oxygen atom of the neighbouring W=O group to give a seven-membered intermediate (Fig. 17) and the other involving hydride transfer from the α-position of the alkoxo ligand to the metal.[143] The Gibbs energy variation profiles calculated for the reaction

$$[W_3S_4(Ph_3)_4(OEt)O]^+ \longrightarrow [W_3S_4(Ph_3)_2(H)O]^+ + MeCHO \quad (15)$$

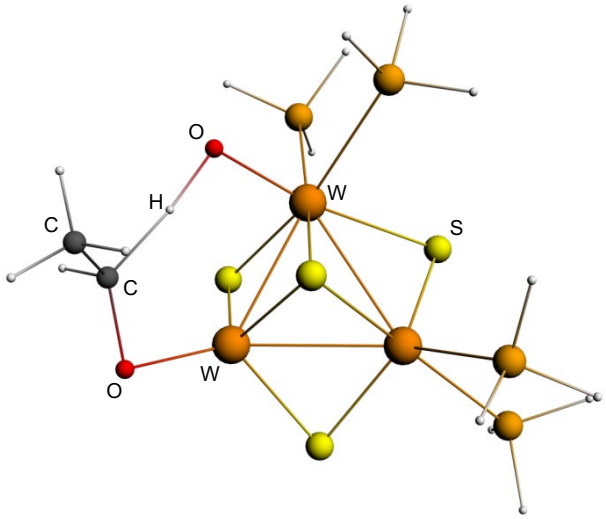


Figure 17. Structure of the seven-membered intermediate formed upon hydrogen atom transfer from the α-position of the ethoxo ligand to the oxygen atom of the neighbouring W=O group.[146]

Table 5. Data on the catalytic activity of molybdenum and tungsten complexes of trinuclear clusters.

Catalyst	Reaction	Ref.
$[M_3S_4X_3(dmpe)_3]^+$ (M = Mo, W; X = H, F)	Microwave-assisted hydrodefluorination of fluorine-containing substrates in the presence of silanes as the source of hydrogen	98
$[M_3S_4X_3(dppe)_3]^+$ (M = Mo, W; X = H, F)	Hydrodefluorination of fluorine-containing substrates in the presence of silanes as the source of hydrogen	99
$[Mo_3S_4X_3(dmpe)_3]^+$ (X = H, Cl)	Selective hydrogenation of aromatic nitro compounds in the presence of HCOOH – Et_3N	109
$[Mo_3S_4Cl_3(dmen)_3]^+$	Selective hydrogenation of aromatic nitro and azo compounds with silanes and hydrogen; reductive amination of nitro compounds with aldehydes	110
$[Mo_3S_4(H_2O)_9]^{4+}$/graphite	Reduction of water to generate hydrogen	128
$[Mo_3S_{13}]^{2-}$/graphite	The same	134
$(Bu_4N)\{[Mo_3S_7Br_4(dcmbpy)]Br\}/TiO_2$	"	19
$[Mo_3S_4(H_2O)_9]^{4+}$/p-Si	Photo- and electrodecomposition of water to give oxygen and hydrogen	131, 132
$[Mo_3S_4(H_2O)_9]^{4+}/NaTaO_3$	Photodecomposition of water	133
$[Mo_3S_{13}]^{2-}$/BiOBr	Photodecomposition of rhodamine B	140
$[Mo_3S_4(H_2O)_9]^{4+}$/zeolites NaY, HUSY, KL, NaMOR, NaH β	Hydrodesulfurization of benzothiophene	147, 148

(for the sake of simplicity, the dmpe ligands are replaced by Ph_3), with the Gibbs energy of the initial $[W_3S_4(dmpe)_2(OEt)O]^+$ being taken to be zero, showed that the former mechanism is thermodynamically favourable and the latter one is kinetically favourable; the energy difference between the two reaction pathways is slight. Thus, these mechanisms can compete in experiment.[146]

The data on the catalytic activity of the above molybdenum and tungsten trinuclear cluster complexes are summarized in Table 5.

5.2. Catalytic properties of heterometallic tetranuclear cluster complexes

5.2.1. Oil hydrotreating: desulfurization with sulfide catalysts

Along with hydrocarbons (alkanes, alkenes, cycloalkanes, arenes), crude oil contains considerable amounts of sulfur compounds (mercaptans, sulfides, disulfides, thiophenes and dibenzothiophenes), nitrogen compounds (anilines, aliphatic amines, quinoline, acridine, carbazole, indole), oxygenates (phenols, ketones and carboxylic acids), and also vanadium and nickel compounds, which occur as $V^{4+}{=}O$ and Ni^{2+} porphyrin complexes. For the production of high-quality oil refining products, these components should be removed during hydrotreating, which includes catalytic reactions such as hydrogenation of unsaturated hydrocarbons, hydrodesulfurization, hydrodenitrogenation, hydrodeoxygenation and hydrodemetallation. The hydrotreating is necessary in order to prevent air pollution, avoid poisoning of the catalysts used in the catalytic reforming and cracking and to improve the fuel quality.

Most of the industrially used hydrotreating catalysts contain active components such as cobalt- and/or nickel-promoted MoS_2/WS_2 supported on a substrate with a high specific surface area (*e.g.*, γ-Al_2O_3) (Fig. 18).[149]

In the absence of a substrate, the activity of noble metal sulfides towards hydrodesulfurization is much higher than the activity of sulfides of other transition metals, which varies in the order [150]

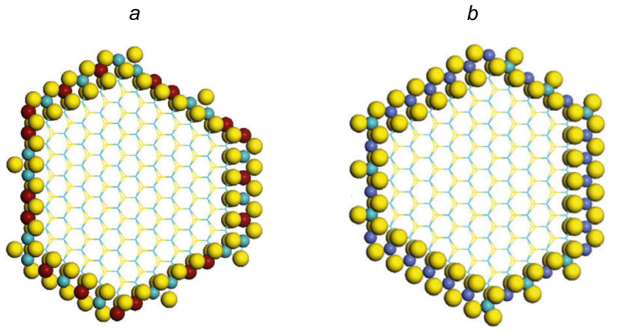


Figure 18. Models of HDS active sites of NiMoS (*a*) and CoMoS (*b*).[149]

$$RuS_2 > Rh_2S_3 > PdS > MoS_2 > NbS_2 > ZrS_2$$

Study of dibenzothiophene hydrodesulfurization catalyzed by MoS_2/Al_2O_3 promoted by noble metals or by cobalt and nickel demonstrated that the activity decreases in the series [151]

$$PtMo \geqslant CoMo \geqslant RuMo > PdMo > Mo$$

For the fabrication of an activated catalyst, tight contacts between the promoter and the catalyst are needed. As a rule, catalysts based on noble metal – molybdenum systems are prepared by successive or joint impregnation of the substrate with aqueous solutions of the metals; this does not ensure close positions of molybdenum and promoter atoms. Heterometallic complexes of the tetranuclear $\{Mo_3S_4M'\}$ cluster (M′ = Co, Ni) contain the desired metal atoms in the appropriate ratio (Mo : M′ = 3 : 1) in one molecule as well as sulfide groups and molybdenum in 4+ oxidation state.[152] Therefore, such complexes are considered as structural

models of the active sites of the industrial Co/MoS_2- and Ni/MoS_2-based hydrotreating catalysts.[153, 154]

Noble metal complexes like $\{(\eta^5\text{-}Cp')_3Mo_3S_4M'L_n\}$ (M' = Ru, Os, Rh, Ir; L = CO, PPh_3, COD, COE, dppp), stabilized by methylcyclopentadienyl and/or cyclooctadienyl ligands and soluble in organic solvent, have been prepared.[155] Presumably, transition to organic solutions would allow the design of homogeneous catalytic systems, with the activity being based on the noble metal heteroatom. However, the catalytic activity of these complexes in hydrotreating processes has not yet been described. Only moderate catalytic activity of analogous nickel complexes $[(\eta^5\text{-}Cp')_3Mo_3S_4NiL]^+$ (L = Me_2S, Et_2S, Bu^t_2S, tetrahydrothiophene, pyridine, quinoline, *etc.*) in hydrotreating processes (HDN and HDS) of a benzothiophene and quinoline mixture in the presence of H_2 (30 bar) at 250 °C has been reported.[155] Most likely, the complexes undergo partial thermal decomposition under these conditions to give catalytically active solid MoS_2/Ni particles. Temperature decrease to 130 °C leads to complete disappearance of the activity. Analysis of structural data for $[(\eta^5\text{-}Cp')_3Mo_3S_4NiL]^+$ confirmed the absence of any activation of the C–S or C–N bonds upon ligand L coordination to nickel.

Study of diphosphine complexes $[M_3NiS_4X_3L_3L']^+$ (M = Mo, W; X = Cl, Br; L = dmpe, dppe; L' = MeCN, py, CO, tetrahydrothiophene) as potential homogeneous catalysts of HDS showed the absence of catalytic activity in reactions with octane-1-thiol.[156]

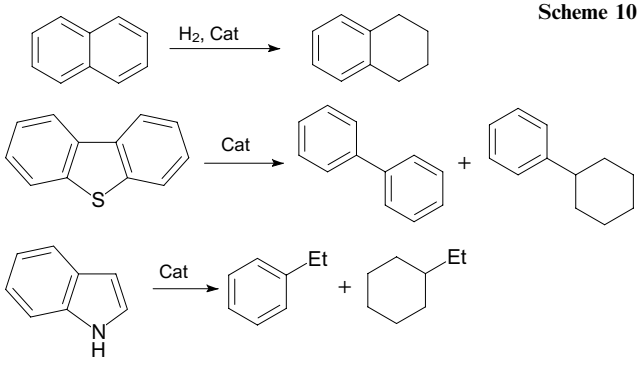
Thermolysis of $[(Cp')_3Mo_3S_4M'L_x](pts)_y$ (M' = Ru, Rh, Ir, Pd, Pt; L = CO, COD, COE, PPh_3, bicyclo[2.2.1]hept-2-ene) (see, for example, structures **X**–**XV**) at 350 °C gives the $\{MoS_xM'\}$ phases, which are preorganized towards the optimal mutual positions of noble metal atoms and the $\{MoS_2\}$ sites.[157]

The catalytic activity of these phases in oil hydrotreating reactions was studied on a model diesel feed containing dibenzothiophene, indole and naphthalene dissolved in n-heptane, because these compounds adequately represent the sulfur and nitrogen compounds and aromatics present in crude oil with boiling points within the diesel fuel boiling range. During the process, naphthalene is hydrogenated to tetralin, dibenzothiophene is converted to biphenyl and cyclohexylbenzene (HDS), and indole is converted to ethylbenzene and ethylcyclohexane (HDN) (Scheme 10). Depending on the metal heteroatom, the catalyst activity increases in the series[157]

$$Mo_3Pd < Mo_3Pt < Mo_3Ru < Mo_3Rh < Mo_3Ir$$

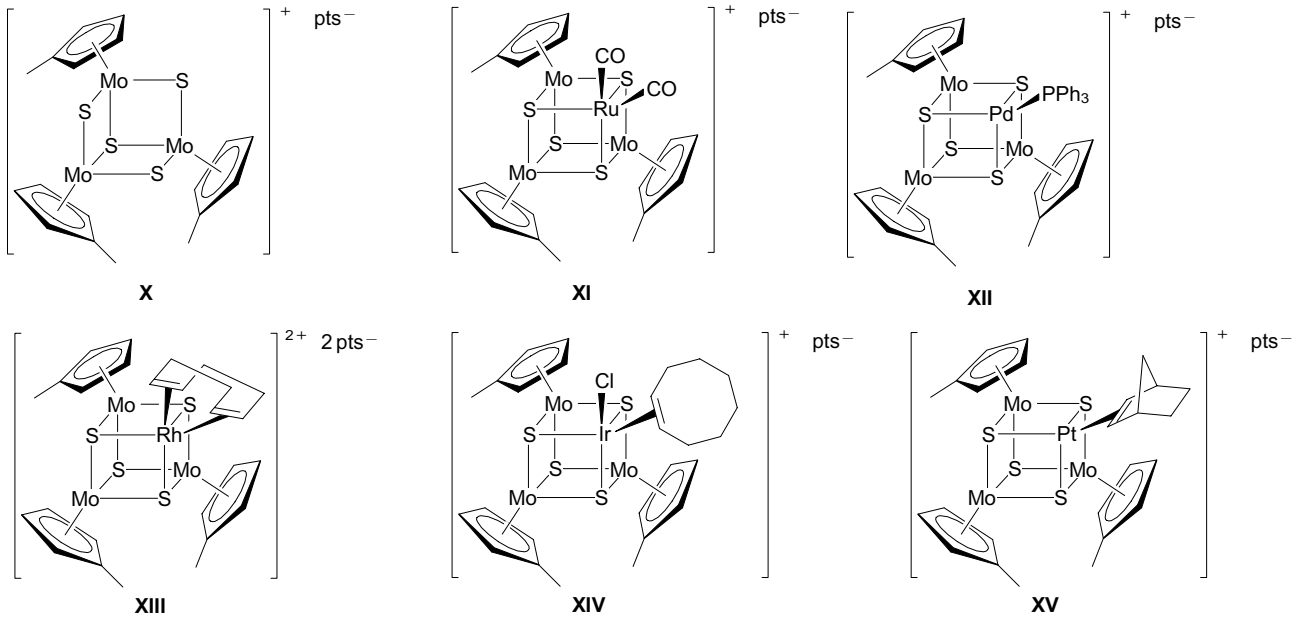
The catalysts based on water-soluble complexes $[Mo_3S_4(H_2O)_9]^{4+}$ and $[Mo_3S_4(NiCl)(H_2O)_9]^{3+}$ and various zeolites (NaY, HUSY, KL, NaMOR, NaH β) obtained by ion exchange showed high catalytic activity in the hydrodesulfurization of benzothiophene. The activity of the tetranuclear $\{Mo_3S_4Ni\}$ cluster-based catalyst is much higher than that of the Ni^{2+} promoted trinuclear $\{Mo_3S_4\}$ cluster-based catalyst, which is more active than the unpromoted analogue.[147, 148]

Scheme 10



Cat = Mo_3S_4M' (M = Ru, Rh, Ir, Pd, Pt)

Structures X–XV

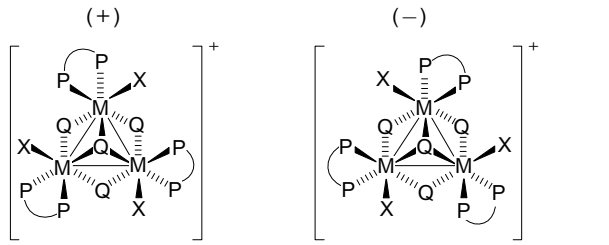


X **XI** **XII** **XIII** **XIV** **XV**

5.2.2. Cyclopropanation of diazo compounds

Specific coordination of bidentate ligands to the trinuclear $\{M_3Q_4\}$ cluster can lead to complexes in which one donor atom (*e.g.*, the phosphorus atom of the diphosphine complexes $[M_3Q_4X_3(\text{diphosphine})_3]^+$) is located in the *trans*-position to the μ_3-capping sulfur atom, while another donor atom is in the *trans*-position to the μ_2-bridging sulfur atom, which leads to chirality of the resulting cluster cations and gives rise to enantiomers **XVI** and **XVII**. In these cluster cations, all three metal sites are asymmetric; therefore, designations for dextro- (+) and levorotatory (−) isomers were introduced to describe the absolute configurations. Evidently, without optically pure reactants, these complexes are formed as racemic mixtures.[158]

Structures XVI, XVII



XVI **XVII**

There are two approaches to the preparation of optically active $\{M_3Q_4\}$ cluster complexes. The first one is to separate racemic mixtures by introducing a chiral ion, for example, TRISPHAT, which gives rise to supramolecular structures.[159] The success of this procedure is based on the configurational stability of the cluster cation at room and higher temperatures. However, in the case of $[Mo_3S_4Cl_3(dppe)_3]^+$, the racemic mixture cannot be separated using the Δ- and Λ-TRISPHAT enantiomers.[160] The second strategy is based on the transfer of chirality to the metal site using organic ligands with easily controllable configuration.

The second approach was used to obtain a family of enantiomerically pure complexes with the $\{M_3Q_4\}$ core *via* stereoselective 'cutting out' of monomers from polymeric chalcohalides $\{M_3Q_7X_2X_{4/2}\}_n$ (X = Cl, Br, H) in the presence of chiral diphosphines such as (+)-1,2-bis[2,5-(dimethylphospholan-1-yl)]ethane.[97] Heterometallic cubane type derivatives of these complexes were prepared and studied as chiral catalysts of cyclopropanation.[161, 162]

Metal-catalyzed cyclopropanation of alkenes with diazo compounds is of both fundamental and practical value; therefore, it attracts attention of researchers. The cyclopropane (the smallest cycloalkane) moiety is present in many natural compounds, including terpenes, pheromones, fatty acid metabolites and unusual amino acids.[163] High ring strain and unique electronic properties make cyclopropanes exceptionally valuable precursors for the preparation of other cyclic and acyclic compounds. Chiral cyclopropanes accessible in enantiomerically pure state serve as versatile synthons for the synthesis of other cyclic compounds. There are three approaches to the synthesis of chiral cyclopropanes:

— transition metal-catalyzed carbene transfer reactions;[164]

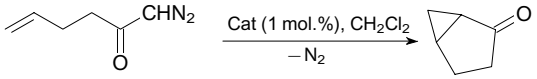
— Simmons – Smith reactions,[165] including transition metal-catalyzed ones;[166]

— nucleophilic addition followed by ring closure in the presence of organic catalysts.[167]

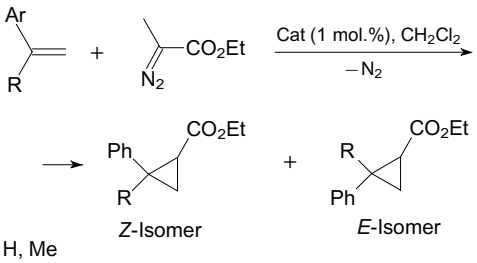
When chiral metal complexes are used as cyclopropanation catalysts, the ligand structure can strongly affect the yield and enantioselectivity of the process, but cases in which the $E:Z$ isomer ratio is >2.5 are very rare.[161]

Enantiomerically pure complexes $[Mo_3CuS_4L_3X_3]X$ (X = Cl, Br, PF_6) with coordinated chiral diphosphines {L = (+)-1,2-bis[(2*R*,5*R*)-2,5-(dimethylphospholan-1-yl)]ethane (*R*,*R*)-L and its enantiomer (*S*,*S*)-L} show relatively high catalytic activity in the intramolecular cyclopropanation of 1-diazo-5-hex-5-en-2-one (Scheme 11) and intermolecular cyclopropanation of alkenes, such as styrene or 2-phenylpropene, with diazoacetates (Scheme 12).[162]

Scheme 11



Scheme 12

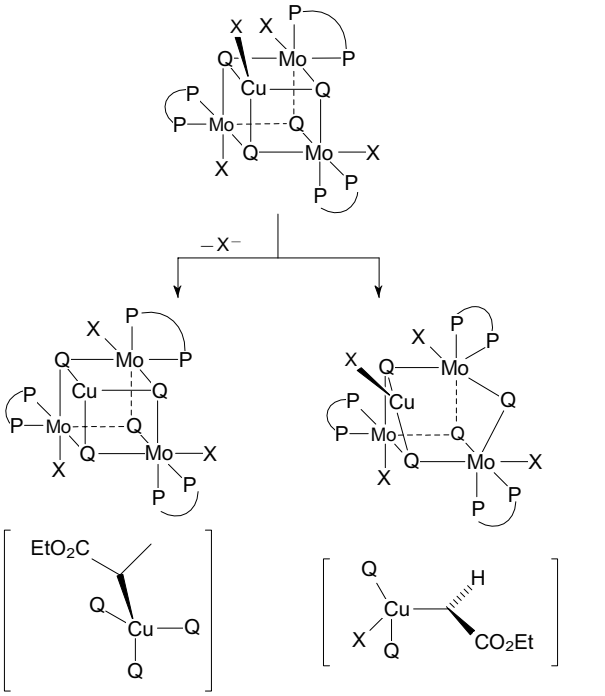


R = H, Me

When styrene reacts with ethyl diazoacetate in the presence of racemic $[Mo_3CuS_4(dmpe)_3Cl_4]^+$ (see Scheme 11), the yield of the product is 80% and the isomer ratio $E:Z = 2.4$; in the presence of the enantiomerically pure catalyst $[Mo_3CuS_4((R,R)\text{-L})_3Cl_4]^+$, the cyclopropane yield increases to 88% and the $E:Z$ ratio increases to 2.6, according to the results of ^{1}H NMR spectroscopy and gas chromatography. In the case of intramolecular cyclopropanation (see Scheme 11), the yields of the product are comparably high for both catalysts (Scheme 12), though the catalyst based on the racemic mixture has a higher activity (the yield is 95% instead of 84% obtained with the chiral catalyst).[162]

Despite the considerable yields of products, the diastereoselectivity (for intermolecular reactions) and the enantioselectivity (for inter- and intramolecular reactions) of the catalyzed processes are moderate. In all probability, this is related to the structure of the catalytically active species. Two alternative mechanisms can be conceived (Scheme 13). One is related to decoordination of the halide ligand from Cu^I to give the carbene intermediate $\{Mo_3Q_4CuCHCO_2Et\}$. The other mechanism implies cleavage of one Cu – Q bond to give the carbene intermediate $\{Mo_3Q_4Cu(X)CHCO_2Et\}$. In both intermediates, the distance between the copper-containing active site and the phosphine chiral centre is rather large, resulting in low enantioselectivity.[168]

Scheme 13



In the series of complexes $[Mo_3CuQ_4L_3X_3]^+$ {L = (+)-1,2-bis[(2*R*,5*R*)-2,5-(dimethylphospholan-1-yl)]-ethane (*R*,*R*)-L and its (*S*,*S*)-L-enantiomer, Q = S, Se; X = Br, Cl}, Se compounds are less reactive, but more selective than S counterparts. The product yields are 77% and $E:Z = 2.3$ (for Q = S, X = Cl) and 70% and $E:Z = 2.6$ (for Q = Se, X = Cl). Meanwhile, replacement of chloride ligands in the sulfur complex by bromide ligands leads to product yields decreasing almost twofold and $E:Z$ ratio increasing to 2.6.[168]

5.2.3. Hybrid materials based on the $\{Mo_3S_4\}$ and $\{Mo_3S_4Cu\}$ clusters

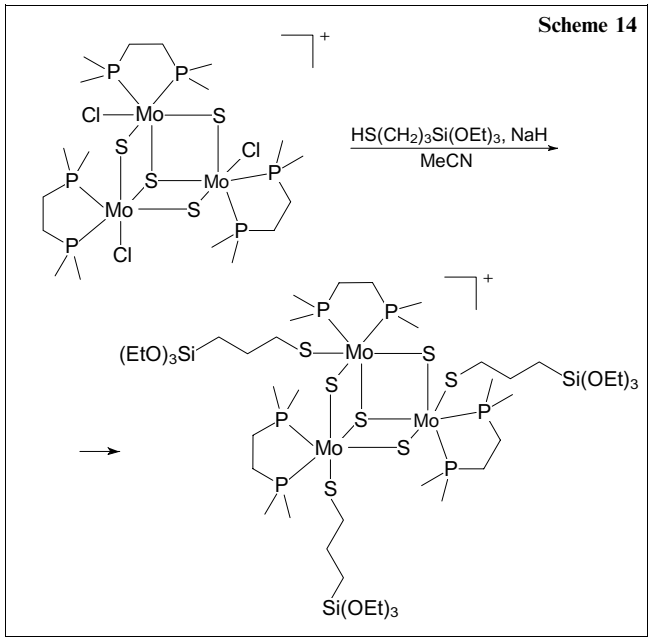
Functionalization of mesoporous silicon oxide *via* adsorption of $[Mo_3S_4(dmpe)_3(MPTES)_3](PF_6)$ can be accomplished by the following procedures (Scheme 14):

— co-deposition of the complex and tetraethyl orthosilicate *in situ* in the presence of a surfactant (cetyltrimethylammonium bromide);

— standard immobilization of the complex on the surface of mesoporous silicon dioxide MCM-41.[169]

The chemical and structural integrity of the cluster complex are retained in materials fabricated by both processes. Depending on the incorporation process, the trinuclear cluster complex is immobilized either within the silicon matrix (the former process) or on the surface (the latter process). In the case of the standard deposition, the materials have an ordered mesoporous structure with a narrow pore size distribution. The materials obtained *in situ* using methanol as the co-solvent have a disordered structure with a pore size ranging from micro- to mesopores due to incomplete extraction of the surfactant. Physicochemical analysis showed that the cluster structure is preserved and that the specific surface area of the materials with various amounts of $[Mo_3S_4(dmpe)_3(MPTES)_3](PF_6)$ exceeds 700 $m^2\ g^{-1}$. The introduction of monovalent copper into the materials fabricated by both the usual deposition and

Scheme 14



the self-assembly *in situ* results in copper coordination to $\{Mo_3S_4\}$ and the formation of the cubane type $\{Mo_3CuS_4\}$ derivative. The interest in these materials is largely associated with the catalytic activity of tri- and tetranuclear heterometallic clusters and with the possibility to develop new heterogeneous catalysts. In particular, $\{Mo_3S_4Cu\}$-based materials could serve as heterogeneous catalysts in cyclopropanation reactions (see above).[162, 168]

5.2.4. Fiedel–Crafts allylation

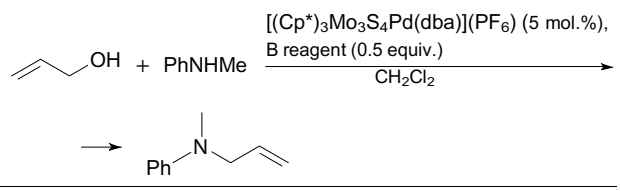
The Fiedel–Crafts allylation of aromatic and heteroaromatic compounds, which is an important tool for the formation of carbon–carbon bonds,[170, 171] is an environmentally benign chemical process. From the economic and environmental standpoints, allyl acetates, allyl carbonates and allyl halides, which are used as substrates in allylation reactions, should better be replaced by allylic alcohols, because water is the only by-product in this case.

Among the catalytic systems involving transition metals that are used in the Fiedel–Crafts allylation of aromatic and heteroaromatic compounds, ruthenium and palladium complexes are best studied.[172, 173] In view of the benefits related to the direct use of allylic alcohols as allylating agents, the search for more efficient and practicable catalytic systems for this process is a topical issue.

The complex $[(Cp^*)_3Mo_3S_4Pd(dba)](PF_6)$ obtained by the reaction of $[(Cp^*)_3Mo_3S_4](PF_6)$ with $Pd(dba)_2$ in CH_2Cl_2[174] is an efficient catalyst for the allylation of amines and methylene compounds under mild reaction conditions (the reaction proceeds within 4 h at room temperature); allylic alcohols are used as allylating agents in the presence of boron-containing reagents (Lewis acids for stimulating C–O bond cleavage).[175]

The allylation of *N*-methylaniline (Scheme 15) and other substrates (aniline, 2,4,6-trimethylaniline, *N*-phenylacetamide, dibenzylamine, phenylbenzylamine) was carried out in the presence of equal amounts of various boron reagents — B_2O_3, BEt_3, H_3BO_3, $PhB(OH)_2$ or $B(OMe)_3$. The yields of the products were 13%–16% in the presence of B_2O_3 and BEt_3. When H_3BO_3, $PhB(OH)_2$ or $B(OMe)_3$ was used, the yields reached 96%–98%. In the absence of

Scheme 15

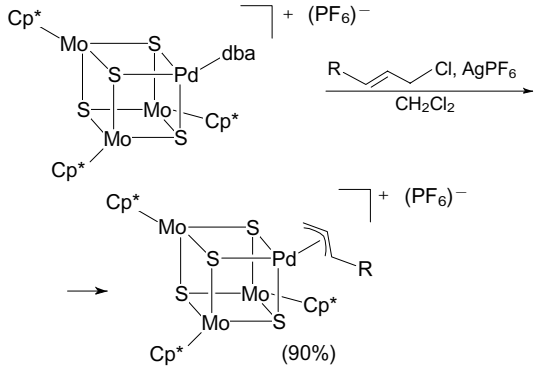


boron reagents, the products were not formed. Catalysts based on mononuclear palladium compounds [$PdCl_2$, $Pd(dba)_2$, $PdCl_2(PPh_3)_2$] did not show catalytic activity. The activity was found only for $Pd(PPh_3)_4$, but it was lower than that of $[(Cp^*)_3Mo_3S_4Pd(dba)](PF_6)$. The trinuclear cluster-based precursor $[(Cp^*)_3Mo_3S_4](PF_6)$ and other heterometallic complexes — $[\{(Cp^*)_3Mo_3S_4Ni\}_2.(COD)](PF_6)$, $[(Cp^*)_3Mo_3S_4RuH_2(PPh_3)](PF_6)_4$, $[(Cp^*)_3Mo_3S_4Pd(PPh_3)](PF_6)$ [174] and $[(Cp^*)_3Mo_3S_4RuCl_3]$ [176] — proved to be inert under these reaction conditions. A moderate activity (26% yield) was found for $[\{(Cp^*)_3Mo_3S_4Ni\}_2(COD)](PF_6)$ for the reaction conducted for 24 h.

The substrates used to study the regioselectivity of the catalyst are allylic alcohols containing methyl or phenyl substituents in the α- or γ-position, *e.g.*, 3-phenylprop-2-en-1-ol (cinnamic alcohol), α-vinylbenzyl alcohol, but-3-en-2-ol, but-2-en-1-ol, 2-methylprop-2-en-1-ol, 3-methylbut-2-en-1-ol and 2-methylbut-3-en-2-ol. The complex $[(Cp^*)_3Mo_3S_4Pd(dba)](PF_6)$ demonstrated high regioselectivity, giving mainly linear products. The lowest yield (in the case of 2-methylbut-3-en-2-ol) was 85%, while for other alcohols, the yields ranged from 89% to 95%, while the $E:Z$ ratio was 7.6 in the case of but-3-en-2-ol and 6.2 in the case of but-2-en-1-ol.

The presumptive mechanism of the reaction is illustrated by Scheme 16 (with H_3BO_3 as the boron-containing agent). The hydroxyl group of the allylic alcohol can donate the electron pair to boron, which facilitates the formation of the π -allylpalladium intermediate. Then the nucleophile (NuH) attacks the intermediate to give the corresponding product.

Scheme 17

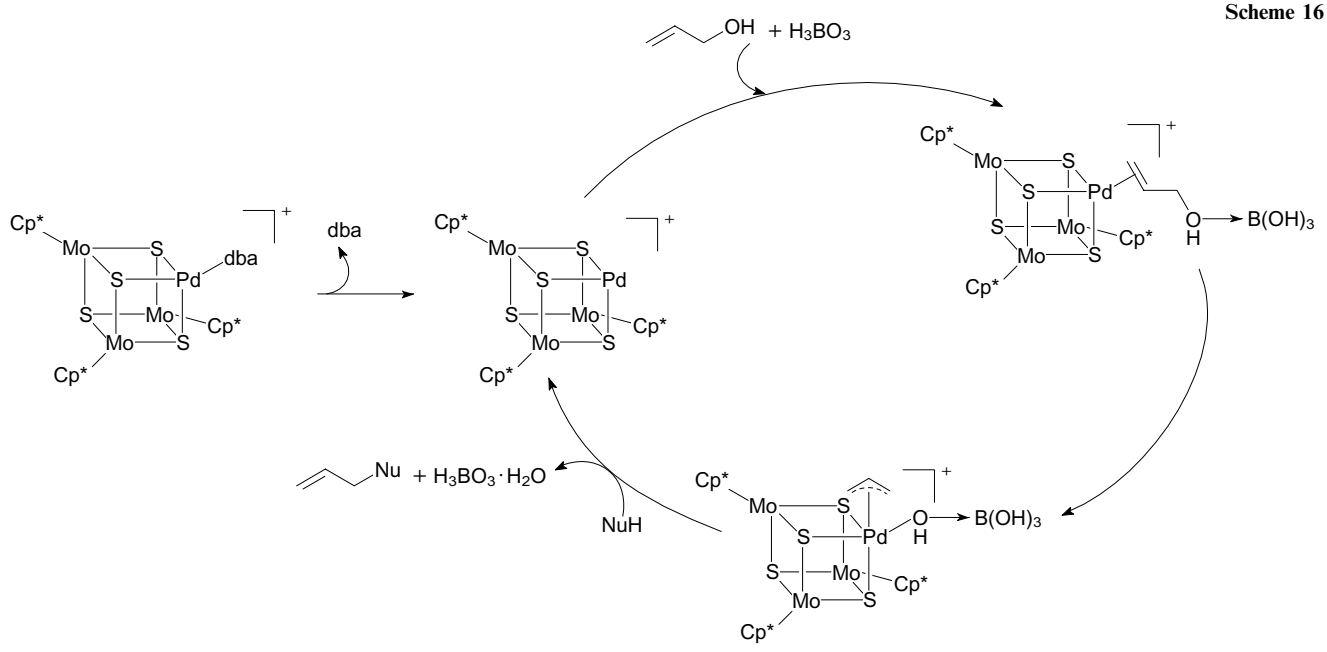


This mechanism is similar to the Pd-catalyzed allylation in the presence of BEt_3.[177] The $\{(Cp^*)_3Mo_3S_4\}$ moiety can be considered as a bulky ligand creating steric hindrance to the formation of branched products.

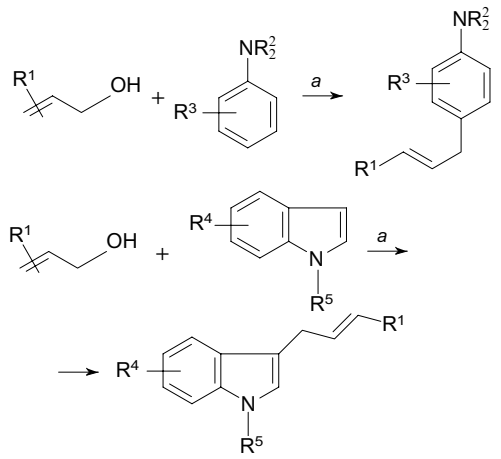
The complex $[(Cp^*)_3Mo_3S_4Pd(\eta^3\text{-All})](PF_6)_2$ synthesized on treatment of $[(Cp^*)_3Mo_3S_4Pd(dba)][(PF_6)$ with vinyl chloride in the presence of $AgPF_6$ (Scheme 17) [178] efficiently catalyzes the Friedel – Crafts allylation of nitrogen-containing aromatic compounds, for example, *N*,*N*-dialkylaniline and indole (Scheme 18; the substituents $R^1 - R^5$ can be represented by ketone, carboxyl, halide, amide and multiple-bonded groups and so on).

In the model reaction of *N*,*N*-dimethylaniline with cinnamic alcohol in the presence of $[(Cp^*)_3Mo_3S_4Pd(\eta^3\text{-All})](PF_6)_2$, the yield of the product reached 87% after stirring of the reaction mixture for 6 h. Meanwhile, palladium(II) chloride, mononuclear complexes $[(\eta^3\text{-All})PdCl]_2$ and $Pd(PPh_3)_4$, gold(III), iron(III) and zinc(II) chlorides and $[\{(Cp^*)_3Mo_3S_4Ni\}_2(COD)](PF_6)$ and $[(Cp^*)_3Mo_3S_4RuH_2(PPh_3)](PF_6)_4$ the cubane type complexes do not exhibit a catalytic activity in this reaction, while the use of $[(Cp^*)_3Mo_3S_4Pd(dba)](PF_6)$ leads to an only 38% product yield.[178] It is noteworthy that the position of the methyl group in the benzene ring markedly

Scheme 16



Scheme 18



(*a*) $[Mo_3S_4Pd(\eta^3\text{-All})]$ (3 mol.%), MeCN, 60 °C, 4 – 24 h

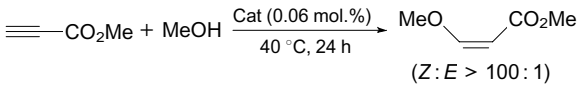
affects the reactivity of the aniline substrate. The *meta*-substituted *N*,*N*-3-trimethylaniline is most reactive and gives the allylation product in 84% yield. In the case of *para*-substituted *N*,*N*,4-trimethylaniline, the yield of the product is noticeably lower (35%), while the *ortho*-substituted *N*,*N*,2-trimethylaniline does not react at all. This may be due to a combination of steric and electronic effects. The highest yield of the product (91%) was found for 3-bromo-*N*,*N*-dimethylaniline.[179]

Cinnamic alcohol or α-vinylbenzyl alcohol reacts with *N*-methylaniline in the presence of $[(Cp^*Mo)_3S_4Pd(\eta^3\text{-All})](PF_6)_2$ to give one and the same product — *N*-methyl-*N*-[(2*E*)-3-phenylprop-2-en-1-yl]aniline — in 95% and 92% yields, respectively, which attests to the formation of a common π-allylpalladium intermediate. The substituted indoles such as 5-methoxy-, 5-bromo- and 2-methylindoles, *N*-methyl- and *N*-phenylindoles and so on are allylated with allylic alcohols in the presence of $[(Cp^*Mo)_3S_4Pd(\eta^3\text{-All})](PF_6)_2$ to give products in up to 98% yields with high regioselectivity.[178]

5.2.5. Addition to the triple bond catalyzed by $[Mo_3S_4(PdCl)(tacn)_3](PF_6)_3$

The complex $[Mo_3S_4(PdCl)(tacn)_3](PF_6)_3$ can promote stereoselective addition of alcohols to esters of alkynoic acids (Schemes 19 and 20) with high efficiency (the *E*-isomer and the saturated addition product are formed in < 3% yield), which cannot be attained using mononuclear palladium complexes $\{Na_2[PdCl_4]$, $Pd(OAc)_2$, $Pd(dba)_2$, $PdCl_2(PhCN)_2$ or $PdCl_2(PPh_3)_2\}$, and suppress the alkyne oligomerization. The minimum conversion is 93%, being observed for ethyl 4-phenylbut-3-ynoate.[180]

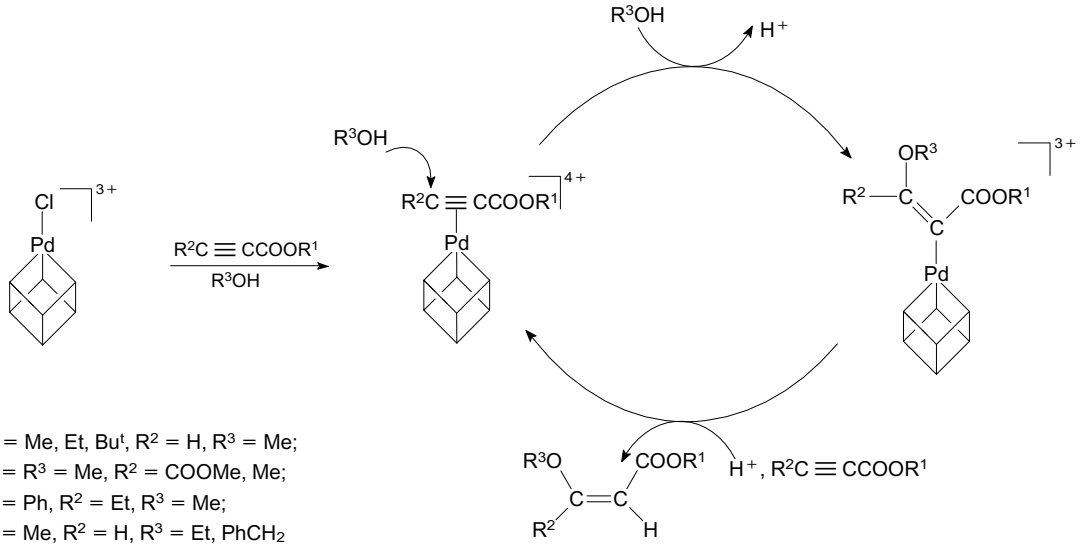
Scheme 19



High selectivity of the *trans*-addition of alcohols can be attributed to the following reaction mechanism (Scheme 20). Presumably, the alkynoic acid ester is first coordinated to Pd incorporated in the cluster, which is followed by nucleophilic attack by the alcohol on an electron-deficient carbon atom in the outer coordination sphere. At the final stage, the proton attacks the Pd – C bond to form the *trans*-addition product. The coordination of the palladium atom in the cubane type complex is tetrahedral and there is only one vacant coordination site, which precludes oligomerization of the alkyne.

Apart from the stereoselective addition of methanol to methyl propiolate, $[Mo_3S_4(PdCl)(tacn)_3](PF_6)_3$ efficiently catalyzes the stereoselective addition of carboxylic acids to electron-deficient terminal alkynes (Scheme 21; the substituents according to this Scheme can be represented by various functional groups: alkyl, aryl, multiple-bonded, ester, halide and amide groups and so on). Common palladium catalysts based on mononuclear complexes $[Pd(OAc)_2$, $PdCl_2(PPh_3)_2$, $PdCl_2(PhCN)_2$, $Pd(PPh_3)_4]$, $[Mo_3S_4PdCl(H_2O)_9]Cl_3$, $[Ru(p\text{-cymene})(PMe_3)Cl_2]$, $[Ru\{\eta_3\text{-}CH_2C(Me)=CH_2\}_2\{Ph_2(CH_2)_4PPh_2\}]$ and $RhCl(PPh_3)_3$ do not give the *Z*-isomer. In the reaction catalyzed by $[Mo_3S_4(PdCl)(tacn)_3](PF_6)_3$, the minimum

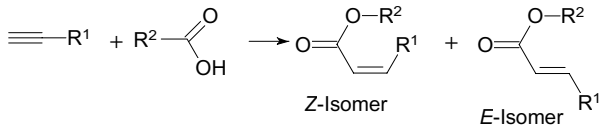
Scheme 20



R^1 = Me, Et, Bu^t, R^2 = H, R^3 = Me;
R^1 = R^3 = Me, R^2 = COOMe, Me;
R^1 = Ph, R^2 = Et, R^3 = Me;
R^1 = Me, R^2 = H, R^3 = Et, $PhCH_2$

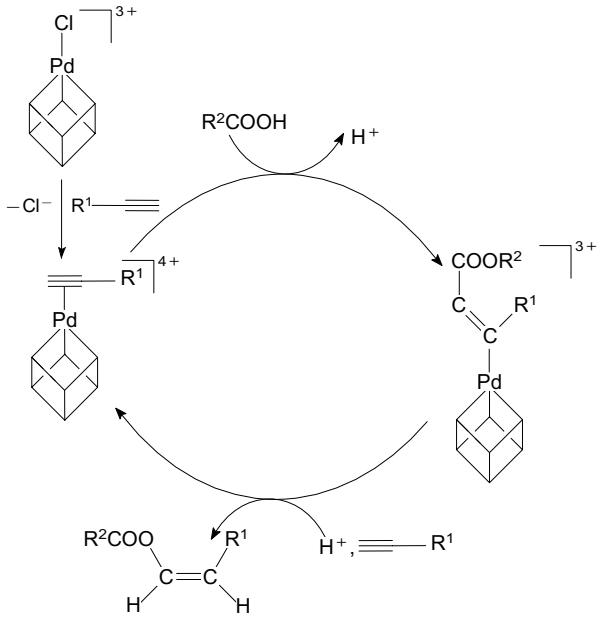
conversion is 91% and the selectivity to *Z*-isomers exceeds 97%, with the yields ranging from 51% (for $HC{\equiv}CSO_2Tol$) to 85% (for $HC{\equiv}CCOPyr$). For the reaction carried out for 18 h, the TON was 2 500 without the loss of selectivity.[181]

Scheme 21



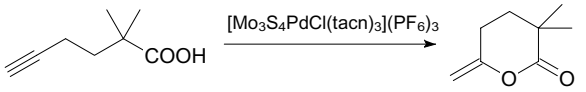
The presumptive reaction mechanism is shown in Scheme 22. In this case, as in the previous Scheme 21, various functional groups can be present as substituents such as alkyl, aryl, multiple-bonded, ester, halide and amide groups and so on. First, acetylene is coordinated to Pd and then the carboxylate anion nucleophilically attacks the terminal acetylenic carbon atom in the outer coordination sphere to give a vinylpalladium intermediate. Then the proton attacks the Pd – C bond with retention of the double bond stereochemistry and formation of the *trans*-product.

Scheme 22



The complex $[Mo_3S_4(PdCl)(tacn)_3](PF_6)_3$ also catalyzes the intramolecular cyclization of alk-3-, alk-4- and alk-5-ynoic acids under mild conditions to give the corresponding enol lactones. Palladium- and rhodium-containing catalysts proved to be inactive towards lactonization of alkynoic acids. As opposed to this, 2,2-dimethylhex-5-ynoic acid is converted to 3,3-dimethyl-6-methylene-2-pyrone in 98% yield after a 3 h reaction in acetonitrile in the presence of $[Mo_3S_4(PdCl)(tacn)_3](PF_6)_3$ and a slight amount of Et_3N (3 mol.%), and the TON reaches 300 (Scheme 23). The reaction mechanism includes intramolecular nucleophilic attack by the carboxylate anion on the C≡C bond of Pd-coordinated acetylene, this is followed by the attack by the proton on the Pd – C bond similar to that described above.[182]

Scheme 23



According to spectroscopic data, in all of the above reactions, the structure of the $[Mo_3S_4(PdCl)(tacn)_3](PF_6)_3$ catalyst is preserved after the reaction.[183]

5.2.6. Cleavage of the N – N bond in hydrazines

The ruthenium complexes $[(Cp^*)_3Mo_3S_4RuH_2(PCy_3)](PF_6)$ and $[(Cp^*)_3Mo_3S_4RuH_2(PPh_3)](PF_6)$ catalyze the hydrazine disproportionation to ammonia and molecular nitrogen. Tetranuclear cluster complexes with NH_3, NH_2 and $NHNH_2$ ligands bound to ruthenium were detected as intermediates. In addition, these complexes also cleave the N – N bond in phenylhydrazine to give ammonia, aniline, benzene and nitrogen.

At a temperature of 333 K in the presence of $[(Cp^*)_3Mo_3S_4RuH_2(PCy_3)](PF_6)$, ~20 mol of NH_3 and ~5 mol of N_2 per mole of the catalyst are formed, while in the presence of $[(Cp^*)_3Mo_3S_4RuH_2(PPh_3)](PF_6)$, the reaction gives only 6.6 mol of ammonia and ~1.6 mol of nitrogen. The authors did not investigate why the replacement of PPh_3 by PCy_3 had a so pronounced effect on the yields of products. The activity of these complexes is lower than that of mononuclear molybdenum and ruthenium thiolate complexes.[184]

5.2.7. Modelling of the active sites of nitrogenase

The reduced nitrogen is a major component of nucleic acids and proteins and, hence, it is vitally important for all organisms. The content of N_2 in the Earth atmosphere is 79%; however, this nitrogen can be converted to usable forms, for example, ammonia, only by biosynthesis. In nature, the MgATP-dependent reduction of N_2 to ammonia is catalyzed by nitrogenase.[185, 186]

$$N_2 + 8\,H^+ + 8\,e + 16\,MgATP \longrightarrow \longrightarrow 2\,NH_3 + H_2 + 16\,MgADP + 16\,Pi \quad (16)$$

The only industrial method for the catalytic reduction of atmospheric nitrogen to ammonia is the Haber process in which N_2 reacts with H_2 at high temperature (300 – 400 °C) and pressure (~250 atm) in the presence of a Fe catalyst. Although this process was developed almost 100 years ago and is associated with enormous economic and environmental expenses, no alternative industrial processes that would be more cost-efficient, environmentally benign or efficacious than the Haber process have yet been found.

Numerous attempts are made to reproduce the topology of the active site of the nitrogenase FeMo cofactor (structure **XVIII**). In particular, complexes with the $\{Mo_2Fe_6S_9\}$, $\{Fe_8S_6O\}$ and $\{MFe_3S_4\}$ cores (M = Mo, W) have been used for this purpose (Fig. 19),[187] although no catalytic activity was found for these complexes towards N_2 reduction to ammonia.

The active site of the FeMo cofactor has been modelled by $[Mo_2Fe_6S_9(SEt)_8]^{3-}$,[188] $[(Tp)_2Mo_2Fe_6S_9(SH)_2]^{3-}$,[189] $[(DmpS)Fe_4S_3O][(DmpS)Fe_4S_3](\mu\text{-}SDmp)_2(\mu\text{-}OCPh_3)$,[190] $[MFe_3S_4(SR)_3((cyclo\text{-}C_3H_5)(cyclo\text{-}C_3H_5)_2cat)L]^{2-/3-}$ (M = Mo,

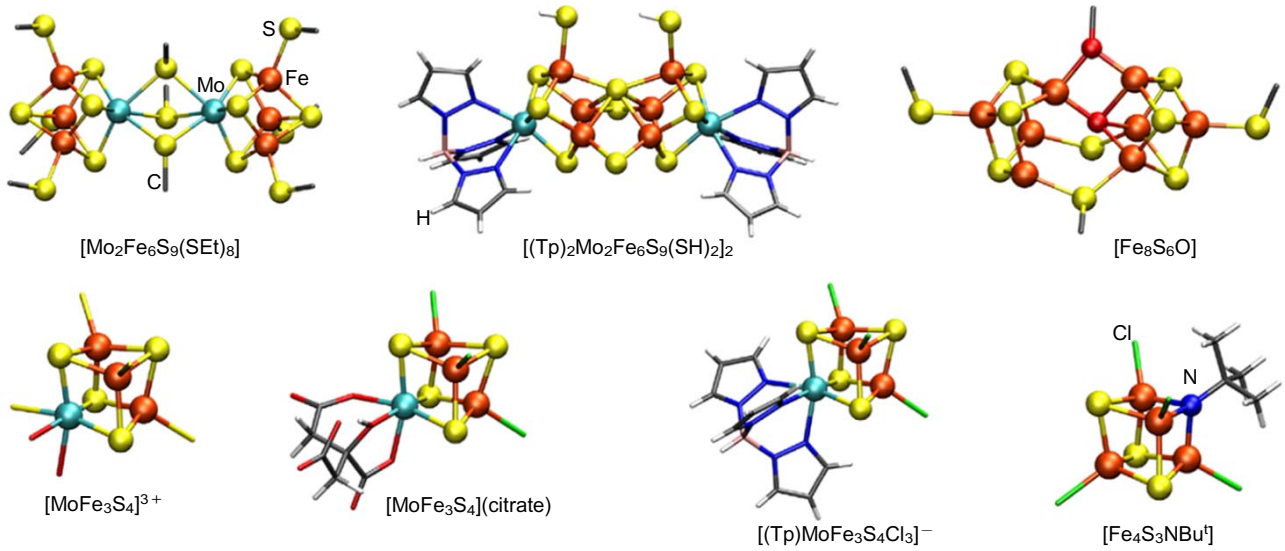
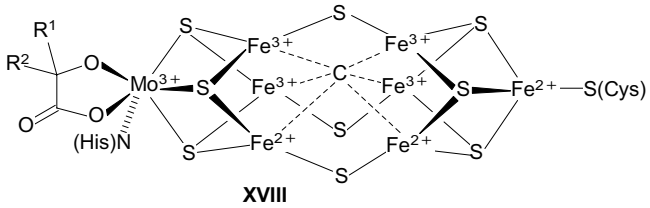


Figure 19. Complexes modelling the FeMo cofactor active site.[187–193]

Structure XVIII



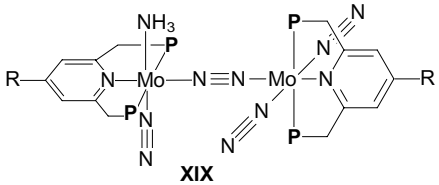
XVIII

$R^1 = CH_2CO_2^-$, $R^2 = (CH_2)_2CO_2^-$

W; R = Et, 4-ClC_6H_4; L = 4-$ClC_5H_4S^-$, PhO^-, CN^-, PEt_3),[191] $[MoFe_3S_4\ Cl_3L]^{3-}$ (L is oxalate, citrate, citramalate)[192] and $[(Tp)MoFe_3S_4Cl_3]^-$.[193]

Meanwhile, mono- and binuclear molybdenum complexes with chelating ligands containing also coordinated nitrogen molecules (structure **XIX**)[194,195] proved to be catalytically active in the reaction

Structure XIX



XIX

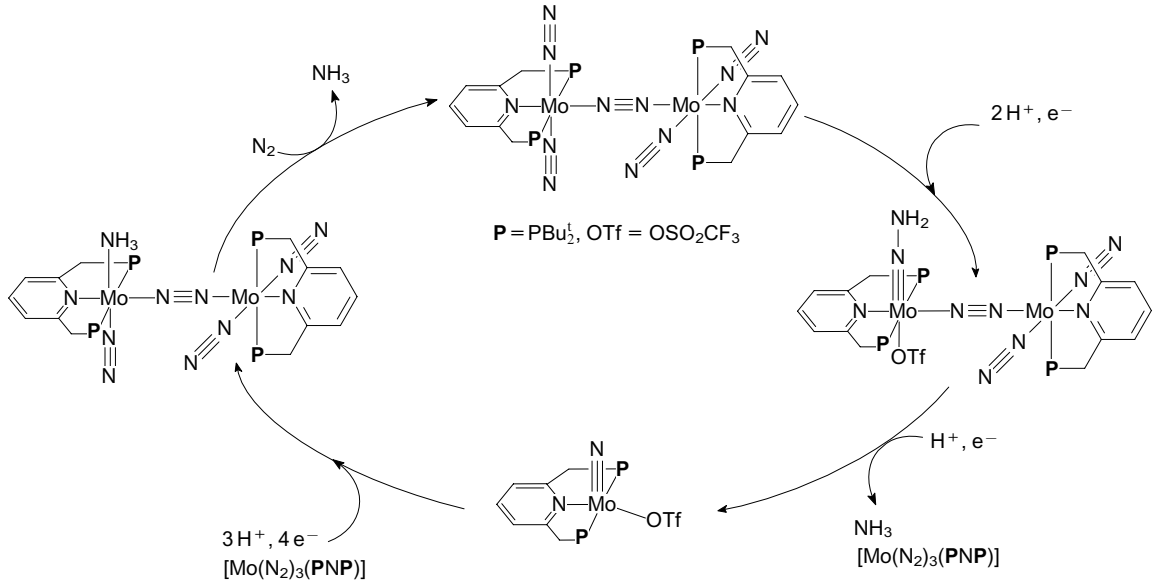
R = H, Me, MeO

$$N_2 + 6e + 6H^+ \xrightarrow{Cat} 2NH_3 \qquad (17)$$

The TOF reaches 28 h^{-1} for TON = 46 and the yield of ammonia is 49%. One more product of the reaction is H_2 formed in a yield of 37%.[195]

The presumptive mechanism of the reaction comprises the protonation of one of the N_2 ligands in the first stage. This is followed by electron transfer from one molybdenum

Scheme 24

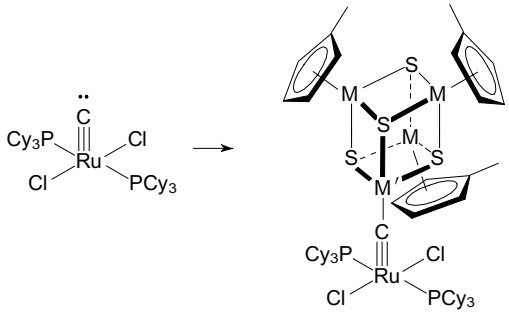


atom to the other *via* the bridging N_2 ligand, which activates the addition of one more proton to the NH_2 group to give the NH_3 molecule (Scheme 24). Ammonia and molecular hydrogen are formed in complementary reactions in this system. The suppression of hydrogen formation leads to increasing yield of ammonia.[195]

As can be seen from structure **XVIII**, the active site of FeMo cofactor of nitrogenase also contains a bridging carbide ligand. Despite the increasing number of complexes with carbide bridges,[196–198] there are virtually no metal sulfide clusters with carbide ligands that could model the active sites of the FeMo cofactor. Only rhenium clusters with bridging carbides have been described.[199] It is still unknown whether the carbide ligand affects the reduction potential of model clusters, because, for example, the replacement of sulfide ligands by imide ones in $\{Fe_4S_3X\}$ (X = S, NR) shifts the reduction potential by -0.4 V.[200]

The reaction of $[(Cp')_3M_3S_4M'L]$pts (M = Mo, W; M′ = Pd, Pt; L′ = dba, nor, pts) with the ruthenium carbide complex $(PCy_3)_2(Cl)_2RuC$[201] gave a number of cluster complexes $[(Cy_3P)_2Cl_2Ru{\equiv}C-M'S_4(MCp')_3]$pts with the cubane type $\{M_3S_4M'\}$ core in which the metal heteroatom is coordinated to the terminal carbide at the ruthenium atom (Scheme 25).[202] According to the results of electrochemical measurements, the Ru≡C ligand has a pronounced electron-withdrawing effect as compared with PPh_3, which results in a considerable positive shift of the redox potential. Cycic voltammograms for

Scheme 25



$[(Cp')_3M_3S_4M'L]^+$ (L is the Ru or PPh_3 carbide complex) showed one reversible one-electron reduction and two successive one-electron oxidation processes. The difference between the redox potentials for complexes with M = W and M′ = Pd and for $(PCy_3)_2(Cl)_2RuC$ with PPh_3 is 0.11, 0.16 and 0.56 V, respectively.[202] Study of these carbide-containing sulfide clusters is a natural development of the works related to modeling of the nitrogenase active sites, which is promising for investigation of the catalytic activity in the N_2 reduction. It is noteworthy that these are the first examples of carbide coordination to molybdenum and tungsten clusters.

The reactions using the above tetranuclear cluster complexes are summarized in Table 6.

Table 6. Complexes of heterometallic tetranuclear clusters as catalysts.

Catalyst	Process	Ref.
$[(Cp')_2Mo_2S_4Co_2(CO)_2]$, $[(Cp')_2Mo_2S_4Fe_2(CO)_6]$, $[(Cp')_2Mo_2S_4Ni_2(CO)_2]$ (see [a])	Hydrodesulfurization of thiophene	152
$[\{(Cp')_3Mo_3S_4Ni\}_2(\mu\text{-}C_4H_8S_2)](pts)_2$, $[\{(Cp')_3Mo_3S_4Ni\}_2(\mu\text{-bpy})](pts)_2$	Hydrodesulfurization and hydrodenitrogenation	153
$[Mo_3S_4\{NiCl\}(H_2O)_9]^{3+}$/NaY zeolites, HUSY, KL, NaMOR, NaH β	Hydrodesulfurization of benzothiophene	147, 148
$[(Cp')_3Mo_3S_4M'L_x](pts)_y$ (M′ = Ru, Rh, Ir, Pd, Pt; L′ = CO, COD, COE, PPh_3, bicyclo[2.2.1]hept-2-ene)	Naphthalene hydrogenation to tetralin; dibenzothiophene hydrodesulfurization to biphenyl and cyclohexylbenzene; and indole hydrodenitrogenation to ethylbenzene and ethylcyclohexane	157
$[Mo_3CuS_4L_3X_3]^+$, L = (+)-1,2-bis[(2*R*,5*R*)-2,5-(dimethylphospholan-1-yl)]ethane (*R*,*R*)-L and its enantiomer (*S*,*S*)-L, dmpe	Intra- and intermolecular cyclopropanation	162, 168
$[(Cp^*Mo)_3S_4Pd(dba)]^+$	Allylation of amines and active methylene compounds with allylic alcohols in the presence of H_3BO_3	175
$[(Cp^*Mo)_3S_4Pd(\eta^3\text{-All})]^+$	Friedel – Crafts allylation of nitrogen-containing aromatic compounds	179
$[Mo_3S_4(PdCl)(tacn)_3]^{3+}$	Stereoselective addition of alcohols to esters of alkynoic acids	180
$[Mo_3S_4(PdCl)(tacn)_3]^{3+}$	Stereoselective addition of carboxylic acids to electron-deficient terminal alkynes	181, 182
$[Mo_3S_4(PdCl)(tacn)_3]^{3+}$	Intramolecular cyclization of 3-, 4- and 5-alkynoic acids to enol lactones	
$[(Cp^*)_3Mo_3S_4RuH_2(PCy_3)](PF_6)$, $[(Cp^*)_3Mo_3S_4RuH_2(PPh_3)](PF_6)$	Cleavage of the N – N bond in hydrazines	184

[a] Cubane type heterometallic clusters $\{Mo_2S_4M'_2\}$ (M′ = Co, Fe, Ni) are not considered in the review: the complexes of these clusters are presented here in relation to their catalytic applications.

6. Conclusion

This review demonstrates a broad diversity of functional properties and potential applications of coordination compounds based on trinuclear molybdenum and tungsten cluster complexes and their heterometallic derivatives. These properties are determined by the natures of both the cluster core (the composition, geometry and electronic structure) and the outer ligand environment. Currently, it is possible to carry out targeted modification of cluster compounds of this type by varying the number and nature of the chalcogenide bridging ligands in the cluster core and the nature of terminal ligands, which gives rise to new compounds and materials with specified properties.

A very important characteristic of trinuclear molybdenum and tungsten chalcogenide clusters and their heterometallic derivatives is the ability to undergo redox transformations, which can be used to prepare magnetically active compounds and electronically conductive materials. The dichalcogenide ligands in $\{M_3Q_7\}$ type clusters tend to undergo irreversible reduction to give $\{M_3Q_4\}$ clusters, which can undergo a series of successive redox transformations (reversible and irreversible) associated with Mo^{4+} to Mo^{3+} reduction. The heterometallic cubane type $\{M_3Q_4M'\}$ clusters can be either reduced $[(M')^{2+}/(M')^0$, $Mo^{4+}/Mo^{3+}]$ or oxidized (Mo^{3+}/Mo^{4+}).

The outer coordination environment can markedly affect the redox processes. A vivid example is the coordination of redox active dithiolates (possessing π-donor properties) to the $\{M_3Q_7\}$ and $\{M_3S_4\}$ clusters, which changes the character of the highest occupied molecular orbital (from metal-centred to ligand-centred), thus providing the clusters with the ability to be reversibly oxidized at moderate potentials. The coordination of π-acceptor diimines (1,10-phenanthroline, 2,2′-bipyridine and their analogues) possessing low-lying π*-orbitals to the $\{M_3Q_7\}$ and $\{M_3S_4\}$ clusters leads to reversible one-, two- and three-electron reduction processes involving both the metal and the ligand.

The presence of reversible oxidation and reduction reactions makes it possible, in some cases, to isolate and study paramagnetic products of chemical or electrochemical redox reactions. In the case of dithiolate derivatives, paramagnetic complexes of the $[Mo_3S_7L_3]$ type (L = dmit, dmit and dsit) exhibing strong antiferromagnetic interactions and electron transport *via* non-covalent S···S contacts (electronic conductivity) were obtained. Upon the reduction of diphosphine derivatives of $\{M_3Q_4\}^{4+}$ with mild reducing agents, it is possible to isolate one-electron reduction products ($\{M_3Q_4\}^{3+}$), which behave as ideal paramagnets.

Luminescent properties are not inherent in this type of clusters. However, the coordination of an imidazophenanthroline derivative to the $\{Mo_3S_7\}$ cluster gives rise to fluorescent complexes in which luminescence is caused by ligand-centred transitions. By means of this coordination, one can control the photophysical properties of imidazophenanthroline, which provides opportunities for the preparation of novel hybrid materials. It is remarkable that the selective reactions of these complexes with halide anions lead to a substantial shift of the emission band (in the case of F^-) or the absence of such shift (in the case of Cl^-, Br^-). This selectivity can be utilized for the design of halide ion sensors.

Another feature of the clusters considered in the review is their high photochemical stability and the applicability as optical limiters of laser radiation. The optical limiting characteristics can be enhanced by introducing dithiolate ligands with an extended π-system and/or electron-donating substituents at bipyridine into the heteroleptic diimine complexes of the $\{Mo_3S_7\}$ cluster.

Perhaps, the best studied property of tri- and tetranuclear clusters is their catalytic activity. The review demonstrates the huge catalytic potential of the chalcogenide clusters towards various chemical transformations. First of all, this is hydrogenation of organic substrates and water reduction to give molecular hydrogen. In the latter case, trinuclear sulfide clusters are considered in comparison with molybdenum disulfide, in view of their chemical and structural similarity. The catalytic activity of heterometallic derivatives is caused, most often, by the presence of a metal heteroatom (Ni, Pd, *etc.*). The active metal sites within the cluster catalyze a broad range of organic transformations.

It is noteworthy that the $\{Mo_3S_4\}$ clusters functionalized by various bidentate ligands (diphosphines, diamines, diimines) efficiently catalyze the reduction of nitro and azo compounds under homogeneous conditions. The reaction is highly selective for substrates containing several potentially active functional groups, which provides the route to functionalized anilines that are difficult to prepare, but are valuable for synthetic and practical purposes. The atom efficiency of these catalytic systems can be increased by using cheap and environmentally benign hydrogen. Under these conditions, diimine and diamine complexes of the $\{Mo_3S_4\}$ cluster are efficient. The diamine complex $[Mo_3S_4Cl_3(dmen)_3](BF_4)$ is also a selective catalyst of tandem *N*-alkylation of amines starting from nitro compounds and aldehydes in the presence of H_2, which can be considered as an efficient way to secondary amines.

Some complexes act as co-catalysts in photo- and electrocatalytic water oxidation and reduction processes. Examples are $[Mo_3S_4(H_2O)_9]^{4+}$ and $[Mo_3S_{13}]^{2-}$ supported on graphite or silicon substrates. The possibility of modification of TiO_2 nanoparticles with diimine complexes of the $\{Mo_3S_7\}$ cluster was demonstrated. The obtained materials show high electrocatalytic activity in the water reduction to hydrogen, comparable with the electrocatalytic activity of molybdenum disulfide-based materials.

The persistent interest in the molybdenum and tungsten chalcogenide clusters expressed, in particular, by specialists engaged in catalysis and materials science gives confidence that we are heading towards the design of novel materials and catalysts.

This review was written with the financial support of the Federal Agency of Scientific Organizations of Russia and the Russian Foundation for Basic Research (Project No. 15-03-02775-a).

References

1. A.A.Opalovskii, V.E.Fedorov, K.A.Khaldoyanidi. *Dokl. Akad. Nauk SSSR*, **182**, 1095 (1968)
2. T.Shibahara. *Coord. Chem. Rev.*, **123**, 73 (1993)
3. G.Sakane, T.Shibahara, in *Transition Metal Sulfur Chemistry. ACS Simp. Ser.* Vol. 653. (Washington, DC: American Chemistry Society, 1996). P. 225
4. T.Saito. *Adv. Inorg. Chem.*, **44**, 45 (1996)
5. R.Llusar, C.Vicent. *Inorg. Chem. Focus III*, 105 (2006)

6. V.E.Fedorov, Yu.V.Mironov, N.G.Naumov, M.N.Sokolov, V.P.Fedin. *Russ. Chem. Rev.*, **76**, 529 (2007)
7. R.Hernández-Molina, M.N.Sokolov, P.A.Abramov, in *Incomplete and Complete Cuboidal Clusters of Molybdenum Chemistry*. (Ed. A.Holders). (New York: Nova Science, 2013). P. 105
8. A.Müller, R.Jostes, F.A.Cotton. *Angew. Chem., Int. Ed. Engl.*, **474**, 875 (1980)
9. K.Hegetschweiler, T.Keller, M.Baeumle, G.Rihs, W.Schneider. *Inorg. Chem.*, **30**, 4342 (1991)
10. A.Müller, R.Jostes, W.Jaegermann, R.Bhattacharyya. *Inorg. Chim. Acta*, **41**, 259 (1980)
11. A.Alberola, R.Llusar, S.Triguero, C.Vicent, M.N.Sokolov, C.Gómez-García. *J. Mater. Chem.*, **17**, 3440 (2007)
12. R.Llusar, S.Triguero, C.Vicent, M.N.Sokolov, B.Domercq, M.Fourmigué. *Inorg. Chem.*, **44**, 8937 (2005)
13. A.L.Gushchin, R.Llusar, C.Vicent, P.A.Abramov, C.J.Gómez-García. *Eur. J. Inorg. Chem.*, 2615 (2013)
14. D.Recatalá, R.Llusar, A.L.Gushchin, E.A.Kozlova, Yu.A.Laricheva, P.A.Abramov, M.N.Sokolov, R.Gómez, T.Lana-Villarreal. *ChemSusChem*, **8**, 148 (2015)
15. J.M.Garriga, R.Llusar, S.Uriel, C.Vicent, A.J.Usher, N.T.Lucas, M.G.Humphrey, M.Samoc. *Dalton Trans.*, 4546 (2003)
16. M.J.Mayor-López, J.Weber, K.Hegetschweiler, M.D.Meienberger, F.Joho, S.Leoni, R.Nesper, G.J.Reiss, W.Frank, B.A.Kolesov, V.P.Fedin, V.E.Fedorov. *Inorg. Chem.*, **37**, 2633 (1998)
17. A.L.Gushchin, M.N.Sokolov, E.V.Peresypkina, A.V.Virovets, S.G.Kozlova, N.F.Zakharchuk, V.P.Fedin. *Eur. J. Inorg. Chem.*, 3964 (2008)
18. R.Llusar, S.Triguero, V.Polo, C.Vicent, C.J.Gómez-García, O.Jeannin, M.Fourmigué. *Inorg. Chem.*, **47**, 9400 (2008)
19. I.J.McLean, R.Hernandez-Molina, M.N.Sokolov, M.S.Seo, A.V.Virovets, M.R.J.Elsegood, W.Clegg, A.G.Sykes. *J. Chem. Soc., Dalton Trans.*, 2557 (1998)
20. R.Llusar, S.Uriel, C.Vicent, J.M.Clemente-Juan, E.Coronado, C.J.Gómez-Garcia, B.Braida, E.Canadell. *J. Am. Chem. Soc.*, **126**, 12076 (2004)
21. R.Llusar, C.Vicent. *Coord. Chem. Rev.*, **254**, 1534 (2010)
22. A.Müller, R.Jostes, W.Eltzner, C.-S.Nie, E.Diemann, H.Bogge, M.Zimmermann, M.Dartmann, U.Reinsch-Vogell, S.Che, S.J.Cyvin, B.N.Cyvin. *Inorg. Chem.*, **24**, 2872 (1985)
23. F.A.Cotton, X.Feng. *Inorg. Chem.*, **30**, 3666 (1991)
24. R.E.Cramer, K.Yamada, H.Kawaguchi, K.Tatsumi. *Inorg. Chem.*, **35**, 1743 (1996)
25. J.Mizutani, H.Imoto, T.Saito. *J. Clust. Sci.*, **8**, 155 (1997)
26. P.A.Petrov, D.Y.Naumov, R.Llusar, C.J.Gómez-García, V.Polo, S.N.Konchenko. *Dalton Trans.*, **41**, 14031 (2012)
27. T.Weber, J.C.Muijsers, J.W.Niemantsverdriet. *J. Phys. Chem.*, **99**, 9194 (1995)
28. J.C.Muijsers, T.Weber, R.M.van Hardeveld, H.W.Zandbergen, J.W.Niemantsverdriet. *J. Catal.*, **157**, 698 (1995)
29. H.Akashi, T.Shibahara. *Inorg. Chim. Acta*, **300**, 572 (2000)
30. J.Andres, M.Feliz, J.Fraxedas, V.Hernandez, J.T.Lopez-Navarrete, R.Llusar, G.Sauthier, F.R.Sensato, B.Silvi, C.Bo, J.M.Campanera. *Inorg. Chem.*, **46**, 2159 (2007)
31. M.Feliz, R.Llusar, J.Andrés, S.Berski, B.Silvi. *New J. Chem.*, **26**, 844 (2002)
32. J.Andrés, S.Berski, M.Feliz, R.Llusar, F.Sensato, B.Silvi. *C. R. Chim.*, **8**, 1400 (2005)
33. J.Li, C.-W.Liu, J.-X.Lu. *Polyhedron*, **13**, 1841 (1994)
34. W.-D.Cheng, G.-C.Guo, J.-S.Huang, L.-J.Lu. *Polyhedron*, **14**, 3649 (1995)
35. Z.Chen, J.Lu, C.Liu, Z.Qianer. *Polyhedron*, **10**, 2799 (1991)
36. C.Wendan, Z.Qianer, H.Jinshun, L.Jiaxi. *Polyhedron*, **9**, 1625 (1990)
37. C.Wendan, Z.Qianer, H.Jinshun, J.Lu. *Polyhedron*, **8**, 2785 (1989)
38. J.Li, C.W.Liu, J.X.Lu. *J. Clust. Sci.*, **5**, 505 (1994)
39. F.Estevan, M.Feliz, R.Llusar, J.A.Mata, S.Uriel. *Polyhedron*, **20**, 527 (2001)
40. M.Feliz, R.Llusar, S.Uriel, C.Vicent, M.G.Humphrey, N.T.Lucas, M.Samoc, B.Luther-Davies. *Inorg. Chim. Acta*, **349**, 69 (2003)
41. R.Hernandez-Molina, M.Sokolov, W.Clegg, P.Esparza, A.Mederos. *Inorg. Chim. Acta*, **331**, 52 (2002)
42. K.Herbst, P.Zanello, M.Corsini, N.D'Amelio, L.Dahlenburg, M.Brorson. *Inorg. Chem.*, **42**, 974 (2003)
43. N.Avarvari, K.Kiracki, R.Llusar, V.Polo, I.Sorribes, C.Vicent. *Inorg. Chem.*, **49**, 1894 (2010)
44. R.Llusar, S.Uriel. *Eur. J. Inorg. Chem.*, 1271 (2003)
45. E.Pedrajas, I.Sorribes, A.L.Gushchin, Yu.A.Laricheva, K.Junge, M.Beller, R.Llusar. *ChemCatChem*, **9**, 1128 (2017)
46. J.A.Pino-Chamorro, Yu.A.Laricheva, E.Guillamón, M.J.Fernández-Trujillo, E.Bustelo, A.L.Gushchin, N.Y.Shmelev, P.A.Abramov, M.N.Sokolov, R.Llusar, M.G.Basallote, A.G.Algarra. *New J. Chem.*, **40**, 7872 (2016)
47. A.L.Gushchin, Yu.A.Laricheva, D.A.Piryazev, M.N.Sokolov. *Russ. J. Coord. Chem.*, **40**, 5 (2014)
48. A.L.Gushchin, Yu.A.Laricheva, P.A.Abramov, A.V.Virovets, C.Vicent, M.N.Sokolov, R.Llusar. *Eur. J. Inorg. Chem.*, 4093 (2014)
49. P.A.Petrov, A.V.Virovets, A.S.Bogomyakov, R.Llusar, C.J.Gomez-Garcia, V.Polo, S.N.Konchenko. *Chem. Commun.*, **48**, 2713 (2012)
50. M.G.Basallote, M.Feliz, M.J.Fernandez-Trujillo, R.Llusar, V.S.Safont, S.Uriel. *Chem. – Eur. J.*, **10**, 1463 (2004)
51. P.A.Petrov, A.V.Virovets, A.Alberola, R.Llusar, S.N.Konchenko. *Dalton Trans.*, **51**, 8875 (2010)
52. T.Saito, N.Tamamoto, T.Yamagata, H.Imoto. *J. Am. Chem. Soc.*, **110**, 1646 (1988)
53. K.Tsuge, H.Imoto, T.Saito. *Inorg. Chem.*, **34**, 3404 (1995)
54. P.A.Petrov, M.R.Ryzhikov, A.V.Virovets, S.N.Konchenko, C.J.Gómez-Garcia, R.Llusar. *Polyhedron*, **81**, 6 (2014)
55. C.S.Bahn, A.Tan, S.Harris. *Inorg. Chem.*, **37**, 2770 (1998)
56. T.Shibahara, G.Sakane, Y.Naruse, K.Taya, H.Akashi, A.Ichimura, H.Adachi. *Bull. Chem. Soc. Jpn.*, **68**, 2769 (1995)
57. K.Hegetschweiler, M.Wöerle, M.D.Meienberger, R.Nesper, H.W.Schmalle, R.D.Hancock. *Inorg. Chim. Acta*, **250**, 35 (1996)
58. R.Miyamoto, S.Kawata, M.Iwaizumi, H.Akashi, T.Shibahara. *Inorg. Chem.*, **36**, 542 (1997)
59. T.Yamauchi, H.Takagi, T.Shibahara, H.Akashi. *Inorg. Chem.*, **45**, 5429 (2006)
60. M.Feliz, J.M.Garriga, R.Llusar, S.Uriel, M.G.Humphrey, N.T.Lucas, M.Samoc, B.Luther-Davies. *Inorg. Chem.*, **40**, 6132 (2001)
61. R.Llusar, S.Uriel, C.Vicent. *J. Chem. Soc., Dalton Trans.*, 2813 (2001)
62. R.Llusar, I.Sorribes, C.Vicent. *Inorg. Chem.*, **48**, 4837 (2009)
63. J.A.A.Pino-Chamorro, Yu.A.Laricheva, E.Guillamón, M.J.Fernández-Trujillo, A.G.Algarra, A.L.Gushchin, P.A.Abramov, E.Bustelo, R.Llusar, M.N.Sokolov, M.G.Basallote. *Inorg. Chem.*, **55**, 9912 (2016)
64. M.Feliz, R.Llusar, S.Uriel, C.Vicent, E.Coronado, C.I.Gómez-Garcia. *Chem. – Eur. J.*, **10**, 4308 (2004)
65. I.Sorribes, F.Lloret, J.C.Waerenborgh, V.Polo, R.Llusar, C.Vicent. *Inorg. Chem.*, **51**, 10512 (2012)
66. A.L.Gushchin, K.A.Kovalenko, M.N.Sokolov, D.Y.Naumov, N.F.Zakharchuk, C.Vicent, V.P.Fedin. *Russ. Chem. Bull.*, **56**, 1701 (2007)
67. A.Alberola, R.Llusar, C.Vicent, J.Andrés, V.Polo, C.J.Gómez-García. *Inorg. Chem.*, **47**, 3661 (2008)
68. H.Akashi, N.Uryu, T.Shibahara. *Inorg. Chim. Acta*, **261**, 53 (1997)

69. P.W.Dimmock, D.P.E.Dickson, A.G.Sykes. *Inorg. Chem.*, **29**, 5120 (1990)
70. N.A.Kryuchkova, M.M.Syrokvashin, A.L.Gushchin, E.V.Korotaev, A.V.Kalinkin, Yu.A.Laricheva, M.N.Sokolov. *Spectrochim. Acta, Part A*, **190**, 347 (2018)
71. S.Krackl, A.Alberola, R.Llusar, G.Meyer, C.Vicent. *Inorg. Chim. Acta*, **363**, 4197 (2010)
72. P.A.Petrov, D.Y.Naumov, T.S.Sukhikh, S.N.Konchenko, C.J.Gómez-Garcia, R.Llusar. *New J. Chem.*, **41**, 7849 (2017)
73. D.Recatala, R.Llusar, F.Galindo, K.A.Brylev, A.L.Gushchin. *Eur. J. Inorg. Chem.*, 1877 (2015)
74. D.Recatalá, A.L.Gushchin, R.Llusar, F.Galindo, K.A.Brylev, M.R.Ryzhikov, N.Kitamura. *Dalton Trans.*, **42**, 12947 (2013)
75. *Optoelectronic Properties of Inorganic Compounds*. (Eds D.M.Roundhill, J.P.Fackler). (Boston: Springer, 1999)
76. W.Zhang, W.Y.Jiao, G.Shi, Y.L.Song, Y.X.Wang, D.J.Liu, Q.Chang, C.Zhang, X.Q.Xin. *Opt. Mater. (Amsterdam)*, **31**, 218 (2008)
77. Q.F.Zhang, Y.N.Xiong, T.S.Lai, W.Ji, X.Q.Xin. *J. Phys. Chem. B*, **104**, 3446 (2000)
78. S.Shi, W.Ji, S.H.Tang, J.P.Lang, X.Q.Xin. *J. Am. Chem. Soc.*, **116**, 3615 (1994)
79. S.Shi, Z.R.Chen, H.W.Hou, X.Q.Xin, K.B.Yu. *Chem. Mater.*, **7**, 1519 (1995)
80. G.Sakane, T.Shibahare, H.W.Hou, X.Q.Xin, S.Shi. *Inorg. Chem.*, **34**, 4785 (1995)
81. R.Philip, P.Chantharasupawong, H.F.Qian, R.C.Jin, J.Thomas. *Nano Lett.*, **12**, 4661 (2012)
82. S.A.Khan, D.Senapati, T.Senapati, P.Bonifassi, Z.Fan, A.K.Singh, A.Neeley, G.Hill, P.C.Ray. *Chem. Phys. Lett.*, **512**, 92 (2011)
83. W.Ji, S.Shi, H.J.Du, P.Ge, S.H.Tang, X.Q.Xin. *J. Phys. Chem.*, **99**, 17297 (1995)
84. P.Ge, S.H.Tang, W.Ji, S.Shi, H.W.Hou, D.L.Long, X.Q.Xin, S.F.Lu, Q.J.Wu. *J. Phys. Chem. B*, **101**, 27 (1997)
85. S.Shi, H.W.Hou, X.Q.Xin. *J. Phys. Chem.*, **99**, 4050 (1995)
86. J.Dai, C.Q.Bian, X.Wang, Q.F.Xu, M.Y.Zhou, M.Munakata, M.Maekawa, M.H.Tong, Z.R.Sun, H.P.Zeng. *J. Am. Chem. Soc.*, **122**, 11007 (2000)
87. G.Chatzikyriakos, I.Papagiannouli, S.Couris, G.C.Anyfantis, G.C.Papavassiliou. *Chem. Phys. Lett.*, **513**, 229 (2011)
88. D.Recatala, R.Llusar, A.Barlow, G.M.Wang, M.Samoc, M.G.Humphrey, A.L.Guschin. *Dalton Trans.*, **44**, 13163 (2015)
89. A.V.Rogachev, A.L.Gushchin, P.A.Abramov, E.A.Kozlova, C.Vicent, D.Piryazev, A.Barlow, M.Samoc, M.G.Humphrey, R.Llusar, V.P.Fedin, M.N.Sokolov. *Eur. J. Inorg. Chem.*, (17), 2865 (2015)
90. A.Nova, R.Mas-Ballesté, A.Lledós. *Organometallics*, **31**, 1245 (2011)
91. E.Clot, O.Eisenstein, N.Jasim, S.A.Macgregor, J.E.McGrady, R.N.Perutz. *Acc. Chem. Res.*, **44**, 333 (2011)
92. X.Ribas. *C – H and C – X Bond Functionalization: Transition Metal Mediation*. (Ed. J.J.Spivey). (Cambridge: The Royal Society of Chemistry, 2013)
93. B.M.Kraft, R.J.Lachicotte, W.D.Jones. *J. Am. Chem. Soc.*, **122**, 8559 (2000)
94. M.F.Kuhnel, D.Lentz. *Angew. Chem., Int. Ed.*, **49**, 2933 (2010)
95. S.Yow, S.J.Gates, A.J.P.White, M.R.Crimmin. *Angew. Chem., Int. Ed.*, **51**, 12559 (2012)
96. M.F.Kuehnel, P.Holstein, M.Kliche, J.Kruger, S.Matthies, D.Nitsch, J.Schutt, M.Sparenberg, D.Lentz. *Chem. – Eur. J.*, **18**, 10701 (2012)
97. A.G.Algarra, M.G.Basallote, M.J.Fernández-Trujillo, M.Feliz, E.Guillamon, R.Llusar, I.Sorribes, C.Vicent. *Inorg. Chem.*, **49**, 5935 (2010)
98. T.F.Beltrán, M.Feliz, R.Llusar, J.A.Mata, V.S.Safont. *Organometallics*, **30**, 290 (2011)
99. C.Alfonso, T.F.Beltrán, M.Feliz, R.Llusar. *J. Clust. Sci.*, **26**, 199 (2015)
100. H.A.Wittcoff, B.G.Reuben, J.S.Plotkin. *Industrial Organic Chemicals*. Wiley, Hoboken. NJ, 2004
101. S.A.Lawrence, in *Amines: Synthesis, Properties and Applications*. (Cambridge: The Press Syndicate of the University of Cambridge, 2012). P. 1
102. S.Farhadi, S.Sepahvand. *J. Mol. Catal. A: Chem.*, **318**, 75 (2010)
103. R.V.Jagadeesh, A.-E.Surkus, H.Junge, M.-M.Pohl, J.Radnik, J.Rabeah, H.Huan, V.Schünemann, A.Brückner, M.Beller. *Science*, **342**, 1073 (2013)
104. S.Ichikawa, M.Tada, Y.Iwasawa, T.Ikariya. *Chem. Commun.*, 924 (2005)
105. A.Corma, P.Serna, P.Concepcion, J.J.Calvino. *J. Am. Chem. Soc.*, **130**, 8748 (2008)
106. L.Q.Liu, B.T.Qiao, Z.J.Chen, J.Zhang, Y.Q.Deng. *Chem. Commun.*, 653 (2009)
107. F.Cardenas-Lizana, S.Gomez-Quero, A.Hugon, L.Delannoy, C.Louis, M.A.Keane. *J. Catal.*, **262**, 235 (2009)
108. R.Joshi, U.Chudasama. *Ind. Eng. Chem. Res.*, **49**, 2543 (2010)
109. I.Sorribes, G.Wienhfer, C.Vicent, K.Junge, R.Llusar, M.Beller. *Angew. Chem., Int. Ed.*, **51**, 7794 (2012)
110. E.Pedrajas, I.Sorribes, K.Junge, M.Beller, R.Llusar. *ChemCatChem*, **7**, 2675 (2015)
111. B.Zhao, Z.Han, K.Ding. *Angew. Chem., Int. Ed.*, **52**, 4744 (2013)
112. F.Haber. *Z. Electr.*, **4**, 506 (1898)
113. A.Corma, P.Concepción, P.Serna. *Angew. Chem., Int. Ed.*, **46**, 7266 (2007)
114. F.A.Cotton, P.A.Kibala, M.Matusz, C.S.McCaleb, R.B.W.Sandor. *Inorg. Chem.*, **28**, 2623 (1989)
115. C.J.Casewit, D.E.Coons, L.L.Wright, W.K.Miller, M.R.Dubois. *Organometallics*, **5**, 951 (1986)
116. E.Pedrajas, I.Sorribes, K.Junge, M.Beller, R.Llusar. *Green Chem.*, **19**, 3764 (2017)
117. K.Maeda, K.Domen. *J. Phys. Chem. Lett.*, **1**, 2655 (2010)
118. W.T.Eckenhoff, R.Eisenberg. *Dalton Trans.*, **41**, 13004 (2012)
119. D.Merki, X.Hu. *Energy Environ. Sci.*, **4**, 3878 (2011)
120. J.Yano, J.Kern, V.K.Yachandra, H.Nilsson, S.Koroidov, J.Messinger, in *Susteining Life on Planet Earth: Metalloenzymes Mastering Dioxygen and Other Chewy Gases. Book Series Metal Ions in Life Sciences*. Vol. 15. (Eds P.M.H.Kroneck, M.E.Sosa Torres). (Springer, 2015). P. 13
121. H.Vrubel, X.Hu. *ACS Catal.*, **3**, 2002 (2013)
122. W.Zhou, Z.Yin, Y.Du, X.Huang, Z.Zeng, Z.Fan, H.Liu, J.Wang, H.Zhang. *Small*, **9**, 140 (2013)
123. Q.Liu, Z.Pu, A.M.Asiri, A.H.Qusti, A.O.Al-Youbi, X.Sun. *J. Nanopart. Res.*, **15**, 2057 (2013)
124. X.Zong, G.Wu, H.Yan, G.Ma, J.Shi, F.Wen, L.Wang, C.Li. *J. Phys. Chem. C*, **114**, 1963 (2010)
125. A.B.Laursen, T.Pedersen, P.Malacrida, B.Seger, O.Hansen, P.C.K.Vesborg, I.Chorkendorff. *Phys. Chem. Chem. Phys.*, **15**, 20000 (2013)
126. P.D.Tran, S.S.Pramana, V.S.Kale, M.Nguyen, S.Y.Chiam, S.K.Batabyal, L.H.Wong, J.Barber, J.Loo. *Chem. – Eur. J.*, **18**, 13994 (2012)
127. Z.Zhang, P.Wang. *J. Mater. Chem.*, **22**, 2456 (2012)
128. T.F.Jaramillo, J.Bonde, J.D.Zhang, B.L.Ooi, K.Andersson, J.Ulstrup, I.Chorkendorff. *J. Phys. Chem. C*, **112**, 17492 (2008)
129. T.F.Jaramillo, K.P.Jorgensen, J.Bonde, J.H.Nielsen, S.Horch, I.Chorkendorff. *Science*, **317**, 100 (2007)
130. J.K.Nørskov, T.Bligaard, A.Logadottir, J.R.Kitchin, J.G.Chen, S.Pandelov, U.Stimming. *J. Electrochem. Soc.*, **152**, J23 (2005)
131. A.B.Laursen, S.Kegnös, S.Dahl, I.Chorkendorff. *Energy Environ. Sci.*, **5**, 5577 (2012)

132. Y.Hou, P.C.Vesborg, L.Bech, B.Seger, S.Dahl, I.Chorkendorff, B.L.Abrams, K.Herbst, M.E.Bjørketun, J.Rossmeisl, J.K.Nørskov, T.Pedersen, O.Hansen. *J. Photon. Energy*, **2**, 026001 (2012)
133. S.W.Seo, S.Park, H.Y.Jeong, S.H.Kim, U.Sim, C.W.Lee, K.T.Nam, K.S.Hong. *Chem. Commun.*, **48**, 10452 (2012)
134. J.Kibsgaard, T.F.Jaramillo, F.Besenbacher. *Nat. Chem.*, **6**, 248 (2014)
135. H.I.Karunadasa, E.Montalvo, Y.Sun, M.Majda, J.R.Long, C.J.Chang. *Science*, **335**, 698 (2012)
136. L.Ye, L.Zan, L.Tian, T.Peng, J.Zhang. *Chem. Commun.*, **47**, 6951 (2011)
137. J.Xiong, G.Cheng, F.Qin, R.Wang, H.Sun, R.Chen. *Chem. Eng. J.*, **220**, 228 (2013)
138. J.Xia, J.Di, S.Yin, H.Xu, J.Zhang, Y.Xu, L.Xu, H.Li, M.Ji. *RSC Adv.*, **4**, 82 (2014)
139. Y.Fang, Y.Huang, J.Yang, P.Wang, G.Cheng. *Environ. Sci. Technol.*, **45**, 1593 (2011)
140. D.Yue, T.Zhang, M.Kan, X.Qian, Y.Zhao. *Appl. Catal., B*, **183**, 1 (2016)
141. A.P.V.Soares, M.F.Portela, A.Kiennemann. *Catal. Rev.*, **47**, 125 (2005)
142. Y.Ono. *Catal. Today*, **81**, 3 (2003)
143. T.Waters, R.A.J.O'Hair, A.G.Wedd. *J. Am. Chem. Soc.*, **125**, 3384 (2003)
144. Y.K.Kim, R.Rousseau, B.D.Kay, J.M.White, Z.Dohnálek. *J. Am. Chem. Soc.*, **130**, 5059 (2008)
145. C.Vicent, M.Feliz, R.Llusar. *J. Phys. Chem. A*, **112**, 12550 (2008)
146. T.F.Beltran, M.Feliz, R.Llusar, V.S.Safont, C.Vicent. *Catal. Today*, **177**, 72 (2011)
147. T.Tatsumi, M.Taniguchi, H.Ishige, Y.Ishii, T.Murata, M.Hidai. *Appl. Surf. Sci.*, **121**, 500 (1997)
148. M.Taniguchi, D.Imamura, H.Ishige, I.Youichi, T.Murata, M.Hidai, T.Tatsumi. *J. Catal.*, **187**, 139 (1999)
149. W.Bensch, in *Comprehensive Inorganic Chemistry II. Superface Inorganic Chemistry Heterogeneous Catalysis.* (2nd Edn). Vol. 7. (Elsevier, 2013). P. 287
150. R.R.Chianelli, G.Berhault, P.Raybaud, S.Kasztelan, J.Hafner, H.Toulhoat. *Appl. Catal., A*, **227**, 83 (2002)
151. L.I.Meriño, A.Centeno, S.A.Giraldo. *Appl. Catal., A*, **197**, 61 (2000)
152. M.D.Curtis. *Appl. Organomet. Chem.*, **6**, 429 (1992)
153. K.Herbst, M.Monari, M.Brorson. *Inorg. Chem.*, **41**, 1336 (2002)
154. A.Puig-Molina, L.P.Nielsen, A.M.Molenbroek, K.Herbst. *Catal. Lett.*, **92**, 29 (2004)
155. K.Herbst, M.Monari, M.Brorson. *Inorg. Chem.*, **40**, 2979 (2001)
156. M.Feliz, R.Llusar, S.Uriel, C.Vicent, M.Brorson, K.Herbst. *Polyhedron*, **24**, 1212 (2005)
157. K.Herbst, M.Brorson, A.Carlsson. *J. Mol. Catal. A: Chem.*, **325**, 1 (2010)
158. E.M.Guillamon, M.Blasco, R.Llusar. *Inorg. Chim. Acta*, **424**, 248 (2015)
159. E.C.Constable. *Chem. Soc. Rev.*, **42**, 1637 (2013)
160. R.Frantz, E.Guillamon, J.Lacour, R.Llusar, V.Polo, C.Vicent. *Inorg. Chem.*, **46**, 10717 (2007)
161. T.Portada, M.Roje, Z.Raza, V.Čaplar, M.Žinić, V.Šunjić. *Eur. J. Org. Chem.*, **5**, 838 (2007)
162. M.Feliz, E.Guillamon, R.Llusar, C.Vicent, S.E.Stiriba, J.Perez-Prieto, M.Barberis. *Chem. – Eur. J.*, **12**, 1486 (2006)
163. R.Faust. *Angew. Chem., Int. Ed.*, **40**, 2251 (2001)
164. H.Pellissier. *Tetrahedron*, **64**, 7041 (2008)
165. J.Long, H.Du, K.Li, Y.Shi. *Tetrahedron Lett.*, **46**, 2737 (2005)
166. É.Lévesque, S.R.Goudreau, A.B.Charette. *Org. Lett.*, **16**, 1490 (2014)
167. M.Ciampini, P.Perlmutter, K.Watson. *Tetrahedron: Asymmetry*, **18**, 243 (2007)
168. E.Guillamon, R.Llusar, J.Perez-Prieto, S.E.Stiriba. *J. Organomet. Chem.*, **693**, 1723 (2008)
169. A.I.Carrillo, J.Garcia-Martinez, R.Llusar, E.Serrano, I.Sorribes, C.Vicent, J.A.Vidal-Moya. *Microporous Mesoporous Mater.*, **151**, 380 (2012)
170. R.A.Sheldon. *Chem. Soc. Rev.*, **41**, 1437 (2012)
171. G.Blay, J.R.Pedro, C.Vila, in *Catalytic Asymmetric Friedel – Crafts Alkylations*. (Eds M.Bandini, A.Umani-Rohcni). (Weinheim: Wiley-VCH, 2009). P. 223
172. A.B.Zaitsev, S.Gruber, P.A.Pluss, P.S.Pregosin, L.F.Veiros, M.Worle. *J. Am. Chem. Soc.*, **130**, 11604 (2008)
173. I.Usui, S.Schmidt, M.Keller, B.Breit. *Org. Lett.*, **10**, 1207 (2008)
174. I.Takei, K.Suzuki, Y.Enta, K.Dohki, T.Suzuki, Y.Mizobe, M.Hidai. *Organometallics*, **22**, 1790 (2003)
175. Y.Tao, Y.Zhou, J.Qu, M.Hidai. *Tetrahedron Lett.*, **51**, 1982 (2010)
176. I.Takei, K.Kobayashi, K.Dohki, M.Hidai. *Inorg. Chem.*, **46**, 1045 (2007)
177. M.Kimura, M.Fukasaka, Y.Tamaru. *Heterocycles*, **67**, 535 (2006)
178. Y.Tao, Bo Wang, Baomin Wang, L.Qu, J.Qu. *Org. Lett.*, **12**, 2726 (2010)
179. Y.Tao, B.Wang, J.Zhao, Y.Song, L.Qu, J.Qu. *J. Org. Chem.*, **77**, 2942 (2012)
180. T.Murata, Y.Mizobe, H.Gao, Y.Ishii, T.Wakabayashi, F.Nakano, T.Tanase, S.Yano, M.Hidai, I.Echizen, H.Nanikawa, S.Motomura. *J. Am. Chem. Soc.*, **116**, 3389 (1994)
181. T.Wakabayashi, Y.Ishii, T.Murata, Y.Mizobe, M.Hidai. *Tetrahedron Lett.*, **36**, 5585 (1995)
182. T.Wakabayashi, Y.Ishii, K.Ishikawa, M.Hidai. *Angew. Chem., Int. Ed. Engl.*, **35**, 2123 (1996)
183. M.Hidai, S.Kuwata, Y.Mizobe. *Acc. Chem. Res.*, **33**, 46 (2000)
184. L.Takei, K.Dohki, K.Kobayashi, T.Suzuki, M.Hidai. *Inorg. Chem.*, **44**, 3768 (2005)
185. B.K.Burgess, D.J.Lowe. *Chem. Rev.*, **96**, 2983 (1996)
186. P.C.Dos Santos, R.Y.Igarashi, H.I.Lee, B.M.Hoffman, L.C.Seefeldt, D.R.Dean. *Acc. Chem. Res.*, **38**, 208 (2005)
187. T.Spatzal, J.Schlesier, E.-M.Burger, D.Sippel, L.Zhang, S.L.A.Andrade, D.C.Rees, O.Einsle. *Nat. Commun.*, **7**, 10902 (2016)
188. T.E.Wolff, J.M.Berg, C.Warrick, K.O.Hodgson, R.H.Holm, R.B.Frankel. *J. Am. Chem. Soc.*, **100**, 4630 (1978)
189. Y.Zhang, J.L.Zuo, H.C.Zhou, R.H.Holm. *J. Am. Chem. Soc.*, **124**, 14292 (2002)
190. S.Ohta, Y.Ohki, T.Hashimoto, R.E.Cramer, K.Tatsumi. *Inorg. Chem.*, **51**, 11217 (2012)
191. P.K.Mascharak, W.H.Armstrong, Y.Mizobe, R.H.Holm. *J. Am. Chem. Soc.*, **105**, 475 (1983)
192. D.Coucouvanis, K.D.Demadis, C.G.Kim, R.W.Dunham, J.W.Kampf. *J. Am. Chem. Soc.*, **115**, 3344 (1993)
193. D.V.Fomitchev, C.C.McLauchlan, R.H.Holm. *Inorg. Chem.*, **41**, 958 (2002)
194. K.Arashiba, Y.Miyake, Y.Nishibayashi. *Nat. Chem.*, **3**, 120 (2011)
195. S.Kuriyama, K.Arashiba, K.Nakajima, H.Tanaka, N.Kamaru, K.Yoshizawa, Y.Nishibayashi. *J. Am. Chem. Soc.*, **136**, 9719 (2014)
196. S.Takemoto, J.Ohata, K.Umetani, M.Yamaguchi, H.Matsuzaka. *J. Am. Chem. Soc.*, **136**, 15889 (2014)
197. E.S.Borren, A.F.Hill, R.Shang, M.Sharma, A.C.Willis. *J. Am. Chem. Soc.*, **135**, 4942 (2013)
198. R.D.Young, A.F.Hill, G.E.Cavigliasso, R.Stranger. *Angew. Chem., Int. Ed.*, **52**, 3699 (2013)
199. Yu.V.Mironov, Yu.M.Gayfulin, S.G.Kozlova, A.I.Smolentsev, M.S.Tarasenko, A.S.Nizovtsev, V.E.Fedorov. *Inorg. Chem.*, **51**, 4359 (2012)

200. X.D.Chen, W.Zhang, J.S.Duncan, S.C.Lee. *Inorg. Chem.*, **51**, 12891 (2012)
201. A.Hejl, T.M.Trnka, M.W.Day, R.H.Grubbs. *Chem. Commun.*, 2524 (2002)
202. A.Reinholdt, K.Herbst, J.Bendix. *Chem. Commun.*, **52**, 2015 (2016)